UNCLASSIFIED UNLIMITED

DRES

CONTRACT REPORT 17/88

THE NEPEAN TRACKED VEHICLE PERFORMANCE MODEL

J.Y. Wong

Vehicle Systems Development Corporation
Ottawa, Ontario

March 1988

DEFENCE RESEARCH ESTABLISHMENT SUFFIELD, RALSTON, ALBERTA

"This work was carried out for DRES under contract. The accuracy of the information presented herein is the responsibility solely of the contractor and is NOT to be construed as an Official Department of National Defence position unless so designated by other authorizing documents."

UNCLASSIFIED

CR12-88/10

VSDC

THE NEPEAN TRACKED VEHICLE PERFORMANCE MODEL (NTVPM-85)

BY

DR. J.Y. WONG

MARCH 1988

VEHICLE SYSTEMS DEVELOPMENT CORPORATION
OTTAWA, CANADA

THE NEPEAN TRACKED VEHICLE PERFORMANCE MODEL (NTVPM-85)

prepared for

Head
Vehicle Mobility Section
Defence Research Establishment Suffield
Department of National Defence

prepared by

Dr. J.Y. Wong
Vehicle Systems Development Corporation
Nepean, Ontario, Canada

under

DSS Contract Serial No. W7702-R6-2680/01-SG

March 1988

Table of Contents

FOREWORD

This report outlines the major features of a computer simulation model, known as the Nepean Tracked Vehicle Performance Model (NTVPM-85), developed by Vehicle Systems Development Corporation (VSDC), Nepean, Ontario, Canada. VSDC is the owner of all right, title and interest in the Intellectual Property in NTVPM-85.

This report was prepared for the Vehicle Mobility Section, Defence Research Establishment Suffield (DRES), Department of National Defence, under contract "Translation and Documentation of Tracked Vehicle Performance Model", Serial No. W7702-R6-2680/01-SG. Dr. G.J. Irwin of DRES was the Scientific Authority for the contract.

The contract was performed by Vehicle Systems Development Corporation. The Project Director was Dr. J.Y. Wong and the Project Engineer was Mr. J. Preston-Thomas.

In the preparation of this document, the author drew heavily on the material contained in some of his previous publications listed as references in the report.

Summary

This report outlines the basic features of a computer simulation model, known as the Nepean Tracked Vehicle Performance Model (NTVPM-85), developed by Vehicle Systems Development Corporation, Nepean, Ontario, Canada.

NTVPM-85 is intended for parametric analysis of tracked vehicle performance over unprepared terrain. It takes into account all major design parameters of the vehicle as well as terrain characteristics. The theoretical basis for NTVPM-85 and its experimental validation are presented. The capabilities and features of NTVPM-85 are compared with those of some of the existing methods for predicting tracked vehicle performance. Examples of the applications of NTVPM-85 to parametric evaluation of tracked vehicle designs are also given.

The model NTVPM-85 is an interactive, user-friendly computer simulation model. It is particularly useful for the designer, as well as the procurement manager, in the evaluation of vehicle candidates or in the optimization of tracked vehicle design for a given mission and environment. NTVPM-85 has found increasingly wide acceptance in vehicle design evaluations for industry and governmental agencies in North America, Europe and elsewhere. For instance, it has been employed to predict the possible changes in mobility of Canada's main battle tank, the Leopard C1, resulting from design modifications for the Canadian Department of National Defence. It has been used to assist AB Hagglund of Sweden in the evaluation of competing designs for a new family of armoured fighting vehicles. It has also been employed to compare the off-road mobility of various military logistics vehicles for an agency of the U.S. Department of the Navy.

INTRODUCTION

With growing demand for improving mobility over a wide range of terrains and in all seasons in resource industries and in military operations, there is an increasing need for a comprehensive and yet realistic mathematical model to guide the development and design of off-road vehicles.

Over the years, particularly since the Second World War, a variety of mathematical models for predicting and evaluating off-road vehicle performance have been developed. They range from entirely empirical to highly theoretical.

Within the context of the intended purposes, properly developed empirical models can play a useful role in estimating the performance of vehicles with design features similar to those that have been tested under similar operating conditions. However, empirical relations are valid only for the specific kinds of vehicle and for the particular types of terrain that have been evaluated. It is by no means certain that they can be extrapolated beyond the conditions upon which they were derived. Consequently, it is uncertain that empirical models can play a significant role in the evaluation of new vehicle design concepts or in the prediction of vehicle performance in new operating environments.

Theoretical models for off-road vehicle performance based on the theory of plastic equilibrium and the finite element method have emerged in recent years. A review of these models has revealed that while they may provide a better understanding of certain aspects of the complex phenomenon of vehicle-terrain interaction, there are severe limitations to their applications to the design and evaluation of off-road vehicles in practice. For instance, existing theoretical models based on the finite element method require the stress boundary conditions on the vehicle-terrain interface as input. This means that vehicle performance parameters, such as sinkage, motion resistance and thrust, can only be predicted if the stress distributions on the vehicle-terrain interface are known in advance. It should be noted, however, that if the stress boundary conditions on the vehicle-terrain interface are known, the tractive performance of the vehicle is completely defined. There is no need to perform a

finite element analysis of terrain response, as far as the prediction of vehicle performance is concerned. Also, in these theoretical models, many of the significant design features of the vehicle, such as roadwheel arrangements, track design and initial track tension of a tracked vehicle, are not taken into account. Furthermore, in many of these models, the stress-strain relationship and the strain-hardening behaviour of the terrain are assumed to be similar to those of metals. It has been shown that these assumptions are far from realistic, particularly for marginal terrain with a high degree of compressibility.

In view of the limitations and deficiencies of the empirical and theoretical models developed so far, a new type of mathematical model specifically developed for parametric evaluation of tracked vehicle design has been formulated by Wong et al. The model takes into account the responses of natural terrains, observed in the field, to loadings similar to those exerted by a tracked vehicle. These include the pressure-sinkage relationship, shearing characteristics, and the responses to repetitive normal and shear loadings of the terrain, measured using a bevameter. In the development of the model, all major design features of a tracked vehicle have also been taken into consideration.

Using the terrain data described above as input and taking the major design features of the vehicle into consideration, a detailed analysis of the mechanics of track-terrain interaction was performed. Based on the analysis, a comprehensive computer simulation model was developed to predict the normal and shear stress distributions on the track-terrain interface, and the external motion resistance, thrust, drawbar pull, and tractive efficiency of the vehicle.

The initial development of a computer simulation model known as CTVPM was made during the period from March 1980 to June 1984 under contract to the Canadian Department of National Defence. This initial model takes into consideration major vehicle design parameters, including vehicle weight, location of centre of gravity, number of roadwheels, roadwheel dimensions and spacing, locations of the sprocket and idler, number of supporting rollers, track dimensions, initial track tension, and angles of approach and departure of the track.

In the development of CTVPM, the following assumptions were made:

A. The track is equivalent to a flexible belt. This assumption is considered to be reasonable for rubber-belt type tracks and for tracks with relatively short track pitch designed for high speed operations, such as those used in fighting vehicles;

B. The track is inextensible;

C. In determining the sinkage of the track under the roadwheels, the effects of the independent suspension of the roadwheels are neglected. This means that the sinkage of the first roadwheel together with the attitude of the track system defines the sinkages of subsequent roadwheels.

In 1985, under the auspices of Vehicle Systems Development Corporation, Nepean, Ontario, Canada, a computer simulation model, known as NTVPM-85, was developed. In this model, the track is no longer assumed to be inextensible, and the track longitudinal elasticity, which is defined as the tension per unit longitudinal strain of the track, is taken into account. The elasticity is determined from the measured relationship between track tension and track link elongation. The track longitudinal elasticity affects the tension distribution in the track and as a result influences the performance of the vehicle to a certain extent over marginal terrain.

Over highly compressible terrain, such as deep snow, track sinkage may be greater than the ground clearance of the vehicle. If this occurs, the belly (hull) of the vehicle will be in contact with the terrain surface, and will support part of the vehicle weight. This will reduce the load carried by the tracks and will adversely affect the traction of the vehicle over terrain that exhibits frictional behaviour. Furthermore, belly contact will give rise to an additional drag component - the belly drag. The problem of belly contact is of importance to vehicle mobility over marginal terrain. In the simulation model NTVPM-85, the characteristics of belly-terrain interaction, including the load supported by the belly and the induced belly drag, are taken into consideration. Furthermore, the modelling of certain aspects of track-terrain interaction, as well as the algorithms that implement the mathematical model on the computer, has been significantly improved in NTVPM-85, as compared with CTVPM.

The model NTVPM-85 is particularly suited for parametric evaluation of vehicle design. It can be an extremely useful tool for the vehicle designer and the procurement manager in the evaluation of competing designs and in the examination of the effects on performance of design modifications and changing operational environments.

1. A REVIEW OF THE METHODS FOR PREDICTING TRACKED VEHICLE PERFORMANCE

The track was first conceived in the 18th century, as a "portable railway" and tracked vehicles have been used on a large scale in agriculture, construction, off-road transport, and military operations since the turn of this century. However, for a long period of time, the development and design of tracked vehicles have been, by and large, guided by empiricism and the "cut and try" methodology. As economic and social conditions change with the rapid progress in technology, the "trial and error" approach to off-road vehicle development has become extremely inefficient and prohibitively expensive. Furthermore, new requirements for greater mobility over a wider range of terrain, and growing demands for energy conservation and environmental protection have emerged. This has led to the recognition of the necessity of establishing realistic mathematical models for vehicle-terrain systems that will enable the development and design engineer, as well as the procurement manager, to evaluate a wide range of options and to establish a rational basis for the selection of an optimum vehicle configuration for a given mission and environment.

To be useful to the development and design engineer and to the procurement manager, a mathematical model for tracked vehicle performance should take into account all major vehicle design and operational parameters as well as terrain characteristics. The performance of a tracked vehicle, usually defined by its motion resistance, tractive effort and drawbar pull as functions of slip, is directly related to the normal and shear stress distributions on the track-terrain interface. A central issue in the mathematical modelling of tracked vehicle performance is, therefore, the establishment of the relationship between the interacting forces on the track-terrain interface and vehicle design parameters and terrain characteristics.

A variety of mathematical models for predicting and evaluating tracked vehicle performance, ranging from entirely empirical to totally theoretical, has been developed over the years. This chapter provides a brief review of some of the methods currently in use (1.1-1.3).

1.1 Empirical Methods

The interaction between an off-road vehicle and the terrain is very complex and considerable effort is required to adequately model it. To circumvent this difficulty, empirical methods have been developed.

One of the well-known empirical methods for evaluating off-road vehicle performance is that developed by the U.S. Army Engineer Waterways Experiment Station (WES). In developing the method, a series of vehicles of interest were tested in a range of terrains considered to be representative and at the same time terrain conditions were measured using a cone penetrometer. The results of vehicle performance testing and terrain measurements were then empirically correlated, and a model, known as the WES VCI model, was proposed for predicting vehicle performance on fine and coarse-grained inorganic soils (1.4). This model forms the basis for the subsequent developments of the AMC-71, AMC-74 and NRMM mobility models.

In the WES model, an empirical equation was established to calculate the mobility index (MI) of a vehicle in terms of certain vehicle design features. For instance, the mobility index for a tracked vehicle is defined as:

$$\text{Mobility Index} = \left[\frac{\text{Contact pressure factor} \times \text{weight factor}}{\text{track factor} \times \text{grouser factor}} + \text{bogie factor} - \text{clearance factor} \right] \times \text{engine factor} \times \text{transmission factor} \qquad (1)$$

where

$$\text{Contact pressure factor} = \frac{\text{gross weight, lb}}{\text{areas of tracks in contact with ground, in.}^2}$$

Weight factor:
- less than 50,000 lb = 1.0
- 50,000 to 69,999 lb = 1.2
- 70,000 to 99,999 lb = 1.4
- 100,000 lb or greater = 1.8

$$\text{Track factor} = \frac{\text{track width, in.}}{100}$$

Grouser factor: Grousers less than 1.5 in. high = 1.0
Grousers more than 1.5 in. high = 1.1

$$\text{Bogie factor} = \frac{\text{gross weight, lb, divided by 10}}{\text{total number of bogies on tracks in contact with ground} \times \text{area, in.}^2\text{, of one track shoe}}$$

$$\text{Clearance factor} = \frac{\text{clearance, in.}}{10}$$

Engine factor: $\geq$ 10 hp/ton of vehicle weight = 1.0
$<$ 10 hp/ton of vehicle weight = 1.05

Transmission factor: Automatic = 1.0; Manual = 1.05

The mobility index (MI) was then empirically correlated to the vehicle cone index (VCI), which is the minimum soil strength in the critical soil layer defined by the rating cone index (RCI) for fine-grained soils or the cone index (CI) for coarse-grained soils for a specified number of passes of a vehicle, such as 1 pass or 50 passes.

Finally, the values of performance parameters of a tracked vehicle, such as the maximum drawbar pull coefficient, maximum slope negotiable and towed motion resistance coefficient, were empirically determined as functions of vehicle type, number of passes to be completed, and the excess of RCI over VCI (i.e., RCI-VCI) for fine-grained soils (or the cone index (CI) for coarse-grained soils).

Another empirical method for evaluating the mobility of tracked vehicles was suggested by Rowland (1.5). He proposed the mean maximum pressure (MMP), which is defined as the mean value of the maxima occurring under all the roadwheel stations, as a criterion for evaluating the soft ground performance of off-road vehicles. Empirical equations were derived from vehicle test data for calculating the MMP for different types of track system.

He proposed that for link and belt tracks on rigid roadwheels,

$$\text{MMP} = \frac{1.26\ W}{2n_r A_\ell b\sqrt{t_t D}} \quad \text{kN/m}^2 \qquad (1.2)$$

and for belt tracks on pneumatic tired road wheels,

$$MMP = \frac{0.5\ W}{2n_r b\sqrt{D\ f_t}} \quad kN/m^2 \tag{1.3}$$

where W - vehicle weight, kN

n_r - number of wheel stations in one track

A_ℓ - rigid area of link (or belt track cleat) as a proportion of track pitch multiplied by wheel width

b - track or pneumatic tire width, m

t_t - track pitch, m

D - outer diameter of roadwheel or pneumatic tire, m

f_t - radial deflection of pneumatic tire under load, m

To evaluate whether a vehicle with a particular value of MMP will have adequate mobility over a specific terrain, Rowland proposed a set of desired values of the mean maximum pressure for different terrain conditions. Table 1.1 shows the desired values of MMP suggested by Rowland (1.6).

Within the context of their intended purposes, the empirical models developed by WES and Rowland are useful in certain types of application. It should be pointed out, however, that strictly speaking, empirical relations are only valid within the specific conditions under which the tests were carried out. Thus, it is by no means certain that empirical relations can be extrapolated beyond the conditions under which they were originally obtained. It appears uncertain, therefore, that an entirely empirical approach could play a useful role in the evaluation of new vehicle design concepts or in the prediction of vehicle performance in new operational environments. Furthermore, an entirely empirical approach is only feasible where the number of variables involved in the problem is relatively small. If a large number of parameters are required to define the problem, then an empirical approach may not be cost-effective.

To provide a more general approach to the prediction and evaluation of tracked vehicle performance, other methods of approach have been developed.

Table 1.1 **Desirable Values of Mean Maximum Pressure**

Terrain	Mean Maximum Pressure* (kN/m^2)		
	Ideal (Multipass Operation)	Satisfactory	Maximum Acceptable (Mostly Trafficable at Single-Pass Level)
Wet fine grained soils			
Temperate	150	200	300
Tropical	90	140	240
Muskeg	30	50	60
Muskeg floating mat and European bogs	5	10	15
Snow	10	25–30	40

1.2 Theoretical Methods

In recent years, attempts have been made to apply the theory of plastic equilibrium, finite element techniques, critical state theory and others to the analysis of vehicle-terrain interaction. Among them, the theory of plastic equilibrium is, perhaps, the most developed. One of the successful examples is the application of the theory of plastic equilibrium to the prediction of the draft of a two-dimensional soil cutting blade. The solution procedures have now been well documented (1.7).

In the late sixties, an extensive experimental investigation into the physical nature of vehicle-terrain interaction under various operating conditions was carried out by Wong and Reece (1.8, 1.9, 1.10). From the study, it was clearly established that failure zones were developed in dense soils under the action of a vehicle running gear and that there was a close correlation between the failure behavior of soil and the performance of the vehicle running gear. As a result of these findings, attempts have been made to apply the theory of plastic equilibrium to the evaluation of the performance of off-road vehicles (1.11). The prediction procedure involves the solution of differential equations for the plastic equilibrium of the soil mass in the failure zones, based on the Mohr-Coulomb yield (failure) criterion. To initiate the solution process and to obtain unique solutions to particular problems, certain information on the vehicle-terrain interface, such as the interface friction angle or more generally the direction of the major principal stresses on the interface, must be specified or assumed at the outset. This is one of the most important issues and yet one of the most uncertain parts of the whole methodology.

The application of the theory of plastic equilibrium could provide a better insight into the physical nature of vehicle-terrain interaction and could establish a theoretical reference with which the actual performance of cross-country vehicles may be compared under certain idealized conditions. It should be recognized, however, that there are severe limitations to the application of the theory to the prediction and evaluation of vehicle mobility in practice (1.12).

Firstly, the theory of plastic equilibrium as presently applied is based on the assumption that the terrain behaves like a rigid, perfectly plastic material. This means that the terrain does not deform significantly until the stresses within certain boundaries reach a certain level at which failure occurs. Beyond this point, the strain increases rapidly, while the stress remains constant. Although dense sand and the like may exhibit behaviour close to that of a rigid, perfectly plastic material, a wide range of natural terrains encountered in cross-country operations, such as snow and muskeg, have a high degree of compressibility, and their behaviour does not conform to that of a rigid, perfectly plastic material. Consequently, failure zones in these terrains under vehicular loads do not develop in a manner similar to that assumed in the theory, and the sinkage of the vehicle running gear is primarily due to the compression of the terrain and not due to the plastic flow of the terrain material. From a vehicle mobility viewpoint, terrains with a high degree of compressibility are of greater concern to vehicle designers and users than dense sand and the like. Thus, the usefulness of the methodology based on the theory of plastic equilibrium in vehicle mobility study is severely limited in practice. Furthermore, the theory of plastic equilibrium is mainly concerned with the prediction of the maximum load that the vehicle can exert on the terrain without causing failure. Consequently, the deformation of the terrain as a result of the application of load by the vehicle, which is of importance to the evaluation of vehicle performance, cannot be predicted.

Secondly, as mentioned previously, to initiate the numerical procedures to predict the performance of vehicle running gear based on the theory of plastic equilibrium, certain information on the vehicle running gear-terrain interface, such as the interface friction angle, must be specified at the outset. The approaches to specifying the required boundary conditions as presently developed are primarily empirical in nature (see reference (1.11)). In other words, the elaborate numerical procedures still heavily rely on empirical data as inputs. For instance, in the prediction of the performance of driven rigid wheels and pneumatic tires, it is suggested in reference (1.11) that the empirical shear stress-slip relationship proposed by Janosi and Hanamoto be used to estimate the interface friction angle. In the analysis of the rigid track-soil interaction, it is suggested that an empirical pressure-sinkage equation proposed by Perloff and Rahim be used as inputs to the solution processes. It is noted that these

empirical relationships suggested as inputs to the elaborate numerical procedures are similar to those used in various semi-empirical methods currently available for predicting off-road vehicle performance. Thus, even though an elaborate numerical procedure has been formulated for the evaluation of vehicle mobility, the solutions to any particular problem still heavily rely on either empirical inputs or assumed boundary conditions on the vehicle-terrain interface, some of which do not necessarily have any justifiable theoretical basis.

Thirdly, the solution procedures based on the theory of plastic equilibrium developed so far are for two-dimensional vehicle-terrain interaction problems. While this may be adequate in some cases, a variety of problems require that three-dimensional effects be taken into consideration. To develop three-dimensional failure patterns beneath a vehicle running gear and to formulate corresponding numerical procedures will greatly increase the complexity of the solution processes.

Because of the problems mentioned above, the methodology based on the theory of plastic equilibrium is not capable of providing a practical engineering tool for the evaluation of cross-country vehicle mobility in the field.

Another theoretical approach to the prediction of vehicle performance over unprepared terrain is based on the finite element method (1.13). Recent applications of this method to the solution of vehicle-terrain interaction problems require the stress or displacement boundary conditions on the interface to be specified at the outset. As pointed out by Wong (1.14), when the stress boundary conditions on the vehicle running gear-terrain interface are specified, the performance of the running gear is completely defined, since performance parameters, such as drawbar pull, motion resistance and input torque to the sprocket or wheel can readily be computed from the specified normal and tangential stresses at the interface using simple integration. Consequently, there is no need whatsoever to follow these approaches to determine the terrain response and then to predict the performance of the running gear. If, on the other hand, displacement boundary conditions at the vehicle-terrain interface are used to initiate the solution process then detailed information on the deformation pattern of the terrain adjacent to the vehicle-terrain interface

must be known at the outset, usually through experiments. Thus, in essence, this solution process begins with acquiring terrain deformation data for specifying the displacement boundary conditions as input, then proceeds to the manipulation of the numerical approximation procedures based on the finite element method, and ends up with providing information on terrain response and vehicle performance that could have been directly obtained during the data acquisition phase at the beginning of the solution process.

In a method recently developed by Karafiath (1.15) for predicting the sinkage and motion resistance of tracked vehicles using the finite element technique, the normal pressure distribution on the track-terrain interface is again required as input. This indicates that in general current methods based on the finite element technique do not provide a complete and self-contained procedure for predicting off-road vehicle performance. They do not address the central issue of vehicle performance modelling and the major concern of the development and design engineer, that is, predicting vehicle performance using vehicle design parameters and terrain characteristics as direct inputs. Also, in these models, the design features of the vehicle system, such as, track system configuration, roadwheel arrangements, track design and initial track tension, are not directly taken into account in the analysis of track-terrain interaction. Furthermore, in many of these theoretical models, the stress-strain relationship and the strain hardening behaviour of the terrain are assumed to be similar to those of metals (1.15). However, very little experimental evidence has so far been produced to support the validity of these assumptions for natural terrains, particularly for marginal terrains where vehicle mobility is of major concern. It appears, therefore, that the usefulness of the theoretical models for off-road vehicle performance developed so far is rather limited in practice, particularly in the development and design processes.

1.3 Methods for Parametric Analysis

One of the better known methods for parametric analysis of tracked vehicle performance is that originally developed by Bekker (1.2, 1.3). In this method, the track in contact with the terrain is assumed to be similar to a rigid footing. If the center of gravity of the vehicle is located at the mid-point of the track contact area, the normal pressure distribution may be taken as uniform, as shown in Fig.1.1. On the other hand, if the center of gravity of the vehicle is located ahead of or behind the mid-point of the contact area, a sinkage distribution of trapezoidal form may be assumed. Based on the assumptions mentioned above, and making use of the pressure-sinkage relationship obtained from the bevameter, the sinkage of the track can be predicted.

For a track with uniform contact pressure p, the sinkage z_0 is given by

$$z_0 = \left(\frac{p}{k_c/b + k_\phi}\right)^{1/n} = \left(\frac{W/b\ell}{k_c/b + k_\phi}\right)^{1/n} \qquad (1.4)$$

where b and ℓ are width and contact length of the track, respectively; W is the normal load on the track, and k_c, k_ϕ and n are the pressure-sinkage parameters in the Bekker equation (1.3).

The motion resistance R_c of the track due to terrain compaction can then be derived from the work done in compacting the terrain and making a rut of depth z_0 (1.3)

$$R_c = \frac{1}{(n+1)b^{1/n}\,(k_c/b+k_\phi)^{1/n}} \left(\frac{W}{\ell}\right)^{(n+1)/n} \qquad (1.5)$$

In very soft ground with noticeable sinkage, Bekker suggested that a bulldozing resistance should be taken into account and that it may be estimated using the retaining wall theory of soil mechanics (1.3).

To predict the tractive effort, use is made of the shear stress-displacement relationship of the terrain obtained using a bevameter (Fig.1.1).

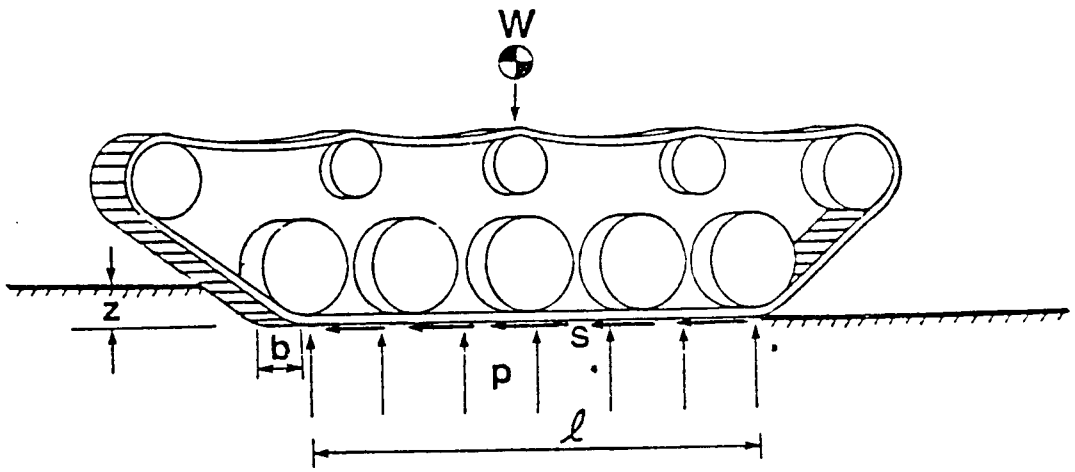

$$p = \frac{W}{2b\ell}$$

$z = f(p)$

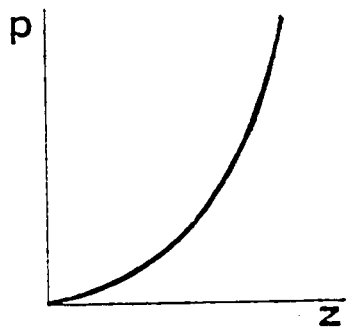

$s = f(p, j)$

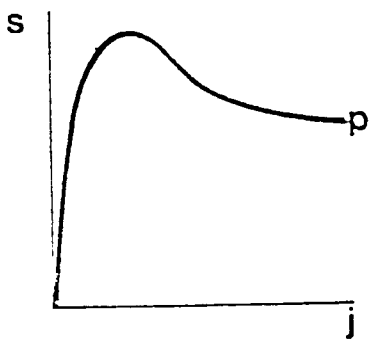

Fig. 1.1 A conventional method for predicting tracked vehicle performance

If the ground pressure is uniformly distributed and the shear stress-shear displacement relationship is described by the simply exponential equation, the tractive effort F of a track can be defined as (1.3, 1.16)

$$F = b \int_0^{\ell} (c + \frac{W}{b\ell} \tan\phi)\ (1-e^{-ix/K})dx$$

$$= (Ac+W\tan\phi)\ [1 - \frac{K}{i\ell}\ (1-e^{-i\ell/K})] \qquad (1.6)$$

where A is the contact area of the track; c, ϕ and K are cohesion, angle of shearing resistance, and shear deformation modulus, respectively.

From the predicted tractive effort and motion resistance, the drawbar pull as a function of slip and the overall tractive performance of the vehicle can be determined.

Experimental evidence has shown that the assumed ground pressure distribution described above is not realistic, particularly for tracked vehicles with high ratios of roadwheel spacing to track pitch designed for high speed operations. Ground pressure under those vehicles is usually concentrated under the roadwheels and is far from uniform. Consequently, performance predictions using the method described above will be unrealistic, particularly with respect to sinkage, motion resistance and tractive effort in soft terrain.

In an attempt to improve the prediction of ground pressure distribution under a track, Bekker performed a pioneering theoretical study about three decades ago (1.2). The analysis is intended for the prediction of static ground pressure distribution when the vehicle is at rest. The effect of vehicle weight, track width, roadwheel spacing and the pressure-sinkage relationship of the terrain were taken into account. The study was, however, limited to the analysis of the shape of the track span between two roadwheels, simplified as knife-edge supports, in a terrain with a linear pressure-sinkage relationship. The effect of roadwheel diameter, suspension characteristics and other design factors were not included in the analysis.

In 1981, an improved method for predicting the static ground pressure distribution was developed by Garber and Wong (1.17). In the analysis, the

major design features of a tracked vehicle, such as the dimensions, spacing and number of roadwheels, vehicle weight, track dimensions, initial track tension, and characteristics of the suspension and the track tensioning device, were taken into consideration. The analysis can accommodate terrain with a linear or non-linear pressure-sinkage relationship. Based on a detailed examination of the interaction between the track and the terrain, the interrelationships of vehicle design parameters, terrain conditions, and static ground pressure distribution under a track were established. Figure 1.2 shows the predicted static ground pressure of various tracked vehicles on different types of terrain, obtained using the analytical method developed by Garber and Wong (1.17). The design parameters of the vehicles used in the analysis are given in Table 1.2. The variation of the mean maximum pressure (MMP), the ratio of MMP to MGP (mean ground pressure, which is the normal load on the track divided by the contact area), and the maximum roadwheel sinkage with terrain stiffness for various types of tracked vehicle is shown in Fig.1.3. It can be seen that both the design configuration of the track system and the terrain conditions have significant influence on the static ground pressure, and that the maximum static pressure under a track is generally much higher than the mean (or nominal) ground pressure.

It can be seen that the analytical method for predicting the static ground pressure developed by Garber and Wong can serve a useful purpose in differentiating the potential performance of vehicles of different designs and in determining the relative significance of the effects of various vehicle design parameters on ground pressure distribution. It should be pointed out, however, that when a tracked vehicle is in straight line motion, a terrain element under the track is subject to the repetitive loading of consecutive roadwheels. The response of the terrain to repetitive loading should, therefore, be taken into account in predicting the ground pressure distribution under a moving vehicle. Furthermore, for a moving tracked vehicle, shear stresses will be developed on the track-terrain interface. To develop a comprehensive model for predicting the tractive performance of tracked vehicles, these factors should be taken into consideration.

Based on the brief review of existing methods for predicting tracked vehicle performance given above it can be seen that most of the methods developed so far are either of empirical nature or based upon assumptions that

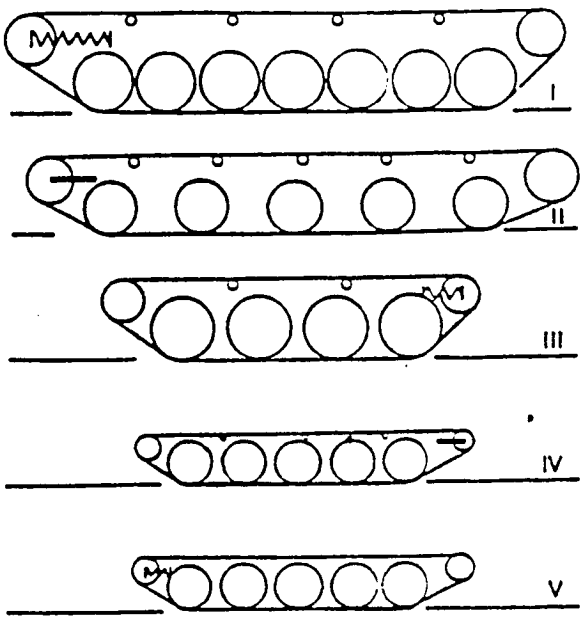

Schematic views of the track systems under consideration.
(I) The tensioning wheel is located in the front.
(II) The tensioning wheel is located in the front and fixed.
(III) The tensioning wheel is located in the rear.
(IV) The tensioning wheel is located in the rear and fixed.
(V) The tensioning wheel is located in the front.

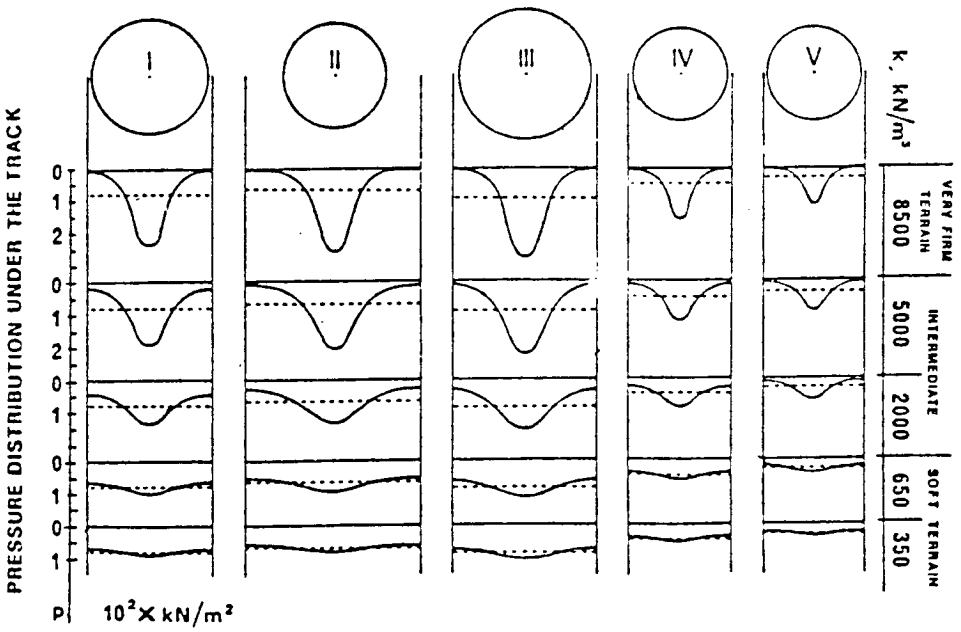

Fig. 1.2 Static normal pressure distribution under various track systems over different terrains

Table 1.2

DESIGN PARAMETERS OF THE TRACK SYSTEMS UNDER CONSIDERATION

Design parameters of the track system	Track System I	Track System II	Track System III	Track System IV	Track System V
W weight of the vehicle, kN	514	370	370	138	78
b width of the track, m	0.65	0.57	0.67	0.50	0.43
L distance between the centres of the front and rear road wheels, m	4.50	4.38	2.65	2.50	2.50
r radius of the road wheel, m	0.35	0.335	0.40	0.28	0.295
N number of the road wheels	7	5	4	5	5
α_0 angle between the track and horizontal surface on the side of the sprocket	45°	22°	37°	33°	30°
β_0 angle between the track and horizontal surface on the side of the tensioning wheel	35°	28.5°	45°	28°	32°
a_0 vertical distance between the centre of the tensioning wheel and the centre of the road wheel, m	0.525	0.335	0.34	0.22	0.175
r_s radius of the sprocket, m	0.28	0.335	0.24	0.17	0.175
r_t radius of the tensioning wheel, m	0.30	0.285	0.22	0.11	0.175
k_t combined stiffness of the suspension springs of the one track, kN/m	1500	1075	1250	545	215
k_t stiffness of the track tensioning device spring, kN/m	1000	∞*	1250	∞*	500
ρ weight of the track per unit track length, kN/m	1.2	0.9	1.1	0.55	0.3
m number of supporting rollers	4	5	2	3	0
T_0 initial track tension per unit width of the track, kN/m	44	25	35.5	12.8	21

*∞ indicates that the tensioning wheel is fixed.

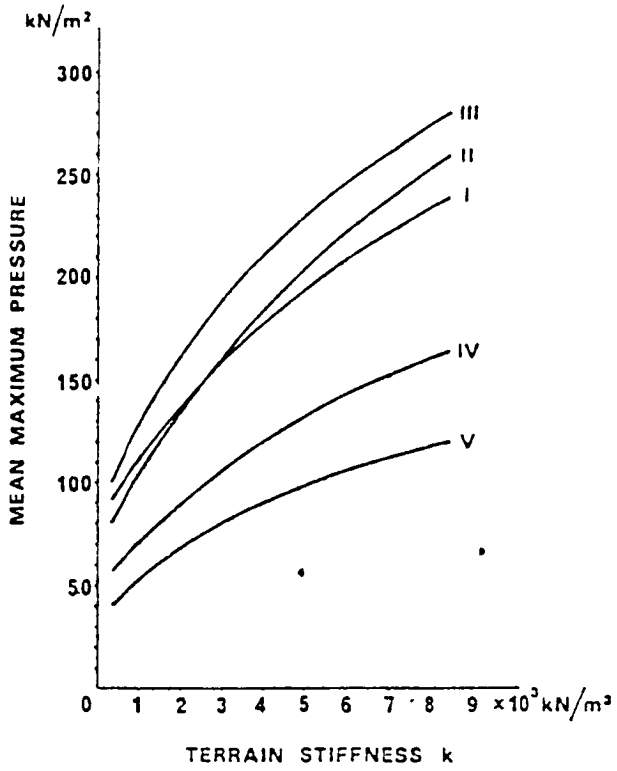

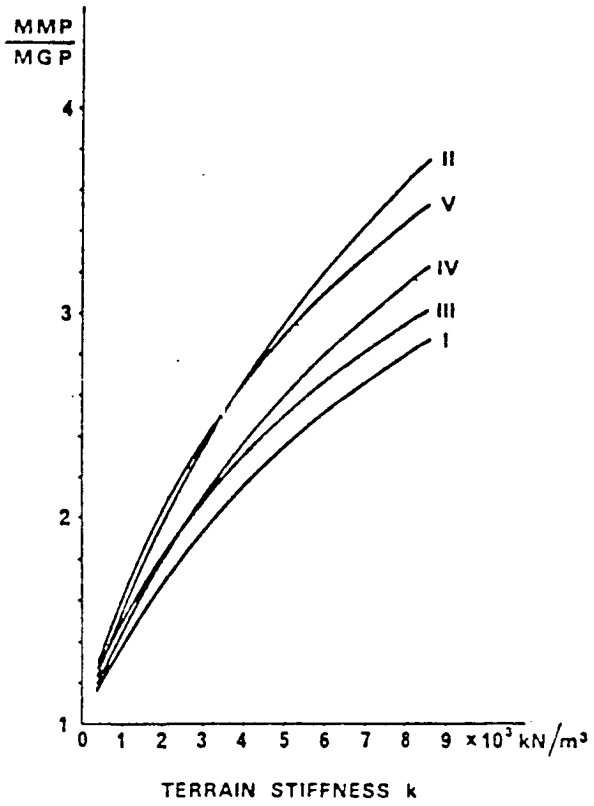

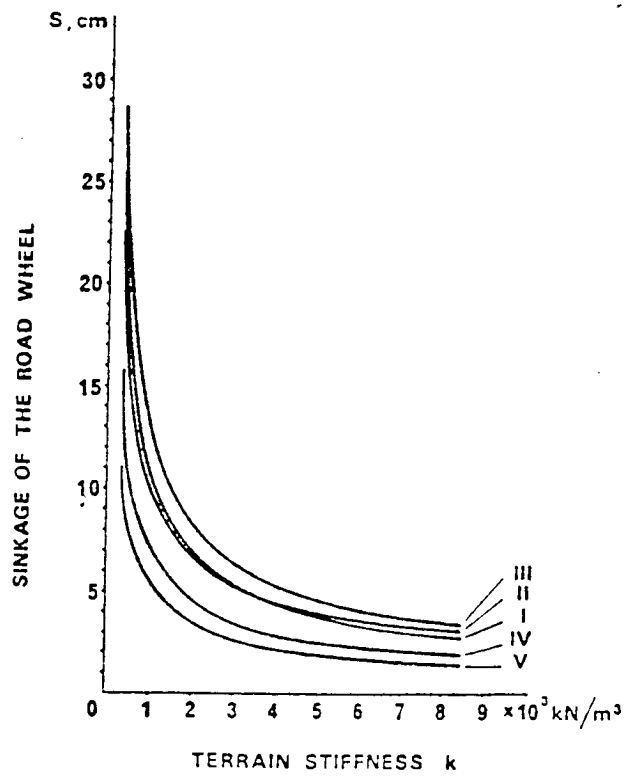

Fig. 1.3 Variation of mean maxium pressure, MMP/MGP, and sinkage of various track systems with terrain stiffness

are not necessarily realistic. Therefore, there is a need for the development of a prediction method that takes into account all major factors of vehicle-terrain interaction in a realistic manner. To satisfy this need, a comprehensive mathematical model has recently been developed by Wong, Garber and Preston-Thomas (1.18) and Wong and Preston-Thomas (1.19).

For many tracked vehicles, particularly those with high ratios of roadwheel spacing to track pitch designed for high speed operations, the normal pressure is usually concentrated under the roadwheels and is far from uniform. Consequently the track in contact with a deformable terrain deflects and has the form of a curve. The contact area is not a flat one as assumed in the methods developed previously. In the region beneath each roadwheel, the track follows the perimeter of the roadwheel, while the shape of the track segment between adjacent roadwheels is largely defined by terrain reaction, track tension, and roadwheel spacing. Since an element of the terrain under the track is subject to the repetitive loading of the consecutive roadwheels, the response of the terrain to repetitive loading has been taken into account in the latest analyses of track-terrain interaction (1.18). Equations governing the shape of the track in contact with the terrain are derived. A numerical procedure is developed to quantitively determine the track shape for a given vehicle over a particular terrain under specific operating conditions. From this and the pressure-sinkage relationship of the terrain, the normal pressure distribution under the track of a moving vehicle can be determined. Based on the predicted normal pressure distribution and on the analysis of the shearing action between the track and the terrain, the shear stress distribution under the track can be predicted. From the predicted normal and shear stress distributions on the track-terrain interface, the sinkage, motion resistance, tractive effort and drawbar pull of a tracked vehicle can be calculated as functions of track slip, thus defining the tractive performance of the vehicle.

The basic features of the mathematical model have been substantiated by means of full-scale tests over a variety of terrains, ranging from sandy terrain, through muskeg to snow-covered terrain. Thus, the model developed has provided a quantitative means with which the effects of vehicle design parameters, as well as terrain conditions, on the performance of tracked vehicles can be evaluated on a more consistent basis and in a more realistic manner than ever before. It is particularly useful for the evaluation of

competing designs and for the examination of the effects on performance of design modifications and changing operational environments (1.18, 1.19).

The model developed can play a significant role in the following:

A. optimization of tracked vehicle design in the development process;

B. selection of tracked vehicle candidates for a given mission and environment from a procurement point-of-view;

C. proper interpretation of vehicle test results and comparison of the performance of vehicle candidates in the evaluation process.

To provide easy access to practicing engineers and vehicle designers, the prediction procedures have been programmed on a microcomputer. It is believed that the computer simulation model developed by Wong et al. has a great potential for making a significant contribution to the rational development, design, evaluation, testing, selection and operation of tracked vehicles.

REFERENCES

1.1 J.Y. Wong, Terramechanics and Its Applications, Volumes I and II, Consiglio Nazionale Delle Ricerche, Istituto Per Le Macchine Movimento Terra E Veicoli Fuoristrada, Ferrara, Italy, March 1987.

1.2 M.G. Bekker, Theory of Land Locomotion, The University of Michigan Press, 1956.

1.3 M.G. Bekker, Introduction to Terrain-Vehicle Systems, The University of Michigan Press, 1969.

1.4 A.A. Rula and C.J. Nuttall, Jr., An Analysis of Ground Mobility Models (An AMOB), Technical Report M-71-4, U.S. Army Waterways Experiment Station, Vicksburg, Mississippi, July 1971.

1.5 D. Rowland, Tracked Vehicle Ground Pressure and Its Effect on Soft Ground Performance, Proceedings of the 4th International Conference of the International Society for Terrain-Vehicle Systems, Vol.I, Stockholm, Sweden, 1972.

1.6 D. Rowland, A Review of the Vehicle Design for Soft Ground Operation, Proceedings of the 5th International Conference of the International Society of Terrain-Vehicle Systems, Vol.1, Detroit, U.S.A., 1975.

1.7 D.R.P. Hettiaratchi and A.R. Reece, The Calculation of Passive Soil Resistance, Geotechnique, Vol.24, No.3, 1974.

1.8 J.Y. Wong and A.R. Reece, Soil Failure Beneath Rigid Wheels, Proceedings of the 2nd International Conference of the International Society for Terrain-Vehicle Systems, University of Toronto Press, 1966.

1.9 J.Y. Wong, Behaviour of Soil Beneath Rigid Wheels, Journal of Agricultural Engineering Research, Vol.12, No.4, 1967.

1.10 J.Y. Wong and A.R. Reece, Prediction of Rigid Wheel Performance Based on the Analysis of Soil-Wheel Stresses. Parts I and II, Journal of Terramechanics, Vol.4, Nos.1 and 2, 1967.

1.11 L.L. Karafiath and E.A. Nowatzki, Soil Mechanics for Off-Road Vehicle Engineering, Trans. Tech. Publications, 1978.

1.12 J.Y. Wong, Discussion on "Soil Mechanics for Off-Road Vehicle Engineering" by L.L. Karafiath and E.A. Nowatzki, Canadian Geotechnical Journal, Vol.16, No.3, 1979, also Journal of Terramechanics, Vol.16, No.4, 1979.

1.13 R.N. Yong and E.A. Fattah, Prediction of Wheel-Soil Interaction and Performance Using the Finite Element Method, Journal of Terramechanics, Vol.13, No.4, 1976.

1.14 J.Y. Wong, Discussion on "Prediction of Wheel-Soil Interaction and Performance Using the Finite Element Method", Journal of Terramechanics, Vol.14, No.4, 1977.

1.15 L.L. Karafiath, Finite Element Analysis of Ground Deformation Beneath Moving Track Loads, Proceedings of the 8th International Conference of the International Society for Terrain-Vehicle Systems, Vol.I, Cambridge, England, August 1984.

1.16 J.Y. Wong, Theory of Ground Vehicles, John Wiley, New York, 1978. (Russian Edition, Machinostroenie Publishing House, Moscow, 1982; Chinese Edition, Machinery Industry Publishing House, Peking, China, 1985).

1.17 M. Garber and J.Y. Wong, Prediction of Ground Pressure Distribution Under Tracked Vehicles, Parts I and II, Journal of Terramechanic, Vol.18, Nos.1 and 2, 1981.

1.18 J.Y. Wong, M. Garber and J. Preston-Thomas, Theoretical Prediction and Experimental Substantiation of the Ground Pressure Distribution and Tractive Performance of Tracked Vehicles, Proceedings of the Institution of Mechanical Engineers, Vol.198, Part D, No.15, 1984.

1.19 J.Y. Wong and J. Preston-Thomas, Parametric Analysis of Tracked Vehicle Performance Using An Advanced Computer Simulation Model, Proceedings of the Institution of Mechanical Engineers, Vol.200, Part D, No.2, 1986.

2. THEORETICAL BASIS FOR THE COMPUTER SIMULATION MODEL FOR TRACKED VEHICLE PERFORMANCE (NTVPM-85)

Based on the review given in the previous chapter, it is fair to say that most of the methods developed so far for predicting the performance of tracked vehicles are either of empirical nature or based upon assumptions that are not necessarily realistic. With a growing demand for improved mobility over a wider range of terrains, there is an increasing need for a comprehensive and yet realistic mathematical model to guide the development and design of tracked vehicles to meet specific requirements.

To be useful to the development and design engineers, as well as the procurement manager, a mathematical model for tracked vehicle performance should take into account all major vehicle design parameters and terrain characteristics. A model that satisfies these requirements has recently been developed by Wong et al. (2.1, 2.2). It takes into account all major design parameters of the vehicle, including track system configuration, number of roadwheels, dimensions of roadwheels, roadwheel spacing, track dimensions, initial track tension, track longitudinal elasticity, suspension heave stiffness, location of the centre of gravity, vehicle belly (hull) shape, and sprocket, idler and supporting roller arrangements. Terrain characteristics, such as the pressure-sinkage relationship, shearing behaviour and the response to repetitive loading, are also taken into consideration. The model can be used to predict the normal and shear stress distributions on the track-terrain interface, and the external motion resistance, tractive effort and drawbar pull of the vehicle as functions of track slip. The basic features of the model have been validated by means of full-scale tests made with an instrumented vehicle on three types of terrain, namely sandy terrain, muskeg and snow.

The model is particularly suited for the evaluation of competing designs and for the examination of the effects on performance of design modifications and changing operational environment.

The initial development of the model was sponsored by the Canadian Department of National Defence, during the period between March 1980 and June 1984. Subsequent developments of the model NTVPM-85, which incorporates the latest features, have been performed under the auspices of Vehicle Systems Development Corporation, Nepean, Ontario, Canada.

The basic approach to the development of the model is outlined below.

2.1 Terrain Input for the Simulation Model

To develop a realistic model for tracked vehicle performance, the mechanical behaviour of the terrain, which forms an integral part of the input, should be measured under loading conditions similar to those exerted by a tracked vehicle. Among the various terrain measuring techniques currently available, the bevameter technique pioneered by Bekker (2.3) appears to provide a close approximation to the loading conditions of a tracked vehicle. Accordingly, in the development of the simulation model, terrain data measured using a bevameter was used. The bevameter is designed to perform two different types of test. One is the pressure-sinkage test and the other is the shear test. To reduce the uncertainty in extrapolating terrain data measured by the bevameter to the prediction of the performance of full-size vehicles, the size of the test piece used in the pressure-sinkage test should be comparable to that of the contact area of a track link. Also, the shear ring used to perform the shear test should be made as large as practicable. Since an element of the terrain under a moving track is subject to the repetitive loading of consecutive roadwheels, the measurement of the response of the terrain to repetitive loading should be included to provide data for predicting the multipass performance of the vehicle running gear. Also, additional sinkage may be induced by the slip of the track, and thus the slip-sinkage relationship should be monitored during the shear test. These characteristics of the terrain are used as input to a detailed analysis of the mechanics of track-terrain interaction, which in turn forms the basis of the simulation model for tracked vehicle performance (2.1, 2.2).

A. Responses of Terrain to Normal Load and to Repetitive Loading

When a tracked vehicle is travelling over an unprepared terrain, an element of the terrain under the track is first subject to the normal load applied by the leading roadwheel. When the leading roadwheel has passed, the load on the terrain element is reduced. Load is reapplied as the second roadwheel rolls over it. A terrain element under the track is thus subject to the repetitive loading of consecutive roadwheels. The loading-unloading-reloading cycle

continues until the rear roadwheel of the vehicle has passed over it. To predict the normal pressure distribution under a moving tracked vehicle, the pressure-sinkage relationship of the terrain as well as its response to repetitive loading must, therefore, be measured.

The response to normal load of a variety of terrains, including sandy terrain, snow-covered terrain and organic terrain (muskeg), has been measured using a vehicle mounted bevameter, together with a portable automatic data processing system, as shown in Figs.2.1 and 2.2, respectively (2.4, 2.5, 2.6, 2.7, 2.8).

Figure 2.3 shows the pressure-sinkage relationship for a sandy terrain, obtained using a circular plate of 5 cm in radius. It can be seen that the pressure initially increases with sinkage along curve OA. However, when the load applied to the terrain by the plate is reduced at A, the pressure-sinkage relationship follows line AB. The inclination of the unloading line AB indicates that a small amount of elastic rebound occurs during unloading. When the load is reapplied at B, the pressure-sinkage relationship follows, more or less, the same path as that during unloading. When the reapplied load exceeds that at which the preceding unloading-reloading cycle begins (i.e., point A), additional sinkage results. With the further increase of load beyond that corresponding to A, the pressure-sinkage relation follows the original pressure-sinkage curve OAC. The characteristics of the subsequent unloading-reloading cycles, such as CD, are quite similar to those of the first one (i.e., AB).

Based on experimental observations described above, the response of the sandy terrain to normal load may be idealized as follows:

a. when the terrain is subject to continuously increasing load without interruption the pressure-sinkage relationship, such as curve OAC shown in Fig.2.3, may be described by the following equation proposed by Bekker

$$p = \left(\frac{k_c}{b} + k_\phi\right) z^n = k z^n \qquad (2.1)$$

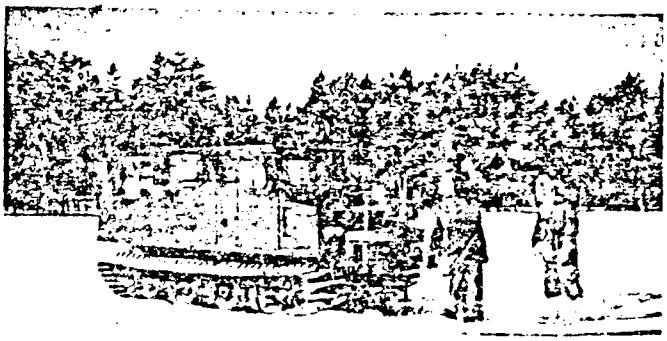

Fig. 2.1(a) Vehicle mounted bevameter in operation

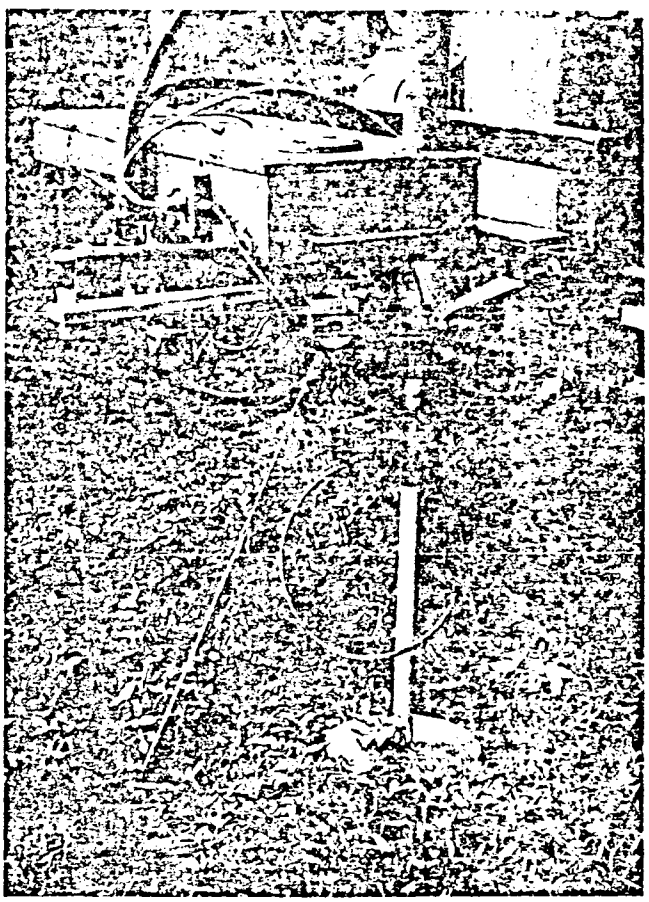

Fig. 2.1(b) Pressure-sinkage tests in muskeg

Fig. 2.1(c) Shear tests in snow

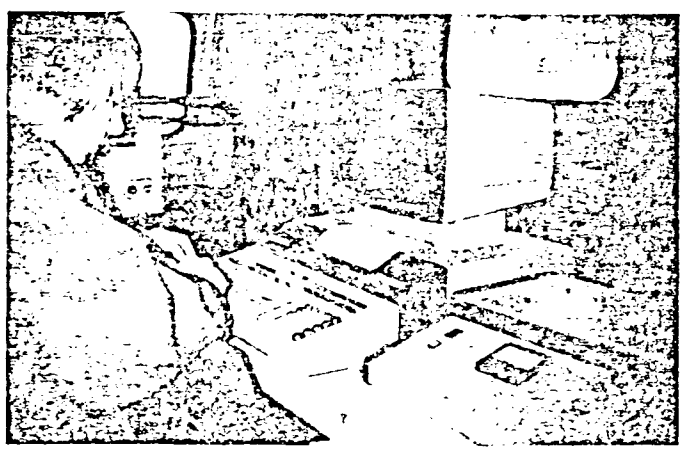

Fig. 2.2 Automatic data processing system developed at Carleton in operation

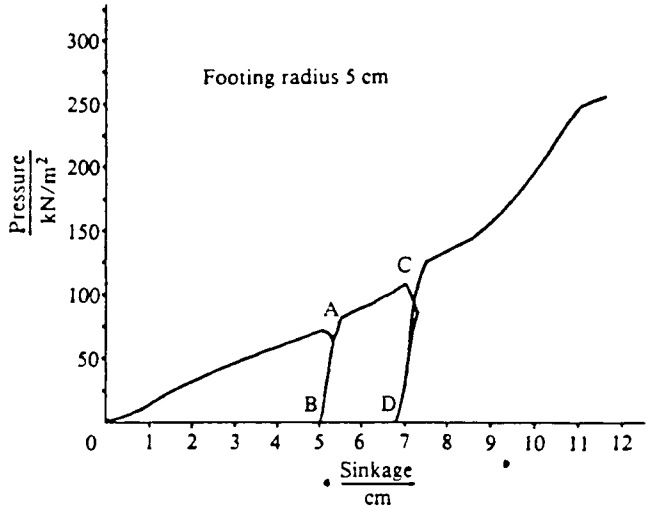

Repetitive loading characteristics of a sand

Fig. 2.3

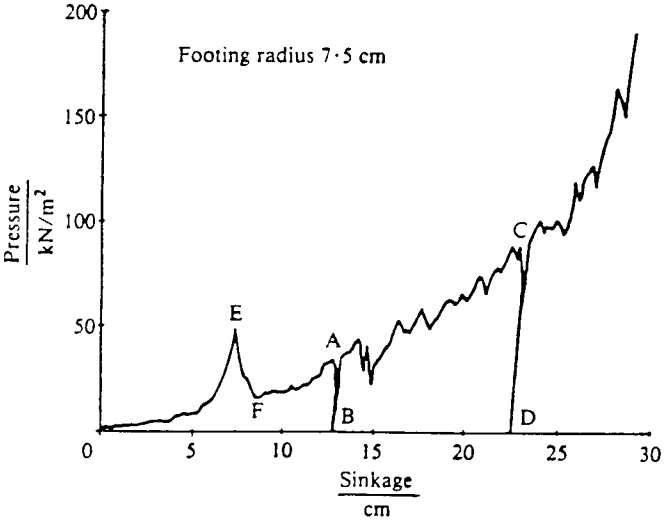

Repetitive loading characteristics of a snow

Fig. 2.4

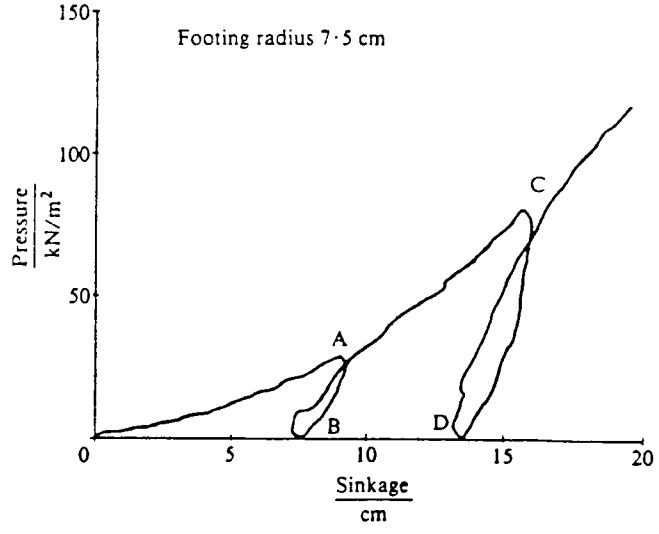

Repetitive loading characteristics of a muskeg

Fig. 2.5

where p is pressure; z is sinkage; k, k_c and k_ϕ are pressure-sinkage parameters; b is the smaller dimension of the contact area; and n is the exponent of terrain deformation.

b. the pressure-sinkage relationship during both unloading and reloading, such as AB and BA shown in Fig.2.3, may be described by

$$\begin{aligned} p &= \left(\frac{k_c}{b} + k_\phi\right) z_u^n - k_u(z_u - z) \\ &= k z_u^n - k_u(z_u - z) \\ &= p_u - k_u(z_u - z) \end{aligned} \tag{2.2}$$

where p_u and z_u are the pressure and sinkage, respectively, when unloading begins; and k_u is the pressure-sinkage parameter representing the average slope of the unloading-reloading line AB.

It is found that k_u is a function of z_u and their relationship, as a first approximation, may be described by

$$k_u = k_0 + A_u z_u \tag{2.3}$$

where k_0 and A_u are parameters, the values of which can be derived from experimental data.

Table 2.1 shows the representative values of the pressure-sinkage and repetitive loading parameters for a sandy terrain (referred to as LETE Sand).

Figure 2.4 shows the pressure-sinkage relationship for a snow cover 33 cm deep, obtained using a plate with a radius of 7.5 cm. It contained a crust approximately 4 cm thick at a depth of 11 cm from the snow surface. The spike at E on the pressure-sinkage curve represents the pressure causing the breaking of the crust, which can be predicted using a method described in reference (2.7). Under continuously increasing load, the pressure-sinkage curve approached an asymptote when the penetration of the plate approached the crust or the frozen ground at the base of the snow cover. When the snow cover was subject to continuously increasing load, the pressure-sinkage relationship

Table 2.1

Values of the pressure–sinkage and repetitive loading parameters for a sandy terrain (LETE sand)

k_c / kN/m^{n+1}	k_ϕ / kN/m^{n+2}	n	k_0 / kN/m^3	A_u / kN/m^2
102	5301	0.793	0	503 000

Table 2.2

Values of the pressure–sinkage and repetitive loading parameters for two snow covers

Snow type	Petawawa snow A		Petawawa snow B	
Section of the pressure–sinkage curve	Before failure of the crust	After failure of the crust	Before failure of the crust	After failure of the crust
K_{p1} (kPA)	3.2	52.7	16.3	10.8
K_{p2} (kPa/m)	234	−48	0	0
K_{z1} (cm)	0.9	14.2	24.8	41.0
K_{z2} (cm^2)	39.7	67.3	0	0
k_0 (kN/m^3)	0		0	
A_u (kN/m^4)	109 600		25 923	

Table 2.3

Values of the pressure–sinkage and repetitive loading parameters for two types of muskeg

Muskeg type	Petawawa muskeg A	Petawawa muskeg B
k_m (kN/m^3)	290	762
m_m (kN/m^3)	51	97
k_0 (kN/m^3)	123	147
A_u (kN/m^3)	23 540	29 700

The values shown in the table were obtained using circular plates

before and after the breaking of the crust, such as OE and FAC, may be described by an exponential function of the following form (2.7)

$$z = z_w\left[1 - \exp\left(\frac{-p}{p_w}\right)\right] \tag{2.4}$$

where p_w and z_w are parameters, the values of which can be derived from experimental data. z_w defines the asymptote of the pressure-sinkage curve.

From experimental evidence, it is found that the size of the contact area has an effect on the pressure-sinkage relationship of the snow cover tested. As a first approximation, the following relationships are proposed

$$p_w = K_{p1} + bK_{p2} \tag{2.5}$$

$$z_w = K_{z1} + \frac{K_{z2}}{b} \tag{2.6}$$

where b is the smaller dimension of the contact area; K_{p1}, K_{p2}, K_{z1} and K_{z2} are parameters, the values of which can be derived from two sets of experimental data obtained using different plate sizes.

The response of the snow cover to repetitive loading, such as AB and CD shown in Fig.2.4, is quite similar to that for the sandy terrain shown in Fig.2.3. Therefore, Equations (2.2) and (2.3) can equally be applied to describing the pressure-sinkage relationship of the snow cover during the unloading-reloading cycle.

Table 2.2 shows the representative values of the pressure-sinkage and repetitive loading parameters for two snow covers with a significant crust (referred to as Petawawa Snow A and B).

The pressure-sinkage relationship for an organic terrain (muskeg) is shown in Fig.2.5. Under continuously increasing load, the pressure-sinkage relationship prior to the failure of the muskeg mat, such as curve OAC, can be described by (2.6)

$$p = k_m z + \frac{2m_m}{b} z^2 \tag{2.7}$$

where k_m and m_m are parameters, the values of which can be derived from experimental data, and b is the smaller dimension of the contact area.

It can be seen from Fig.2.5 that during unloading and reloading, the pressure-sinkage relationship follows different paths. This shows that the muskeg exhibits a certain amount of hysteresis. However, as a first approximation, the pressure-sinkage relationship during unloading as well as reloading can be linearized and represented by Equation (2.2). It is found that for the types of muskeg tested, Equation (2.3) also holds.

Table 2.3 shows the values of the pressure-sinkage and repetitive loading parameters for two types of muskeg (referred to as Petawawa Muskeg A and B).

The pressure-sinkage relationship and the response to repetitive loading of the terrain constitute the basic terrain inputs to the simulation model for predicting the normal pressure distribution under a moving tracked vehicle.

B. Shearing Behaviour of Terrain

To predict the shear stress distribution under a track, the shear stress-displacement relationship of the terrain must be known. This can be obtained using a bevameter with a shear ring. During the test, the torque and angular displacement of the shear ring are measured, from which the shear stress-displacement relationship can be determined (2.4, 2.5, 2.8).

Based on the results of a large number of shear tests on a variety of natural terrains, it is found that there are three basic types of shear stress-displacement relationship (2.8):

a. The first type of shear stress-displacement curve does not display a "hump" of maximum shear stress but rather the shear stress increases with shear displacement and approaches a constant value. This type of characteristic is observed in the internal shearing of a dry sand and a peat, and in rubber-sand, rubber-snow, rubber-peat and rubber-muskeg mat shearing, as shown in Fig.2.6. This type of shear stress-displacement relationship may be described by

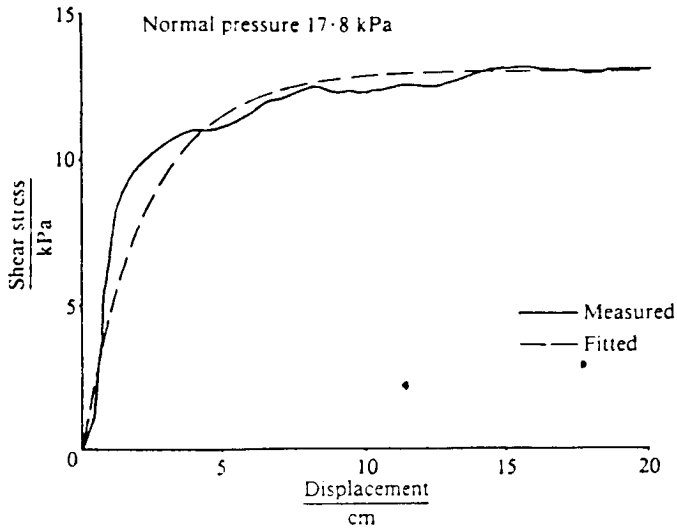

Shear stress–displacement relationship of a sand

Fig. 2.6

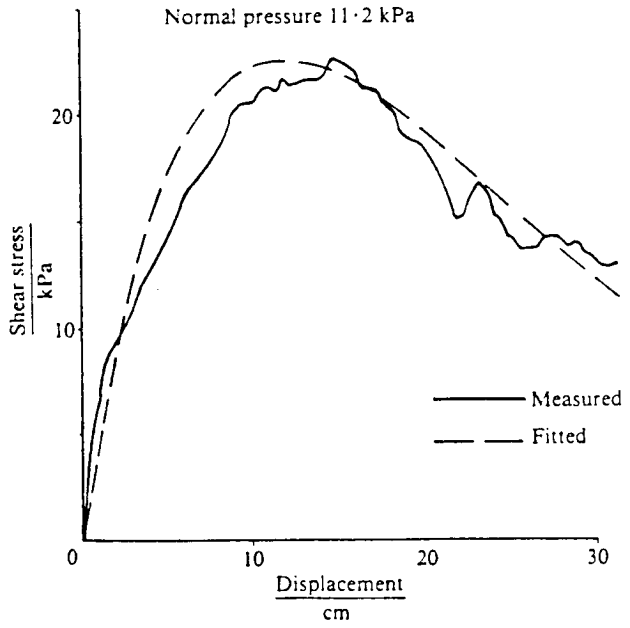

Shear stress–displacement relationship of a muskeg mat

Fig. 2.7

$$\frac{s}{s_{max}} = 1 - \exp\left(\frac{-j}{K}\right) \tag{2.8}$$

where s is the shear stress, s_{max} is the maximum shear stress, j is the shear displacement, and K is a parameter usually referred to as the shear deformation modulus.

b. The second type of shear curve exhibits a "hump" of maximum shear stress and then the shear stress decreases continually with the increase of shear displacement. This type of curve is observed in the internal shearing of a muskeg mat, as shown in Fig.2.7 and may be described by

$$\frac{s}{s_{max}} = \left(\frac{j}{K_w}\right) \exp\left(1 - \frac{j}{K_w}\right) \tag{2.9}$$

where K_W is a parameter which represents the shear displacement where the maximum shear stress occurs.

c. The third type of shear curve displays a "hump" of maximum shear stress and then the shear stress decreases with the increase of shear displacement to a more or less constant value of residual stress. This kind of curve is observed in certain types of loam and snow, as shown in Fig.2.8, and may be described by

$$\frac{s}{s_{max}} = K_r\left[1 + \left(\frac{1}{K_r[1 - \exp(-1)]} - 1\right) \times \exp\left(1 - \frac{j}{K_w}\right)\right]\left[1 - \exp\left(-\frac{j}{K_w}\right)\right] \tag{2.10}$$

where K_r is a parameter which represents the ratio of the residual shear stress to the maximum shear stress, and the parameter K_W is the same as that in Equation (2.9).

For many types of terrain, the relationship between the maximum shear stress s_{max} and the normal pressure p may be described by the Mohr-Coulomb equation

$$s_{max} = c + p \tan \phi \tag{2.11}$$

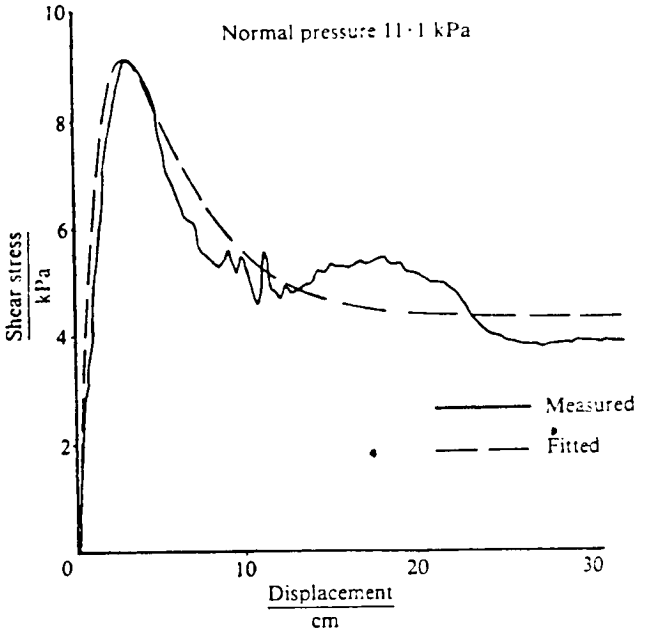

Shear stress–displacement relationship of a snow

Fig. 2.8

Table 2.4

Shear strength parameters of various types of terrain

Terrain type	Type of shearing	Cohesion (adhesion) kPa	Angle of shearing resistance degrees	$\frac{K}{cm}$	K_r	$\frac{K_w}{cm}$
LETE sand	Internal	1.3	31.1	1.2	—	—
	Rubber–sand	0.7	27.5	1.0	—	—
Petawawa snow A and B	Internal	0.4	24.0	—	0.655	2.2
	Rubber–snow	0.12	16.4	0.4	—	—
Petawawa muskeg A	Peat (internal)	2.8	39.4	3.1	—	—
Petawawa muskeg B	Peat (internal)	2.6	39.2	3.1	—	—

where c is the cohesion (or adhesion) and ϕ is the angle of shearing resistance. The values of the shear strength parameters of various types of terrain are given in Table 2.4.

For certain kinds of terrain, the shear strength is affected by the shear rate. In the prediction of shear stress on the track-terrain interface, the shear strength of the terrain at a shear rate equivalent to the slip velocity of the track should be used.

Traditionally, the prediction of shear stress distribution under a track is based on the assumption that the normal pressure is uniformly distributed on the track-terrain interface. Consequently, the shear stress at a particular point under the track is determined by the shear displacement at that point.

As described previously, when a tracked vehicle is travelling over an unprepared terrain, an element of the terrain under the track is subject to the repetitive normal load applied by the consecutive roadwheels, and thus the normal pressure is not uniformly distributed. Consequently, for a frictional terrain this element will also be subject to repetitive shear loading. To predict the shear stress distribution on the track-terrain interface more realistically, the response to repetitive shear loading of the terrain should be known. Figure 2.9 shows the response of a frictional terrain (a dry sand) to repetitive shear loading under a constant normal load. It indicates that when the shear loading is reduced from B to zero and is then reapplied to C, the shear stress-displacement relationship during reshearing, such as CDE, is similar to that when the terrain is being sheared in its virgin state, such as OAB. This means that when reshearing takes place after unloading, the shear stress does not instantaneously reach its maximum value for a given normal pressure. Rather, a certain amount of shear displacement must take place before the maximum shear stress can be developed, similar to that when the frictional medium is being sheared in its virgin state.

Results of an investigation into the shearing force developed beneath a shear plate under a cyclic normal load lead to similar conclusions (2.1). Figure 2.10 shows the variation of the shearing force beneath a rectangular shear plate on a dry sand subject to a vertical harmonic load with a frequency of 10.3 Hz. It indicates that during the loading portion of each cycle, the

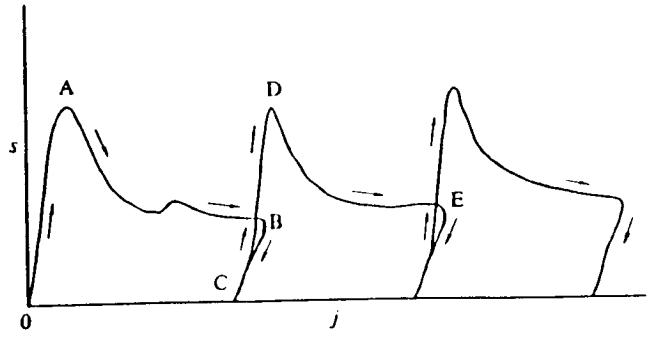

Fig. 2.9 Response of a frictional terrain to repetitive shear load

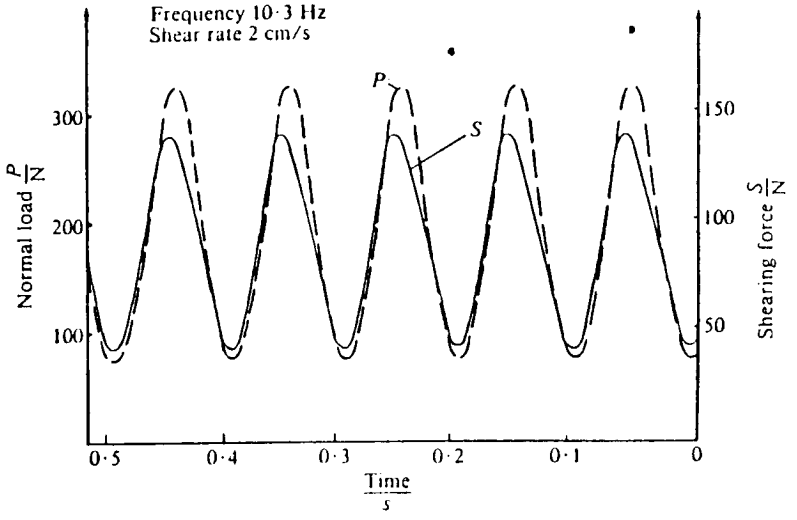

Fig. 2.10 Shearing force developed under a shear plate subject to cyclic loading on a dry sand

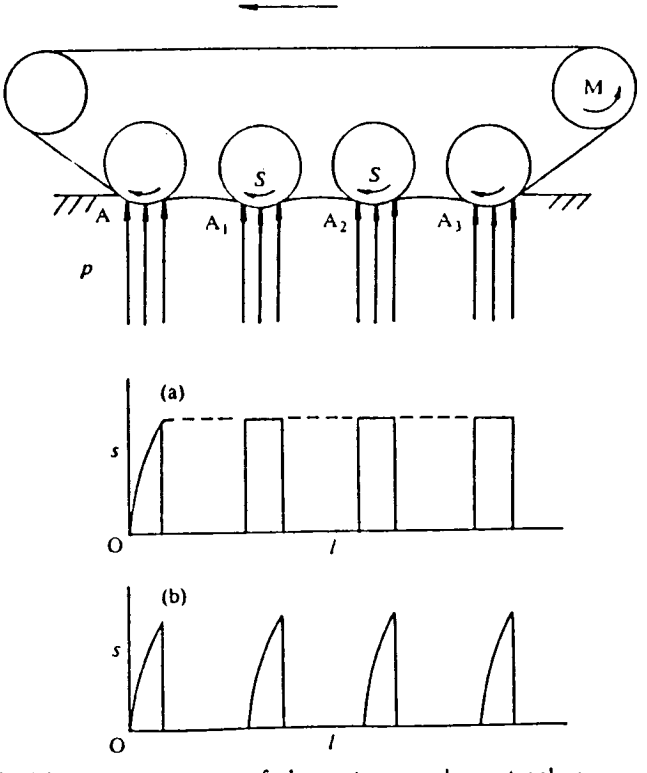

Fig. 2.11 Development of shear stress under a track over a frictional terrain predicted by
(a) the conventional method
(b) the improved method taking into account the response of terrain to repetitive shear loading

shearing force does not reach its maximum value S_{max} instantaneously ($S_{max} = P \tan \phi$, where P is the value of the instantaneous normal load and ϕ is the angle of shearing resistance). This is demonstrated by the fact that the slope of the normal load curve is steeper than that of the shearing force curve. During the unloading portion of the cycle, however, the shearing force decreases in proportion to the instantaneous value of the normal load.

The response of the terrain under repetitive shear loading and its behaviour under cyclic normal load described above have a significant effect on the development of shear stress under the track. Figure 2.11 illustrates how the development of the shear stress may be modified if the response to repetitive shear loading of a frictional terrain is taken into account for an idealized case. It should be pointed out that when the repetitive shearing characteristics of the terrain are taken into consideration, the predicted total tractive effort of the vehicle may be considerably lower than when they are not taken into account, particularly at low track slips, as can be noted from Fig.2.11.

It should be mentioned that the sandy terrain, two muskegs and two snow-covered terrains tested exhibit predominant frictional properties. Consequently, the behaviour of the terrain under repetitive shear loading described above is applicable to these terrains.

2.2 Approach to the Prediction of the Normal Pressure Distribution Under A Moving Track

When a tracked vehicle rests on a hard surface the tracks lie flat on the ground. In contrast, when the vehicle travels over a deformable terrain the normal load applied through the track system causes the terrain to deform. The track sections between the roadwheels take up load, and as a result they deflect and have the form of a curve. The actual length of the track in contact with the terrain between the front and rear roadwheels increases in comparison with that when the track rests on firm ground. This causes a reduction in the sag of the top run of the track and a change in track tension. Furthermore, the passage of each consecutive roadwheel will usually cause additional sinkage, and the vehicle may assume a noise-up attitude.

When the terrain characteristics are known, the prediction of the normal pressure distribution is reduced to the determination of the shape of the deflected track in contact with the terrain. To achieve this, the mechanics of track-terrain interaction has to be examined.

In the development of the analytical method for predicting the normal pressure distribution, the following assumptions are made (2.1, 2.2):

A. The track is modelled as a flexible belt. This assumption is reasonable, particularly for the rubber belt track and for tracks with relatively short pitch. The elongation of the track under tension has been taken into account in the current version of the simulation model, NTVPM-85.

B. In determining the sinkages of the track under the roadwheels, the effects of the independent suspension of the roadwheels are neglected in NTVPM-85. This means that the sinkage of the first roadwheel together with the attitude (inclination) of the vehicle body completely defines the sinkages of the subsequent roadwheels.

Based on these assumptions, the mechanics of track-terrain interaction is analyzed, and a set of equations for the equilibrium of the forces and moments acting on the track system, and for the evaluation of the overall track length are derived. They establish the relationship between the shape of the deflected track in contact with the terrain and vehicle design parameters and terrain characteristics. The solution of this set of equations defines the sinkage of the leading roadwheel, the inclination of the vehicle, the track tension and the track shape. From these, the normal pressure distribution under a moving tracked vehicle can be determined.

It should be mentioned that a new version of the simulation model, NTVPM-86, in which the characteristics of the independent suspension for the roadwheels have been taken into consideration, is currently under development.

2.3 The Shape of the Deflected Track

The schematic of a track-roadwheel system travelling on a deformable terrain under steady-state conditions is shown in Fig.2.12. The deflected track in contact with the terrain may be divided into two sections: one in contact with both the roadwheel and the terrain (such as segments AC and FH), and the other in contact with the terrain only (such as segment CF). The shape of the track segment in contact with the roadwheel, such as AC, is defined by the shape of the roadwheel, whereas the shape of the track segment in contact with the terrain only, such as CF, is determined by the results of the interaction between the track and the terrain.

Along segment AB, the pressure exerted on the terrain increases from A to B. From B to D the pressure decreases corresponding to the unloading portion of the repetitive loading cycle of the terrain shown in Figs. 2.3, 2.4 and 2.5. Along segment DE, the pressure increases again, corresponding to the reloading portion of the repetitive loading cycle shown in Figs.2.3, 2.4 and 2.5. Beyond point E, which is at the same level as point B, the sinkage is higher than that at B. As a result the pressure increases and the sinkage of roadwheel i+1 will be greater than that of roadwheel i. Beyond point G the pressure exerted on the terrain decreases again, and another unloading-reloading cycle begins.

To determine the shape of the track segment that is in contact with the terrain only, let us consider the equilibrium of an element of the track as shown in Fig.2.13.

In the analysis, the pressure exerted on the track by the terrain is assumed to be normal to the track-terrain interface, and equal to that acting on a plate at the same sinkage as discussed in Section 2.1.

Considering the equilibrium of the track element along the normal and tangential directions, one obtains

$$p\,dl - (T + dT)\sin d\alpha = 0 \qquad (2.12)$$

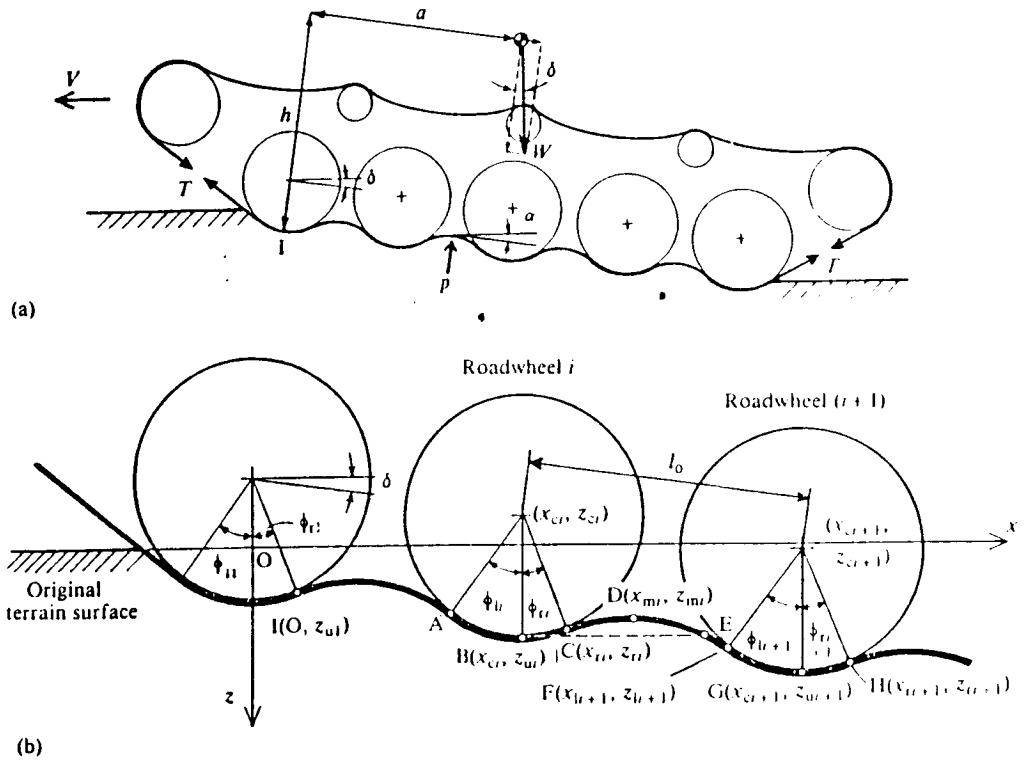

Geometry of a track system in contact with a deformable terrain

Fig. 2.12

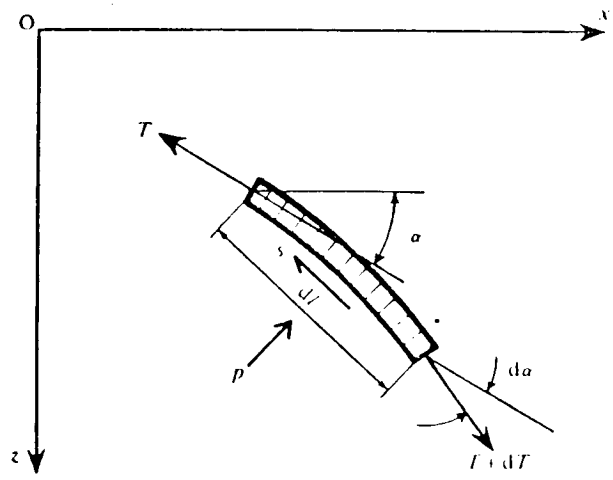

Forces acting on an element of the track

Fig. 2.13

$$T + s\,dl - (T + dT)\cos d\alpha = 0 \tag{2.13}$$

where T is the tension in the track per unit width, p is the normal pressure exerted by the terrain, and s is the shear stress acting on the track element. Other parameters are illustrated in Fig.2.13. If the vehicle is operating at very low slip and the shear stress s is not significant, its effects on normal pressure distribution can be neglected. In this section the prediction of the normal pressure distribution under a track in the absence of shear stresses will be discussed. At higher slip, however, the effects of the shear stress will be significant and should be included in the prediction of normal pressure distribution. This will be discussed later in Section 2.5.

If the shear stress is neglected, and $d\alpha$ is small, which implies $\cos d\alpha = 1$ and $\sin d\alpha = d\alpha$, Equation (2.12) may be rewritten as

$dT = 0$ and T = constant

and Equation (2.13) becomes

$$T = p\frac{dl}{d\alpha} = pR \tag{2.14}$$

where R is the radius of curvature of the track and is expressed by

$$R = \left[1 + \left(\frac{dz}{dx}\right)^2\right]^{3/2} \Big/ \frac{d^2z}{dx^2} \tag{2.15}$$

Substituting Equation (2.15) into Equation (2.14), one obtains

$$T\frac{d^2z}{dx^2} - p\left[1 + \left(\frac{dz}{dx}\right)^2\right]^{3/2} = 0 \tag{2.16}$$

This is the basic question that governs the shape of the track segment between two roadwheels in contact with the terrain only, such as CF shown in Fig.2.12. Dependent upon whether the terrain is being loaded, unloaded or reloaded, the pressure-sinkage relationship will take different forms as described in Section 2.1.

When the terrain under the track is subject to continuously increasing load, such as that under segment EF shown in Fig.2.12, (equivalent to loading along the path OA or AC shown in Figs.2.3, 2.4 and 2.5) the pressure-sinkage relationship may be described by Equations (2.1), (2.4) or (2.7), dependent on the type of terrain.

In the following analysis of track-terrain interaction, the sandy terrain described in Section 2.1 is used as an example to illustrate the procedures involved. Over the sandy terrain, the pressure-sinkage relationship under continuously increasing load is described by Equation (2.1) and therefore Equation (2.16) can be rewritten as

$$T\frac{d^2z}{dx^2} - kz^n\left[1+\left(\frac{dz}{dx}\right)^2\right]^{3/2} = 0 \tag{2.17}$$

Setting $\frac{dz}{dx} = u$, the above equation becomes a first-order differential equation

$$T\frac{u\,du}{(1+u^2)^{3/2}} = kz^n\,dz \tag{2.18}$$

Integrating the above equation, one obtains

$$\frac{-T}{\sqrt{\left[1+\left(\frac{dz}{dx}\right)^2\right]}} = \frac{kz^{n+1}}{(n+1)} + C_1 \tag{2.19}$$

where C_1 is an integration constant. Equation (2.19) may be rewritten as

$$dx = dz\Big/\left\{\sqrt{\left[\left(\frac{-T}{kz^{n+1}/(n+1)+C_1}\right)^2 - 1\right]}\right\} \tag{2.20}$$

Integrating the above equation, one obtains

$$x = \int dz\Big/\left\{\sqrt{\left(\frac{-T}{kz^{n+1}/(n+1)+C_1}\right)^2 - 1\right]}\right\} + C_2 \tag{2.21}$$

where C_2 is an integration constant.

Equation (2.21) defines the shape of track segment EF, shown in Fig.2.12, over a sandy terrain. For other types of terrain a similar approach can be followed to obtain the equation that governs the shape of the track segment.

After a roadwheel has passed, the pressure exerted on the terrain along track segment CD, shown in Fig.2.12, is gradually reduced. As described in Section 2.1, during unloading the pressure-sinkage relationship is expressed by Equation (2.2) and the shape of track segment CD is, therefore, governed by

$$T\frac{d^2z}{dx^2} - k_u(z - z_a)\left[1 + \left(\frac{dz}{dx}\right)^2\right]^{3/2} = 0 \qquad (2.22)$$

where $z_a = z_u - kz_u^n/k_u$ and z_u is the sinkage of the preceding roadwheel, such as that at point B in Fig.2.12.

Equation (2.22) can be integrated twice to obtain the following equation governing the shape of track segment CD,

$$x = \int dz \Big/ \left\{\sqrt{\left[\left(\frac{-T}{k_u z(z/2 - z_a) + C_1}\right)^2 - 1\right]}\right\} + C_2 \qquad (2.23)$$

Under segment DE of the track shown in Fig.2.12, the terrain is being reloaded during which the pressure-sinkage relationship is described by Equation (2.23). Therefore, Equation (2.23) also defines the shape of track segment DE. As the track is modelled as a flexible belt, the transition from BC to CD and from DF to FG, shown in Fig.2.12, should be smooth. This means that track segment CD should be tangent to roadwheel i at C. Similarly, track segment DF should also be tangent to roadwheel i+1 at F.

At point C, defined by coordinates x_{ri} and z_{ri}, the condition that should be met to ensure smooth transition may be expressed by

$$\left.\frac{dz}{dx}\right|_{x = x_{ri}} = -\tan\phi_{ri} \quad (i = 1, 2, \ldots, N - 1) \qquad (2.24)$$

where N is the number of roadwheels on a track.

Making use of Equation (2.23), one may rewrite the above equation as follows:

$$\left[\frac{-T}{k_u z_{ri}(z_{ri}/2 - z_{ai}) + C_{1i}}\right]^2 - 1 = \tan^2 \phi_{ri} \qquad (2.25)$$

$$(i = 1, 2, \ldots, N-1)$$

or

$$k_u z_{ri}\left(\frac{z_{ri}}{2} - z_{ai}\right) + C_{1i} = -T \cos \phi_{ri} \qquad (2.26)$$

$$(i = 1, 2, \ldots, N-1) \ .$$

where $z_{ai} = z_{ui} - kz_{ui}^{n}/k_u$ and z_{ui} is the sinkage of point B.

From Equation (2.26), C_{1i}, which is the integration constant for roadwheel i, can be defined in terms of ϕ_{ri};

$$C_{1i} = -T \cos \phi_{ri} - k_u z_{ri}\left(\frac{z_{ri}}{2} - z_{ai}\right) \qquad (2.27)$$

It should be noted that $z_{ri} = z_{ui} - R(1-\cos\phi_{ri})$, where R is the radius of the roadwheel.

Point F in Fig.2.12, where track segment DF should be tangent to roadwheel i+1, may be below or above the level of point B of roadwheel i (i.e., z_{ui}). If point F is level with or above point B (i.e., $z_{\ell i+1} \leq z_{ui}$), then under the entire segment DF the terrain is being reloaded (corresponding to the reloading path BA in Figs. 2.3, 2.4 and 2.5). Accordingly, the slope of segment DF can be derived from differentiating Equation (2.23) with integration constant C_{1i} defined by Equation (2.27);

$$\frac{dz}{dx} = \sqrt{\left[\left(\frac{-T}{\frac{1}{2}k_u(z - z_{ri})(z - 2z_{ai} + z_{ri}) - T \cos \phi_{ri}}\right)^2 - 1\right]} \qquad (2.28)$$

The slope of the tangent to roadwheel i+1 can be defined by

$$\frac{dz}{dx} = \frac{(x_{ci+1} - x)}{(z - z_{ci+1})} = \frac{\sqrt{[R^2 - (z - z_{ci+1})^2]}}{(z - z_{ci+1})} \qquad (2.29)$$

where x_{ci+1} and z_{ci+1} are the coordinates of the center of roadwheel i+1.

At point F, the slope of track segment DF should match that of the tangent to roadwheel i+1. As a consequence the sinkage $z_{\ell i+1}$ at point F is defined by setting Equation (2.28) equal to Equation (2.29) and $z=z_{\ell i+1}$.

$$z_{\ell i+1} = z_{ai} - \frac{T}{Rk_u} + \sqrt{\left\{(z_{ai} - z_{ri})^2 + \frac{2T}{Rk_u} \times \left[\frac{T}{2Rk_u} - z_{ai} + R\cos\phi_{ri} + z_{ci+1}\right]\right\}} \tag{2.30}$$

Equation (2.30) defines $z_{\ell i+1}$ as a function of ϕ_{ri}, T, and other parameters. For a given set of parameters, if the value of $z_{\ell i+1}$ is found to be greater than the sinkage z_{ui} of roadwheel i, then point F will be below point B.

When point F is below point B (i.e., $z_{\ell i+1} > z_{ui}$); then under segment DE the terrain is being reloaded (corresponding to the reloading path BA in Figs. 2.3, 2.4 and 2.5), whereas under segment EF the pressure applied to the terrain exceeds the maximum value applied to the preceding roadwheel at B and as a result additional sinkage occurs (corresponding to the loading path AC in Figs. 2.3, 2.4 and 2.5). Consequently, the shape of track segment DE is governed by Equation (2.23) whereas the shape of segment EF is governed by Equation (2.21). Since the track is modelled as a flexible belt, the transition from segment DE to segment EF must also be smooth. This means that both segments should have the same slope at E. The slope of DE at E (i.e., $z=z_{ui}$) can be determined from Equation (2.28) by setting $z=z_{ui}$, and is expressed by

$$\left.\frac{dz}{dx}\right|_{z=z_{ui}} = \sqrt{\left\{\left(\frac{-T}{\frac{1}{2}k_u(z_{ui} - z_{ri})(z_{ui} - 2z_{ai} + z_{ri}) - T\cos\phi_{ri}}\right)^2 - 1\right\}} = S_E \tag{2.31}$$

The slope of track segment EF is governed by Equation (2.20). The integration constant C_1 in Equation (2.20) can be obtained by setting the slope of track segment EF at E equal to that defined by Equation (2.31).

$$C_1 = -\left\{T + [\sqrt{(S_E^2 + 1)}]\frac{kz_{ui}^{n+1}}{n+1}\right\} \Big/ \sqrt{(S_E^2 + 1)} \tag{2.32}$$

The general expression for the slope of segment EF is therefore given by

$$\frac{dz}{dx} = \sqrt{\left[\left\{ -T \Big/ \left[\frac{k}{n+1}(z^{n+1} - z_{ui}^{n+1}) - \frac{T}{\sqrt{(S_E^2+1)}} \right] \right\}^2 - 1 \right]} \tag{2.33}$$

Track segment EF shoud be tangent to roadwheel i+1 at F. By setting Equation (2.29) equal to Equation (2.33) the sinkage, $z_{\ell i+1}$, at F can be defined by

$$\frac{kR}{n+1}(z_{li+1}^{n+1} - z_{ui}^{n+1}) - T\left[\frac{R}{\sqrt{(S_E^2+1)}} - (z_{li+1} - z_{ci+1})\right] = 0 \tag{2.34}$$

This indicates that when point F is below point B (i.e., $z_{\ell\ i+1} > z_{ui}$) the sinkage $z_{\ell\ i+1}$ at point F can be determined by solving Equation (5.23) for a given set of parameters including ϕ_{ri}, T, and z_{ui}.

It should be mentioned that Equation (2.30) and Equation (2.34) only define the sinkage $z_{\ i+1}$ at which the slope of track segment DF will match that of a corresponding point at the same sinkage on the circumference of roadwheel i+1. To ensure that point F on track segment DF actually coincides with the corresponding point on the circumference of roadwheel i+1, additional requirements should be met.

Considering the horizontal projection of the track section between the centres of two adjacent roadwheels, i and i+1 shown in Fig.2.12, one finds that one of the following two conditions should be satisfied, dependent upon the sinkage of point F:

A. When point F is above point B (i.e., $z_{\ell i+1} < z_{ui}$);

$$R(\sin\phi_{ri} + \sin\phi_{li+1}) + \int_{z_{mi}}^{z_{ri}} dz \Big/ \sqrt{\left\{\left[\frac{-T}{\frac{1}{2}k_u(z - z_{ri})(z - 2z_{ai} + z_{ri}) - T\cos\phi_{ri}}\right]^2 - 1\right\}} + \int_{z_{mi}}^{z_{li+1}} dz \Big/ \sqrt{\left\{\left[\frac{-T}{\frac{1}{2}k_u(z - z_{ri})(z - 2z_{ai} + z_{ri}) - T\cos\phi_{ri}}\right]^2 - 1\right\}} = l_0\cos\delta \tag{2.35}$$

where ℓ_0 is the distance between the centres of two adjacent roadwheels, δ is the inclination of the vehicle frame with respect to the horizontal, and z_{mi} is the ordinate of point D which is the minimum sinkage of the track between two adjacent roadwheels. At point D the slope of the track is zero. Therefore, by setting dz/dx in Equation (2.28) to zero, z_{mi} can be expressed by

$$z_{mi} = z_{ai} + \sqrt{\left[(z_{ai} + z_{ri})^2 - \frac{2T}{k_u}(1 - \cos\phi_{ri})\right]} \quad . \tag{2.36}$$

B. When point F is below point B (i.e., $z_{\ell i+1} > z_{ui}$)

$$R(\sin\phi_{ri} + \sin\phi_{ii+1}) + \int_{z_{mi}}^{z_{ri}} dz \Big/ \sqrt{\left\{\left[\frac{-T}{\frac{1}{2}k_u(z - z_{ri})(z - 2z_{ai} + z_{ri}) - T\cos\phi_{ri}}\right]^2 - 1\right\}}$$
$$+ \int_{z_{mi}}^{z_{ui}} dz \Big/ \sqrt{\left\{\left[\frac{-T}{\frac{1}{2}k_u(z - z_{ri})(z - 2z_{ai} + z_{ri}) - T\cos\phi_{ri}}\right]^2 - 1\right\}}$$
$$+ \int_{z_{ui}}^{z_{ii+1}} dz \Big/ \sqrt{\left\{\left[\frac{-T}{k/(n+1)(z^{n+1} - z_{ui}^{n+1}) - T/\sqrt{(S_E^2 + 1)}}\right]^2 - 1\right\}} = l_0\cos\delta \tag{2.37}$$

It should be noted that in Equation (2.35) and Equation (2.37) there are four basic unknowns; ϕ_{ri} for roadwheel i, vehicle inclination angle δ, track tension T, and sinkage of the first roadwheel, z_{u1}. All other parameters, such as z_{ai}, $z_{\ell i+1}$, z_{mi} and z_{ri} can be expressed in terms of the four basic unknowns. It should be noted that the sinkage, z_{ui}, of the lowest point of roadwheel i (i.e., point B shown in Fig.2.12) can be expressed in terms of z_{u1} and δ.

$$z_{ui} = z_{u1} + (i - 1)l_0 \sin\delta \quad (i = 1, 2, \ldots, N) \tag{2.38}$$

For each track segment between two roadwheels, an equation of the form of Equation (2.35) or Equation (2.37), which contains ϕ_{ri}, δ, and z_{u1}, can be derived. Therefore, for a track system of N roadwheels, N-1 equations

containing δ, T, z_{u1} and ϕ_{ri} (i=1,2,...,N-1) can be established. To completely define the deflected shape of the N-1 track segments between adjacent roadwheels, three additional independent equations containing δ, T, and z_{u1} should be established. These additional equations can be derived by considering the equilibrium of the normal forces and the moments acting on the track system and the track length. It should be mentioned that the increase in length of the track segments between roadwheels in contact with the terrain causes an increase in track tension and hence additional compression of the suspension springs and elongation of the track. This means that the decrease in the sag of the top run of the track, the additional compression of the suspension springs and the elongation of the track under tension compensate for the increase in length of the track between roadwheels in contact with the terrain. The effects on track tension of the additional compression of the suspension springs, the changes in the sag of the top run of the track and the track elongation have been taken into account in the analysis.

The solution to this set of N+2 equations will yield the values of ϕ_{ri}(1=1,2,...,N-1), δ, T and z_{u1}. Thus the shape of the deflected track between the front and rear roadwheels is completely defined. Making use of the information on the pressure-sinkage relationship and the response to repetitive loading of the terrain, the normal pressure distribution under a moving track at low slip with insignificant shear stresses can then be determined.

2.4 Prediction of the Shear Stress Distribution Under A Moving Track

The tractive performance of a tracked vehicle is closely related to its normal pressure and shear stress distributions on the track-terrain interface. In Section 2.3 the prediction of the normal pressure distribution, neglecting the effects of shear stresses, is discussed. In this section the shearing action of a flexible track will be analyzed and a method for predicting the shear stress distribution will be presented. Based on these, the effects of shear stresses on the normal pressure distribution will be discussed in the next section.

To predict the shear stress distribution under a track, the shear stress-shear displacement relationship, the shear strength and the response to repetitive shear loading of the terrain, as discussed in Section 2.1, must be known. Over a given terrain, the shear stress at a given point on the track-terrain interface is a function of the shear displacement, measured from the point where shearing (or reshearing) begins, and the normal pressure at that point. The shear displacement developed under a flexible track, shown in Fig.2.14, may be determined from the analysis of the slip velocity V_j, similar to that for a rigid track or a rigid wheel (2.1, 2.3, 2.9). The slip velocity V_j of a point P on a flexible track relative to the terrain surface is the tangential component of the absolute velocity V_a shown in Fig.2.14. The magnitude of the slip velocity V_j is expressed by

$$\begin{aligned} V_j &= V_t - V\cos\alpha \\ &= r\omega - r\omega(1-i)\cos\alpha \\ &= r\omega[1-(1-i)\cos\alpha] \end{aligned} \tag{2.39}$$

where r and ω are the radius and angular speed of the sprocket, respectively, i is the slip of the track, α is the angle between the tangent to the track at point P and the horizontal, V_t is the theoretical speed of the vehicle (i.e., $V_t=r\omega$), and V is the actual speed of the vehicle. The shear displacement j along the track-terrain interface is given by

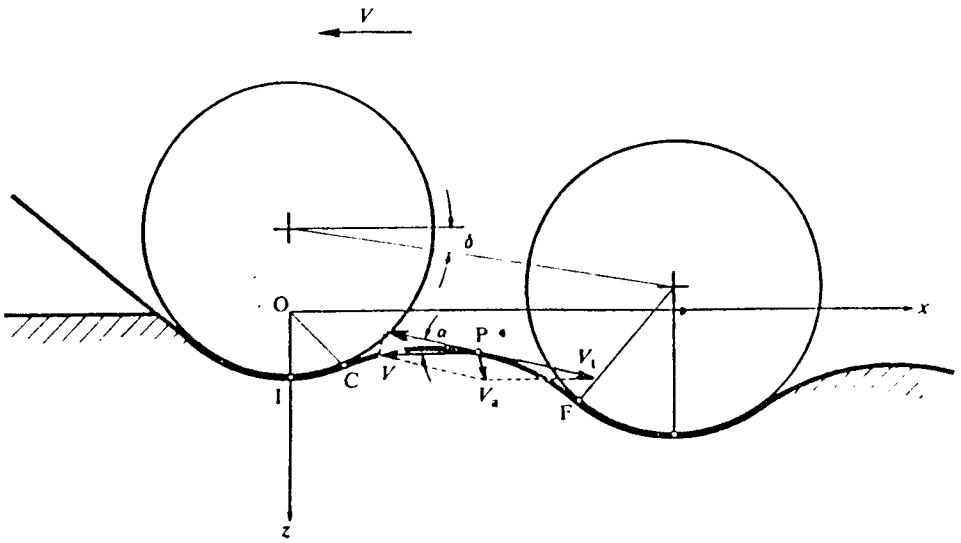

Slip velocity of a point on the track in contact with a deformable terrain

Fig. 2.14

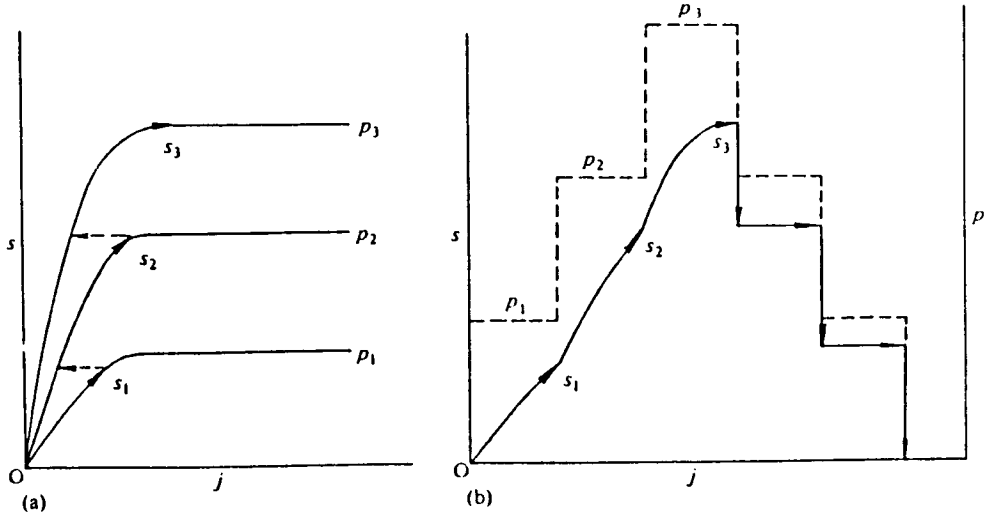

(a) Shear stress-displacement relationships under constant normal pressures
(b) Shear stress-displacement relationship under varying normal pressure

Fig. 2.15

$$
\begin{aligned}
j &= \int_0^t r\omega[1-(1-i)\cos\alpha]\,dt \\
&= \int_0^l r\omega[1-(1-i)\cos\alpha]\,\frac{dl}{r\omega} \\
&= \int_0^l \left[1-(1-i)\frac{dx}{dl}\right] dl \\
&= l-(1-i)x
\end{aligned}
\tag{2.40}
$$

where ℓ is distance along the track between point P and the point where shearing (or reshearing) begins, and x is the corresponding horizontal distance between point P and the initial shearing (or reshearing) point.

If the shear stress-displacement relationship of the terrain is described by Equation (2.8), then the shear stress distribution may be expressed by

$$
s(x) = [c + p(x)\tan\phi]\left[1-\exp\left(-\frac{(l-(1-i)x)}{K}\right)\right] \tag{2.41}
$$

where p(x) is the normal pressure on the track, which is a function of x.

For terrain with a shear stress-displacement relationship described by Equation (2.9) or (2.10) a similar approach may be followed to derive an appropriate expression for the shear stress distribution.

In using Equation (2.41) to predict the shear stress distribution under a track, attention should be paid to the following points:

A. As mentioned previously, an element of the terrain under a moving track is subject to the repetitive normal load applied by the consecutive roadwheels. Consequently, for a terrain with frictional properties, the terrain element will be subject to repetitive shear loading. The behaviour of the terrain under repetitive shear loading should, therefore, be taken into account in predicting shear stress distribution under a track. Based on the behaviour of the terrain under repetitive shear loading described in Section 2.1, for an idealized case shown in Fig.2.11, the shear displacement should be calculated either from the initial shearing point

for the first track segment, such as point A, or from the points where reshearing begins for the subsequent track segments, such as points A_1, A_2 and A_3. This will lead to the development of shear stress under various segments of the track as illustrated in Fig.2.11(b).

B. As pointed out previously, the normal pressure under a track is rarely uniformly distributed. Consequently, shearing takes place with varying normal load under a track segment. However, the shear stress-shear displacement relationships of the terrain are usually measured under constant normal pressures. To predict the shear stress under varying normal pressure, a special procedure must be followed. This procedure is illustrated in Fig.2.15 for an idealized case with discrete steps in normal pressure. Although in practice the normal pressure under the track usually varies continuously, its variation may be represented by small steps. The shear stress-shear displacement relationships of a terrain under different normal pressures of p_1, p_2 and p_3 are shown in Fig.2.15(a). If the normal pressure on a track segment increases by equal steps from 0 to p_3 and then decreases by the same steps from p_3 to 0, as shown in Fig.2.15(b), then during the loading part of the cycle, from 0 to p_3, the variation of shear stress with shear-displacement under the track segment will follow the path $OS_1S_2S_3$. It will be noted that the path OS_1 in Fig.2.15(b) is identical to the path OS_1 in Fig.2.15(a) and that paths S_1S_2 and S_2S_3 in Fig.2.15(b) correspond to those shown in Fig.2.15(a). This is based on the observation of the shearing behaviour of terrain described previously in Section 2.1, which indicates that the maximum shear stress under a given normal pressure is reached only after a certain amount of shear displacement has taken place. During the unloading part of the cycle, however, the shear stress decreases instantaneously with the decrease of normal pressure for a terrain with predominantly frictional characteristics, as shown in Fig.2.15(b).

C. Over terrains exhibiting both frictional and cohesive properties, the shear stress developed on the track-terrain interface is composed of two components. One is due to friction and depends on the normal pressure and shear displacement calculated from the initial shearing point (or reshearing point) as described above. The other is due to cohesion (or

adhesion) and does not depend on normal pressure. It is dependent on the shear displacement measured from the initial shearing point of the track.

Based on the above analysis of the shear displacement under a flexible track and the development of shear stress under varying normal pressure, the shear stress distribution under a track can be predicted. The prediction procedure is used in the simulation model NTVPM-85.

2.5 Effects of Shear Stresses on the Normal Pressure Distribution

In Section 2.3, an analytical method for predicting the normal pressure distribution under a track at low slip and neglecting the effects of shear stresses is presented. As a result, the tension is assumed to be constant throughout the track. At higher slip, however, the shear stresses on the track-terrain interface becomes significant, and their presence changes the tension of the track. Since the shape of the track segments between adjacent roadwheels is dependent upon track tension, the normal pressure distribution is affected by the presence of shear stress.

As described in the preceding section, the shear stress on the track-terrain interface varies along the contact length. Thus, the track tension changes from one segment to another. To simplify the analysis, in determining the deflected shape of track segments between adjacent roadwheels, such as CF shown in Fig.2.14, an average track tension is used. This average track tension is taken as the mean of the tensions at points C and F, which are determined by the shear stress distribution on the track-terrain interface. It can be shown that the shear stresses acting on track segments (such as CF) between adjacent roadwheels are usually relatively low and hence cause only a small change in track tension between C and F. Therefore, using an average track tension in determining the deflected shape of track segments between adjacent roadwheels is reasonable. Following this approach, an iterative procedure is developed for predicting the normal pressure and shear stress distributions under a track at a given slip. The basic steps of this procedure are outlined below:

A. Following the procedure described in Section 2.3 first calculate the normal pressure distribution when no shear stresses are present;

B. Use the method developed in the preceding section to calculate the shear stress distribution under the track for a given slip, using the normal pressure distribution determined at the preceding step;

C. Based on the shear stress distribution, calculate the tractive effort, which

can be obtained by integrating the shear stresses over the entire contact area, and determine the difference between the tensions at either end of each track segment between adjacent roadwheels, such as that between C and F shown in Fig.2.14; calculate the average tension in each track segment between adjacent roadwheels;

D. Use the average tensions in the track segments to initiate an iterative process to recalculate the normal pressure distribution. Check whether the conditions that define the equilibrium of forces and moments acting on the track system and the track length are satisfied. If the conditions are not met, select a set of new values for the variables, including track tension T_u, sinkage of the first roadwheel z_{u1}, and inclination angle δ. When a tension change is necessary increase or decrease all tensions by a constant amount. If the tension between the sprocket and the front roadwheel decreases to zero, slack may be introduced.

E. Repeat the procedure described above until the errors in the equilibrium equations for forces and moments and in the calculations of track length are less than the preassigned values.

In the equation for moment equilibrium, the moment due to drawbar pull, which causes load transfer from the front to the rear, has been taken into consideration (see. Fig.2.16). Furthermore, the role that the shear stresses play in supporting the vertical load applied to the track has also been taken into account in the calculations.

It should be mentioned that the presence of shear stresses not only will affect the normal pressure distribution but also may induce additional sinkage, usually referred to as slip-sinkage. For the types of terrain described in Section 2.1, it was found that slip-sinkage is not significant, and is therefore not included in the present analysis. However, if slip-sinkage is found to be significant for the terrain in question, it can readily be incorporated into the present analytical framework.

2.6 Prediction of Motion Resistance and Drawbar Pull

When the normal pressure and shear stress distributions under a tracked vehicle at a given slip have been determined, the tractive performance of the vehicle can then be predicted. The tractive performance of an off-road vehicle is usually characterized by its motion resistance, tractive effort, and drawbar pull (the difference between tractive effort and motion resistance) as functions of slip.

The motion resistance R_t of the vehicle can be determined from the horizontal component of the normal pressure acting on the track in contact with the ground. For a vehicle with two tracks, R_t can be described by (see Fig.2.16)

$$R_t = 2b \int_0^{L_t} p \sin \alpha \, dl \tag{2.42}$$

where b is the contact width of the track, L_t is the length of the track in contact with the terrain, p is normal pressure, and α is the angle of the track element with respect to the horizontal.

The tractive effort F of the vehicle can be calculated from the horizontal component of the shear stress acting on the track in contact with the terrain. For a vehicle with two tracks, F is given by (see Fig.2.16)

$$F = 2b \int_0^{L_t} s \cos \alpha \, dl \tag{2.43}$$

where s is the shear stress.

Since both the normal pressure p and shear stress s are functions of track slip, the motion resistance R_t and tractive effort F vary with slip.

For a track with rubber pads, part of the total tractive effort is generated by the rubber-terrain shearing. To predict the tractive effort developed by the rubber pads, the portion of the vehicle weight supported by the

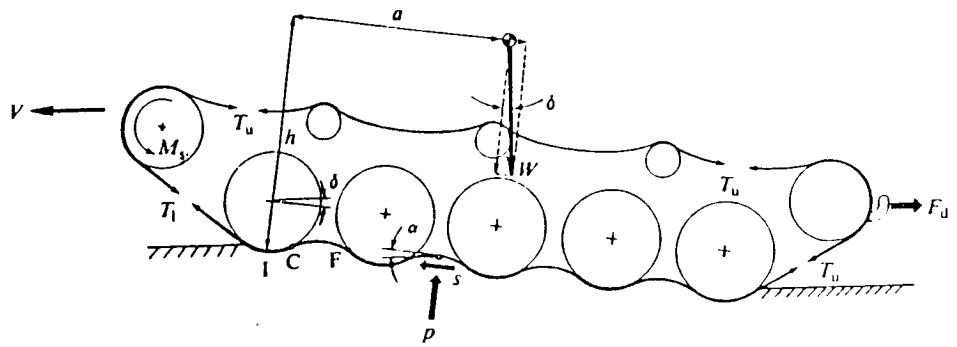

Fig. 2.16 Forces acting on a track system

Table 2.5 Vehicle and track parameters

Vehicle parameters	
Weight	88.71 kN
x-coordinate of the centre of gravity (in front of the mid-point of the track)	12.7 cm
y-coordinate of the centre of gravity	99 cm
Number of roadwheels (on one track)	5
Radius of the roadwheels	30.5 cm
Distance between roadwheel centres	66.7 cm
Distance between sprocket and tensioning wheel centres	403 cm
Initial track tension	10 kN
Number of supporting rollers	0
Angle of approach of the track	26
Angle of departure of the track	16
Drawbar x-coordinate (behind the mid-point of the track)	229 cm
Drawbar y-coordinate	68 cm
Track parameters	
Weight per unit length	0.56 kN/m
Width	38 cm
Pitch	15 cm
Height of the grousers	4.7 cm

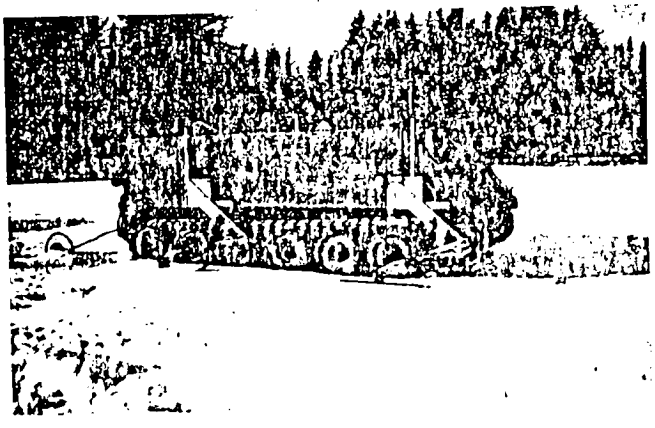

Fig. 2.17 Instrumented test vehicle

rubber pads should be estimated and the characteristics of rubber-terrain shearing should be taken into account.

It should be mentioned that the tractive effort F calculated by Eq.(2.43) is due to the shearing action of the track across the grouser tips (or due to rubber-terrain shearing for a track with rubber pads). For a track with long grousers, additional thrust will be developed due to the shearing action on the vertical surfaces on either side of the track. According to Reece (2.10), the maximum shear force per unit track length S_{vmax} from the two sides of a track is given by

$$S_{vmax} = 4ch \sin^2\left(\frac{\pi}{4} + \frac{\phi}{2}\right) + 2hz_m\gamma \tan\left(\frac{\pi}{4} + \frac{\phi}{2}\right) \cos\left(\frac{\pi}{2} - \phi\right) \tag{2.44}$$

where c, γ and ϕ are the cohesion, weight density, and angle of shearing resistance of the terrain, respectively; h is the grouser height and z_m is the mean sinkage of the grouser.

The relationship between the shear force developed on the two sides of a track and shear displacement may be assumed to be similar to that between the shear stress and shear displacement described in Section 2.1. Therefore, the distribution of the shear force on the two vertical sides along the length of the track can be predicted in the same way as that described in Section 2.1 and the thrust F_v from the two sides of a track can be expressed by

$$F_v = \int_0^{L_t} S_v \cos\alpha \, dl \tag{2.45}$$

where S_v is the shear force per unit length of the track. The drawbar pull F_d of the vehicle can be considered as the difference between the tractive effort and the motion resistance, and can be expressed by

$$\begin{aligned} F_d &= F + 2F_v - R_t \\ &= 2b\int_0^{L_t} s\cos\alpha \, dl + 2\int_0^{L_t} S_v \cos\alpha \, dl - 2b\int_0^{L_t} p\sin\alpha \, dl \end{aligned} \tag{2.46}$$

From this equation, the relationship between drawbar pull F_d and track slip i can be determined.

The simulation model described above has been programmed on microcomputer and the resulting computer simulation model is referred to as NTVPM-85. The

simulation model can be used to predict the normal pressure and shear stress distributions, sinkage, motion resistance, tractive effort, and drawbar pull as functions of slip.

2.7 Experimental Substantiation

To substantiate the basic features of the computer simulation model NTVPM-85, full-scale tests of an instrumented vehicle, shown in Fig.2.17, over various types of terrain were carried out. The basic parameters of the test vehicle, an M113A1, are given in Table 2.5. The mechanical properties of the terrain were measured at the time of vehicle testing and are described in Tables 2.1 to 2.3.

To measure the normal pressure under the track of the test vehicle, four Kulite IPT-750, flush stainless steel diaphragm pressure transducers were used. These transducers employ semiconductor strain gauge elements, glass bonded directly to the diaphragm. The diameter of the diaphragm in contact with the terrain is 1.89 cm (0.745 in).

The transducers were mounted on a track link, two on the rubber pad and two on the side, as shown in Fig.2.18. The signals from these transducers were transmitted through an adapter and a cable (shown in Fig.2.19) to a Vishay model 2100 multichannel signal conditioner (amplifier) installed inside the test vehicle. The transducer signals, after being amplified, were recorded on a Midwestern Instruments model 800, galvanometer type recording oscillograph.

In addition to the normal pressure, a number of operational parameters of the test vehicle were monitored during tests. To measure the dynamic sinkages of the track at the front and rear roadwheels, as well as the trim angle of the vehicle, four Research Incorporated 4040 linear displacement transducers were used. Since it is difficult to install mechanical devices for directly monitoring the sinkage of the track with respect to the terrain surface, a special monitoring system was developed. In this system, two linear displacement transducers were employed to monitor the displacements of the vehicle body at locations immediately above the front and rear roadwheels with respect to the terrain surface. Over snow, skis were used as the sensing element as shown in Fig.2.17, while over muskeg or mineral terrain, bicycle wheels were used as the sensing element. Two additional displacement transducers were used to monitor the displacements of the front and rear roadwheels relative to the

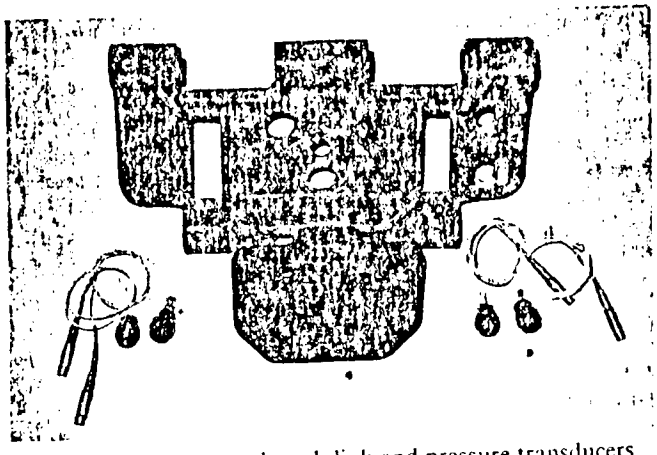

Instrumented track link and pressure transducers

Fig. 2.18

Adapter and cable for transmitting pressure transducer signals

Fig. 2.19

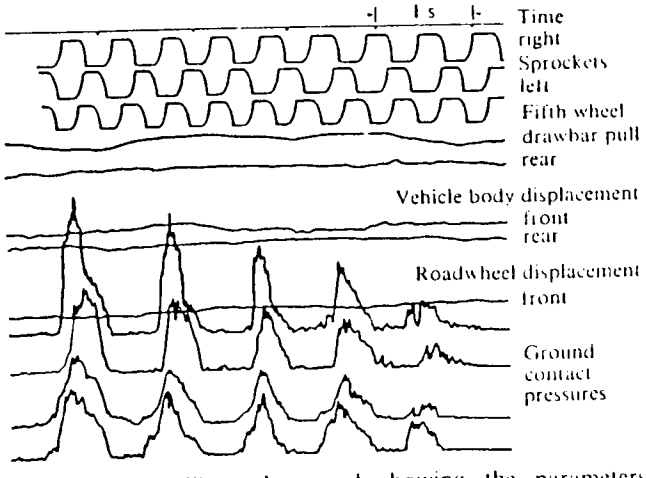

An oscillograph record showing the parameters monitored during a test

Fig. 2.20

vehicle body. Based on these measurements, the dynamic sinkages of the front and rear roadwheels of the track system with respect to the terrain surface and the trim angle of the vehicle can be derived.

The distance the vehicle travelled during tests was measured using a fifth wheel running in the rut made by the track. It was found that the fifth wheel worked well over the types of terrain tested. The revolutions of the sprockets of both tracks of the test vehicle were measured using photoelectric counters and were recorded on the oscillograph. Based on the signals from the fifth wheel and the sprocket counters, the slip of the tracks can be derived. A time signal was also provided on the oscillograph. Thus, from the fifth wheel signal and the time signal, the vehicle speed can be calculated. The drawbar pull of the test vehicle was monitored by a strain-gauge load cell.

Figure 2.20 shows a typical record of the parameters monitored during a test, which include ground contact pressures, distance as measured by the fifth wheel, sprocket revolutions, vehicle body and roadwheel displacements, time and drawbar pull.

The data recorded by the oscillograph was later digitized and processed using a Hewlett-Packard 9111A graphics tablet and a Hewlett-Packard 9845T microcomputer.

The measured normal pressure on the rubber pad of the track and the drawbar pull-slip curves of the test vehicle over various types of terrain are shown in Figs.2.21-2.24 and Figs. 2.25-2.28, respectively. The predicted normal pressure on the rubber pad of the track and the predicted drawbar pull-slip curves of the vehicle are also shown in the figures.

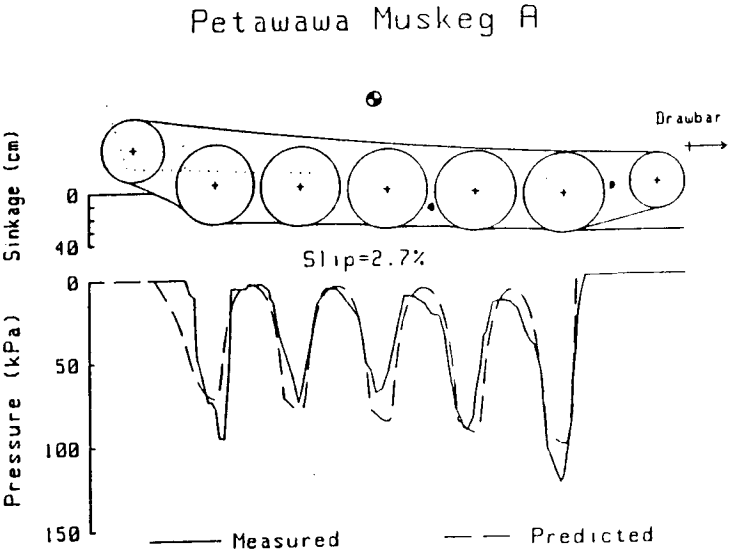

Measured and predicted normal pressure distributions under the track pad of an M113A1 on Petawawa Muskeg A.

Fig. 2.21

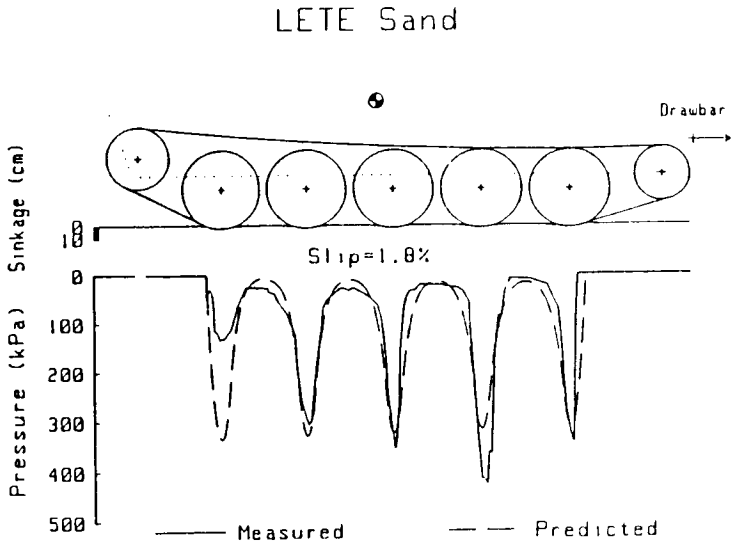

Measured and predicted normal pressure distrbutions under the track pad of an M113A1 on LETE sand.

Fig. 2.22

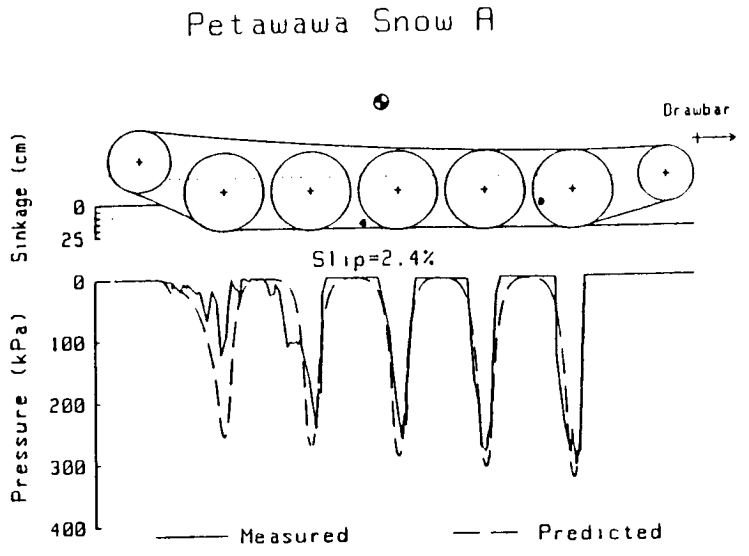

Measured and predicted normal pressure distributions under the track pad of an M113A1 on Petawawa Snow A.

Fig. 2.23

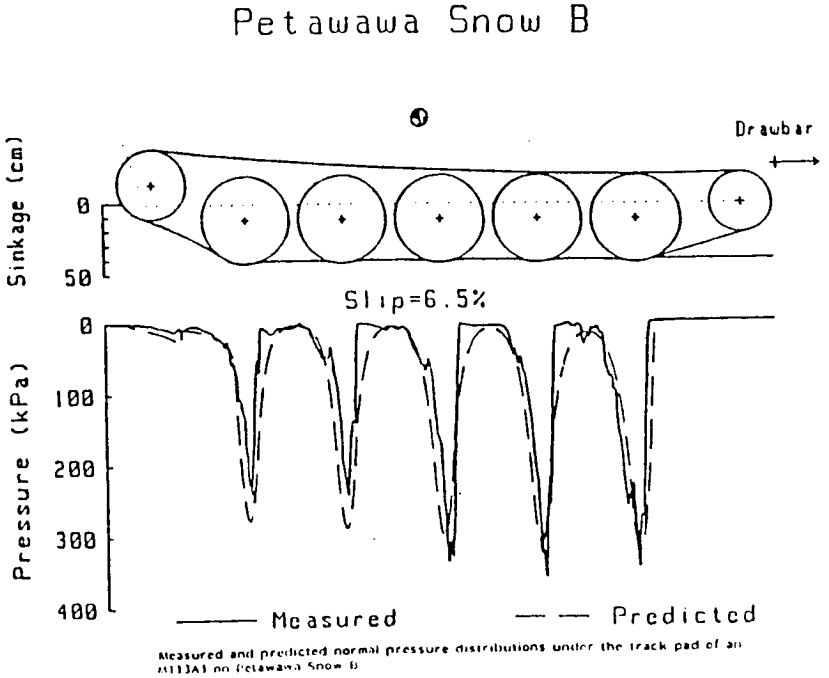

Measured and predicted normal pressure distributions under the track pad of an M113A1 on Petawawa Snow B

Fig. 2.24

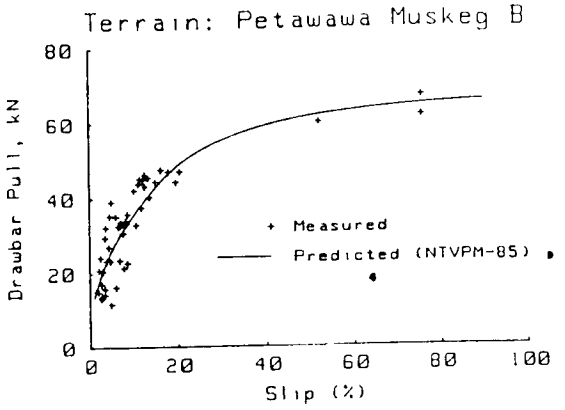

Measured and predicted drawbar performance of an M113A1 on Petawawa Muskeg B

Fig. 2.25

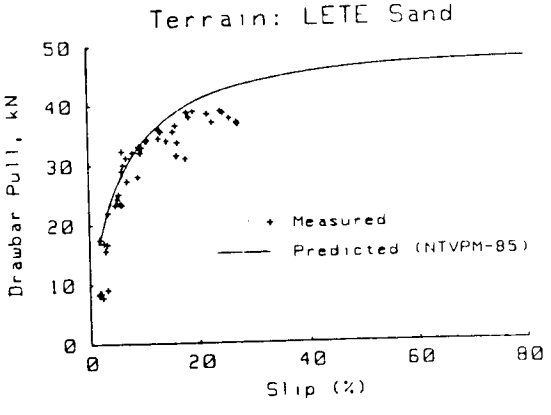

Measured and predicted drawbar performance of an M113A1 on LETE sand

Fig. 2.26

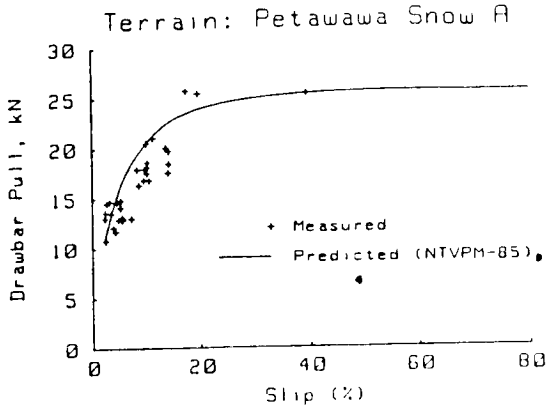

Measured and predicted drawbar performance of an M113A1 on Petawawa Snow A.

Fig. 2.27

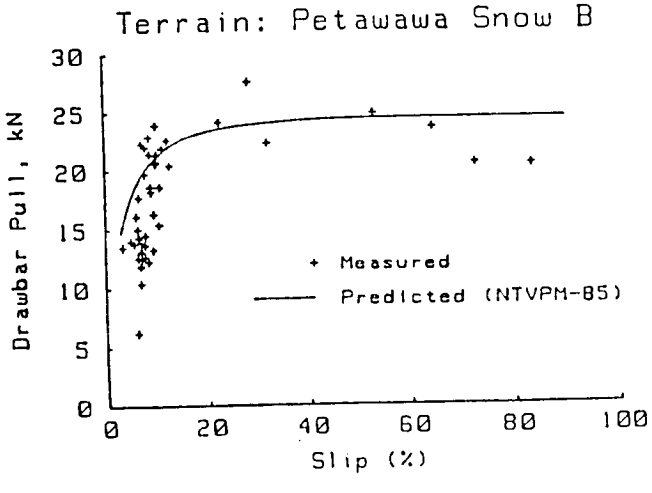

Measured and predicted drawbar performance of an M113A1 on Petawawa Snow B.

Fig. 2.28

2.8 Comparison of Predictions with Experimental Results

1. Comparisons between the predicted normal pressure distributions obtained using the computer simulation model NTVPM-85 and the measured ones over various types of terrain are shown in Figs.2.21-2.24. Over a muskeg (Petawawa Muskeg A), a good agreement exists between the predicted normal pressure distribution and the measured one as shown in Fig.2.21. The measured maximum normal pressure under the track pad over this muskeg is approximately 130 kPa, in contrast with the nominal ground pressure of 43.7 kPa, obtained by dividing the vehicle weight by the track contact area. This means that the nominal ground pressure is only about 34% of the measured maximum pressure. Over a sandy terrain (LETE Sand), the normal pressure distribution predicted using NTVPM-85 is very close to those measured, as shown in Fig.2.22. The maximum normal pressure measured under the track pad over this sandy terrain is about 430 kPa, which is approximately ten times the nominal ground pressure of 43.7 kPa. Over two types of snow-covered terrain (Petawawa Snow A and B), good-to-excellent agreement again exists between the measured and predicted normal pressure distributions, as shown in Figs.2.23 and 2.24. The nominal ground pressure of 43.7 kPa is again only about 12% of the measured maximum normal pressure.

The generally good agreement between the measured and predicted normal pressure distributions using NTVPM-85 is due primarily to the inclusion of the response of the terrain to repetitive normal load and to the detailed analysis of the track-terrain interaction. As mentioned previously, an element of the terrain under the track is subject to the repetitive loading of consecutive roadwheels. The terrain, after being compacted by the first (or preceding) roadwheel, becomes much stiffer than in its virgin state. Consequently this promotes the concentration of normal pressure under the roadwheels, and significant pressure peaks are always observed, even on a terrain like muskeg which is relatively soft in its virgin state.

Furthermore, the behaviour of the terrain during the unloading-reloading cycle described in Section 2.1 also explains why it is possible that the pressure at a point on the track segments between two adjacent roadwheels can be

as low as zero, while the sinkage at that point, measured from the original terrain surface, is not zero.

The good agreement between the measured and the predicted normal pressure distributions also indicates that the assumption that the track may be modelled as a flexible belt is reasonable for the type of track system examined.

2. Comparisons between the measured drawbar pulls and the predicted ones at various slips over different terrains are shown in Figs.2.25-2.28. As can be seen from the figures, there is a good-to-excellent agreement between the measured drawbar pulls and the predicted ones using the simulation model NTVPM-85.

The good agreement between the measured and predicted drawbar pulls is primarily due to the inclusion of the terrain response to repetitive shear loading and the shearing characteristics of terrain under varying normal load in the prediction of shear stress distribution under the track. The behaviour of the terrain under repetitive shearing has a significant effect on the development of tractive effort, particularly at low track slips, as described previously. Furthermore NTVPM-85 gives a realistic prediction of normal pressure under the track, and hence sinkage and motion resistance. This results in a fairly accurate prediction of drawbar pull.

The close agreement between the predicted and measured normal pressure distributions and drawbar performance shows that the basic features of the computer simulation model NTVPM-85 have been substantiated. Thus, the model can be an extremely useful tool for the development and design engineer, as well as the procurement manager.

Since the model takes into account all major design parameters of the vehicle as well as terrain characteristics, it is particularly suited for the evaluation of competing designs and for the examination of the effects on performance of design modifications and changing operational environments. The model provides a rational basis for the selection of the most promising design for a given mission and environment, prior to expensive hardware construction.

References

2.1 J.Y. Wong, M. Garber and J. Preston-Thomas, Theoretical prediction and experimental substantiation of the ground pressure distribution and tractive performance of tracked vehicles, Proceedings of the Institution of Mechanical Engineers, Vol.198, Part D, No.15, 1984.

2.2 J.Y. Wong and J. Preston-Thomas, Parametric analysis of tracked vehicle performance using an advanced computer simulation model, Proceedings of the Institution of Mechanical Engineers, Vol.200, Part D, No.2, 1986.

2.3 M.G. Bekker, Theory of Land Locomotion, The University of Michigan Press, 1956.

2.4 J.Y. Wong, Data processing methodology in the characterization of the mechanical properties of terrain, Journal of Terramechanics, Vol.17, No.1, 1980.

2.5 J.Y. Wong, P.S. Harris and J. Preston-Thomas, Development of a portable automatic data processing system for terrain evaluation. Proceedings of the 7th International Conference of the International Society for Terrain-Vehicle Systems, Vol.III, Calgary, Canada, 1981.

2.6 J.Y. Wong, J.R. Radforth and J. Preston-Thomas, Some further studies on the mechanical properties of muskeg in relation to vehicle mobility, Journal of Terramechanics, Vol.19, No.2, 1982.

2.7 J.Y. Wong and J. Preston-Thomas, On the characterization of the pressure-sinkage relationship of snow covers containing an ice layer, Journal of Terramechanics, Vol.20, No.1, 1983.

2.8 J.Y. Wong and J. Preston-Thomas, On the characterization of the shear stress-displacement relationship of terrain, Journal of Terramechanics, Vol.19, No.4, 1982.

2.9 J.Y. Wong, Theory of Ground Vehicles, John Wiley, New York, 1978. Russian translation, Machinostroenie Publishers of Moscow, U.S.S.R., 1982. Chinese translation, Machinery Industry Publishing House, Peking, China, 1985.

2.10 A.R. Reece, Principles of soil-vehicle mechanics, Proceedings of the Institution of Mechanical Engineers, Vol.180, Part 2A, No.2, 1965-66.

3. APPLICATIONS OF THE COMPUTER SIMULATION MODEL (NTVPM-85) TO PARAMETRIC ANALYSIS OF TRACKED VEHICLE PERFORMANCE

As mentioned previously, the model NTVPM-85 is particularly suited for the evaluation of competing designs and for the examination of the effects on performance of design modifications and changing operational environments. Thus, it is an extremely useful tool for the development and design engineer in the optimization of tracked vehicle design and for the procurement manager in the selection of vehicle candidates for a given mission and environment.

As NTVPM-85 takes into account all major vehicle design parameters, it can be used in the evaluation and optimization of vehicle configuration and design parameters, such as track system configuration, number of roadwheels, roadwheel radius, roadwheel spacing, sprocket radius and location, idler radius and location, track supporting roller radius and location, suspension heave stiffness, vehicle weight, location of the centre of gravity, track width and pitch, grouser height, track elasticity, track link and rubber pad geometry, track weight per unit length, initial track tension, belly (hull) shape, and drawbar location. In addition, the model takes into consideration terrain characteristics. Thus, it can also be employed to examine the effects of terrain conditions on vehicle mobility and to optimize vehicle design for a given operating environment. To demonstrate the application of NTVPM-85, a parametric analysis of the tractive performance of a tracked vehicle over various types of terrain has been performed (3.1, 3.2). The baseline vehicle used in the analysis has parameters similar to those of a widely used armored personnel carrier (M113). The major design parameters of the baseline vehicle with 5 roadwheels (on each of the two tracks) are given in Table 3.1. To examine the effects of track system configuration on performance, two derivatives of the baseline vehicle, one with 6 roadwheels and the other with 8 overlapping roadwheels (on each of the two tracks), are selected. Their design parameters are also given in Table 3.1.

To evaluate the effects of terrain conditions on vehicle performance, three types of terrain, referred to as Hope Valley snow, Petawawa Muskeg A, and LETE

Table 3.1

BASIC PARAMETERS OF THE TRACKED VEHICLES USED IN THE STUDY

Vehicle parameters	Baseline vehicle	Vehicle with six roadwheels	Vehicle with eight overlapping roadwheels
Weight, kN	104.62	104.62	104.62
C.G.X-co-ordinate*, cm	136	141.9	142.5
C.G.Y-co-ordinate, cm	99	99	99
Number of roadwheels (per track)	5	6	8
Roadwheel radius, cm	30.5	25	25
Roadwheel spacing, cm	66.8	55.8	40
Sprocket pitch radius, cm	24.3	24.3	24.3
Sprocket center X-co-ordinate, cm	−65	−59.1	−58.5
Sprocket center Y-co-ordinate, cm	55.3	55.3	55.3
Idler radius, cm	21.4	21.4	21.4
Idler center X-co-ordinate, cm	338	343.9	345.5
Idler center Y-co-ordinate, cm	41.4	41.4*	41.4
Drawbar X-co-ordinate, cm	362.5	368.4	369
Drawbar Y-co-ordinate, cm	68	68	68
Suspension stiffness (per track), kN/cm	4.8	4.8	4.8
Track weight per unit length, kN/m	0.56	0.56	0.56
Track width, cm	38	38	38
Track pitch, cm	15	15	15
Height of grouser, cm	4.7	4.7	4.7
Track elasticity, kN	3000	3000	3000
Number of track supporting rollers	0	3	3

*Co-ordinate origin is at the bottom of the front roadwheel.

Table 3.2

VALUES OF THE PRESSURE–SINKAGE AND REPETITIVE LOADING PARAMETERS

Parameters	Hope Valley Snow	Petawawa Muskeg A	LETE Sand
k_c, kN/m^{n+2}	6.16	–	102
k_ϕ, kN/m^{n+2}	149.35	–	5,301
n	1.525	–	0.793
k_m, kN/m^3	–	290	–
M_m, kN/m^3	–	51	–
k_0, kN/m^3	0	123	0
A_u, kN/m^4	40,000	23,540	503,000

Table 3.3

VALUES OF SHEAR STRENGTH PARAMETERS

Terrain	Type of shearing	Cohesion (adhesion), c (kPa)	Angle of shearing resistance, ϕ (°)	Shear deformation modulus, K (cm)
Hope Valley Snow	Internal	0.76	23.2	4.24
	Rubber-snow	0.12	16.4	0.39
	Vehicle belly-snow	0	5.7	–
Petawawa Muskeg A	Internal (peat)	2.83	39.4	3.1
	Vehicle belly-muskeg	0	13.5	–
LETE Sand	Internal	1.3	31.3	1.2
	Rubber-sand	0.7	27.5	1.0

sand, are used in the study. They are selected to represent a wide range of terrain conditions, from highly compressible to fairly firm. The Hope Valley snow had an average depth of 128 cm, which represents a challenge to vehicle mobility (3.3). The Petawawa Muskeg A had a surface mat approximately 5-10 cm thick and an underlying peat about 5 m deep (3.4). It was a muskeg with a fragile surface easily disturbed by vehicles. The LETE sand was a fairly firm terrain (3.1).

Table 3.2 summarizes the values of the pressure-sinkage and repetitive loading parameters of the three types of terrain used in the study. The basic mechanical properties of the Hope Valley snow are taken from reference (3.3). Certain parameters that are required as input to the simulation model are not available from reference (3.3). For these parameters, estimated values based on those of similar terrains are used. Terrain parameters for LETE sand and Petawawa Muskeg A are the same as those shown in Tables 2.1 and 2.3.

For Hope Valley snow and LETE sand, the Bekker equation, Eq.(2.1), is used to characterize the pressure-sinkage relationship. For Petawawa Muskeg A, Eq.(2.7) is used to describe the pressure-sinkage characteristics. The pressure-sinkage relationship during the unloading and reloading cycle is assumed to be linear and is described by Eqs.(2.2) and (2.3).

Table 3.3 summarizes the values of the shear strength parameters of the three types of terrain used in the study. It should be mentioned that for the three types of terrain, Eq.(2.8) is used to characterize their shear stress-shear displacement relationships, and the Mohr-Coulomb equation, Eq.(2.11), is used to describe their shear strengths.

Parametric analysis was performed using the computer simulation model NTVPM-85 to examine the effects of design parameters on the tractive performance of the three vehicle configurations over the three types of terrain. The prime vehicle design parameters examined in this study include track system configuration and initial track tension.

3.1 Effects of Design Parameters on Performance Over Hope Valley Snow

The drawbar pull to weight ratio as a function of slip for three different track system configurations (5 roadwheels, 6 roadwheels and 8 overlapping roadwheels) at various initial track tension to weight ratios, T_0/W, over Hope Valley snow are shown in Figs.3.1, 3.2 and 3.3, respectively (3.1, 3.2). The initial track tension referred to in this study is the tension in the track when the vehicle rests on firm, level ground. It should be mentioned that T_0/W=0.096 corresponds to an initial track tension of 10 kN, which is the recommended value for the baseline vehicle. It can be seen that for a given track system configuration, increasing the initial track tension noticeably improves the drawbar performance of the vehicle. For the baseline vehicle with 5 roadwheels, increasing the value of T_0/W from 0.096 to 0.382 results in an increase of the drawbar pull to weight ratio from 0.006 to 0.130 at 20% slip. This indicates that when the initial track tension is set at the recommended value, the vehicle is nearly immobilized on Hope Valley snow. However, the mobility of the vehicle is greatly improved with the increase of the initial track tension. It can also be seen from Figs.3.1 and 3.3 that for the same initial track tension to weight ratio of 0.191, the track system with 8 overlapping roadwheels has a drawbar pull to weight ratio of 0.122 at 20% slip, as compared with a value of 0.049 for the track system with 5 roadwheels. This represents an increase of 149% in drawbar pull.

Figures 3.4 and 3.5 show the normal pressure distributions under the track system with 8 overlapping roadwheels at initial track tension to weight ratios of 0.096 and 0.287, respectively. It is shown that for a given track system configuration, an increase in the initial track tension greatly increases the load supported by the track segments between roadwheels over marginal terrain. Consequently, the normal pressure is more uniformly distributed and the peak pressure is reduced. This results in the reduction of both the sinkage and the load supported by the vehicle belly.

Figure 3.6 shows the effect of the initial track tension on the load supported by the belly for the three track systems, with a ground clearance of

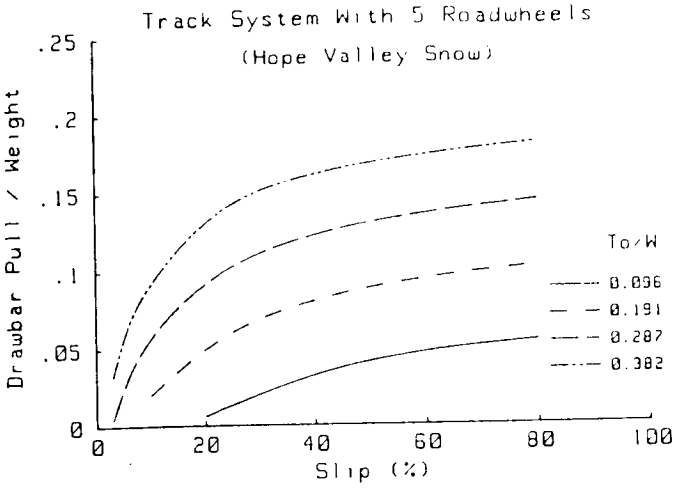

Drawbar performance of a track system with five roadwheels at various ratios of initial track tension to weight on Hope Valley snow.

Fig. 3.1

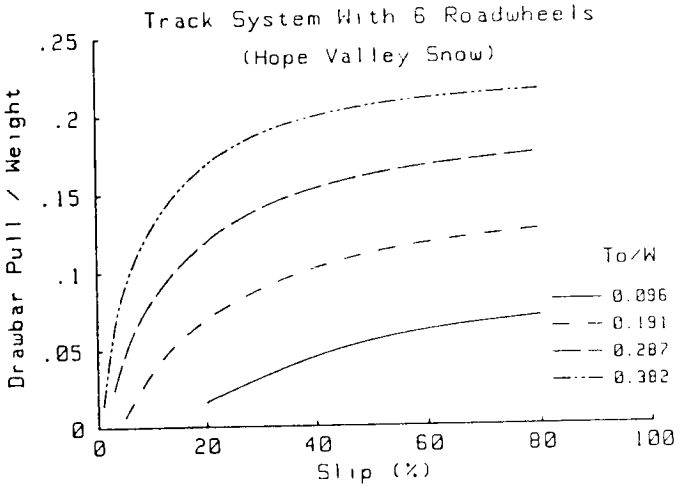

Drawbar performance of a track system with six roadwheels at various ratios of initial track tension to weight on Hope Valley snow.

Fig. 3.2

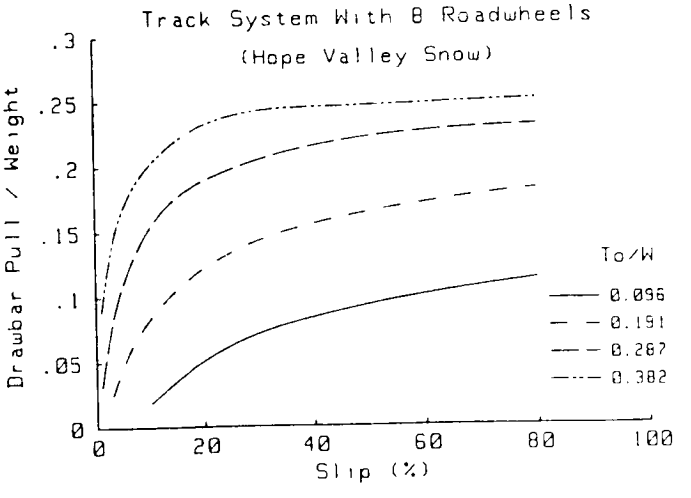

Drawbar performance of a track system with eight overlapping roadwheels at various ratios of initial track tension to weight on Hope Valley snow.

Fig. 3.3

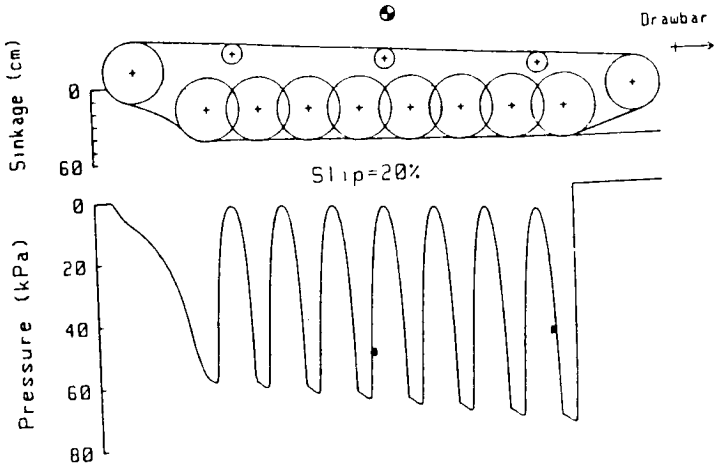

Predicted normal pressure distribution under a track system with eight overlapping roadwheels at initial track tension to weight ratio of 0.096 on Hope Valley snow.

Fig. 3.4

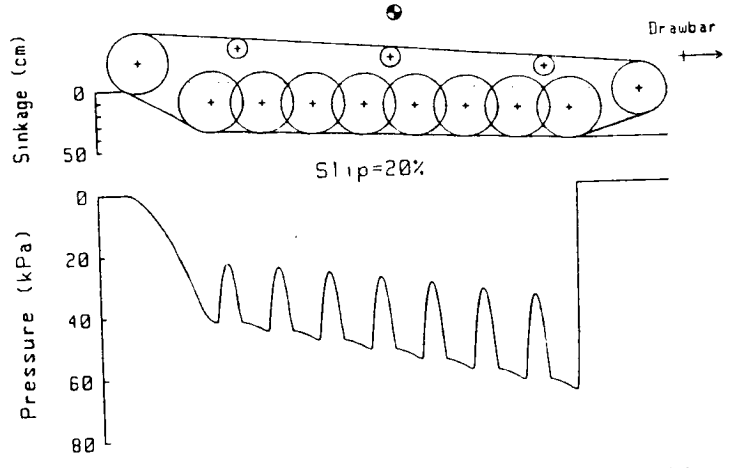

Predicted normal pressure distribution under a track system with eight overlapping roadwheels at initial track tension to weight ratio of 0.287 on Hope Valley snow.

Fig. 3.5

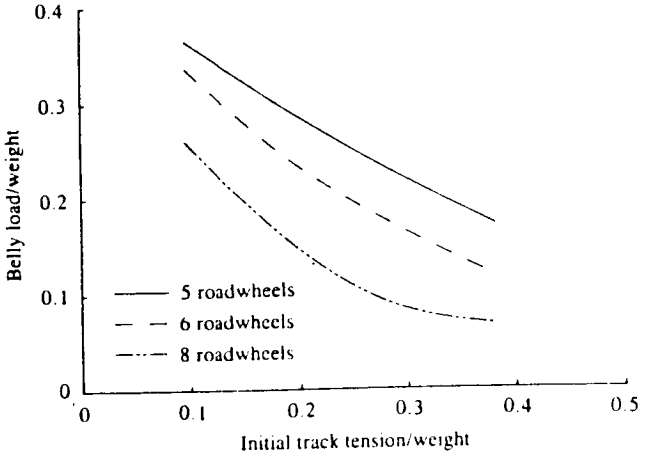

Variation of belly load to weight ratio with initial track tension to weight ratio for three track systems (ground clearance 41 cm, slip 20 per cent)

Fig. 3.6

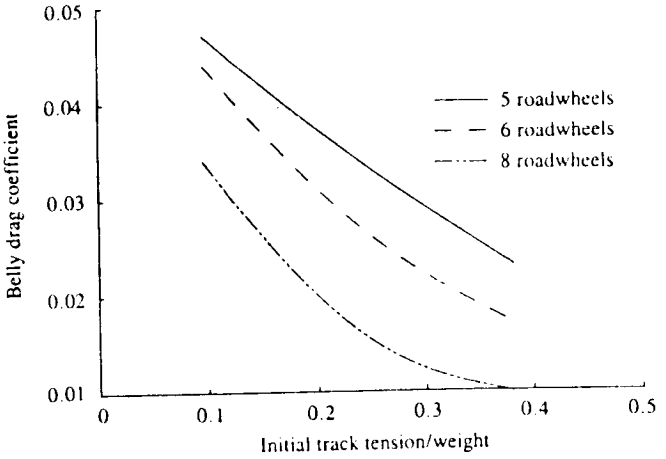

Variation of belly drag coefficient with initial track tension to weight ratio for three track systems (ground clearance 41 cm, slip 20 per cent)

Fig. 3.7

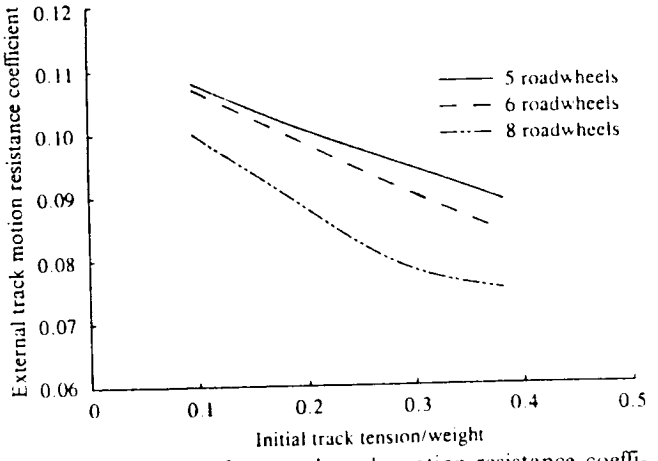

Variation of external track motion resistance coefficient with initial track tension to weight ratio for three track systems (ground clearance 41 cm, slip 20 per cent)

Fig. 3.8

41 cm and operating at 20% slip. It can be seen that in general as the initial track tension increases, the load supported by the track increases and that supported by the belly decreases. For the track system with 5 roadwheels, increasing the initial track tension to weight ratio from 0.096 to 0.287 causes the percentage of the vehicle weight supported by the belly to drop from 36.5% to 22.6%. For the same initial track tension to weight ratio of 0.096, increasing the number of roadwheels from 5 to 8 causes the percentage of the vehicle weight supported by the belly to drop from 36.5% to 25.2%. The decrease of the load supported by the belly causes a reduction in the belly drag as shown in Fig.3.7. The belly drag coefficient is the ratio of the belly drag to vehicle weight.

As shown in Fig.3.8, increasing the initial track tension for a given track system reduces the external motion resistance acting on the track, which is the resistance due to track-terrain interaction. It can be seen that for the basic track system with 5 roadwheels with a ground clearance of 41 cm and a track slip of 20%, the external track motion resistance coefficient, defined as the ratio of the external track motion resistance to vehicle weight, decreases slightly from 0.108 to 0.095 as the ratio of initial track tension to weight increases from 0.096 to 0.287. For the same initial track tension to weight ratio of 0.096, increasing the number of roadwheels from 5 to 8 causes the external track motion resistance coefficient to decrease slightly from 0.108 to 0.099. As a result of the reduction in belly drag and in external track motion resistance, the total external motion resistance coefficient of the vehicle (i.e., the sum of both the belly drag coefficient and external track motion resistance coefficient) decreases noticeably with the increase of initial track tension as shown in Fig.3.9.

As the load supported by the belly decreases with the increase of the initial track tension, the percentage of the vehicle weight supported by the track increases. Over a terrain exhibiting significant frictional behaviour, such as the snow-covered terrain used in this study, the tractive effort of the vehicle increases accordingly. Since the total external motion resistance decreases noticeably with the increase of the initial track tension, as described previously, the drawbar pull of the vehicle increases significantly with the increase of initial track tension as shown in Fig.3.10.

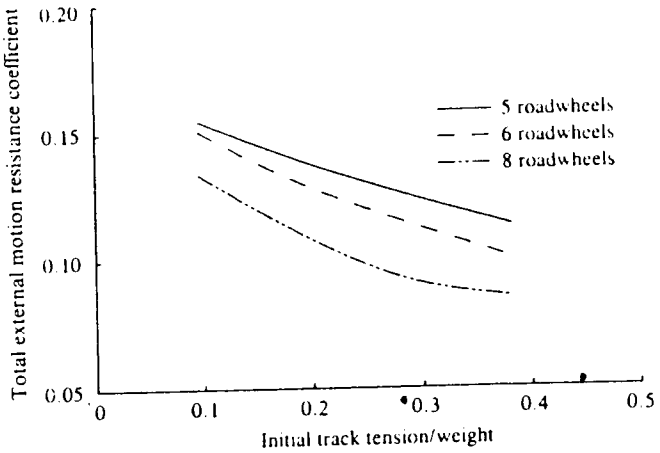

Fig. 3.9 Variation of total external motion resistance coefficient with initial track tension to weight ratio for three track systems (ground clearance 41 cm, slip 20 per cent)

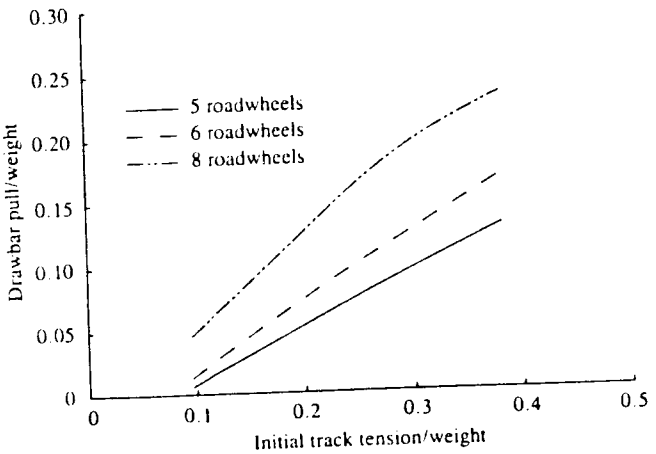

Fig. 3.10 Variation of drawbar pull to weight ratio with initial track tension to weight ratio for three track systems (ground clearance 41 cm, slip 20 per cent)

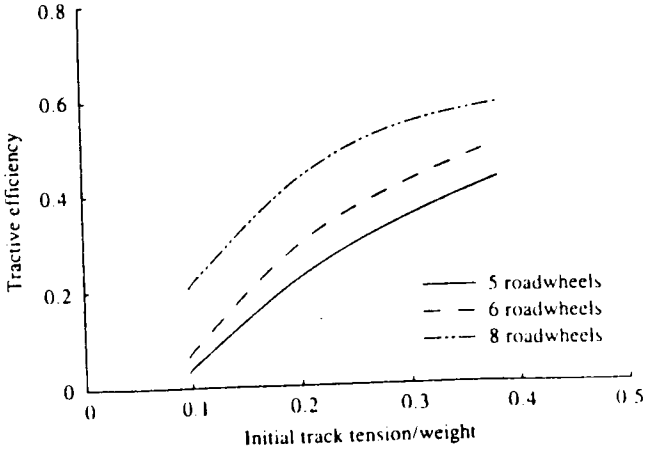

Fig. 3.11 Variation of tractive efficiency with initial track tension to weight ratio for three track systems (ground clearance 41 cm, slip 20 per cent)

Figure 3.11 shows the effect of the initial track tension on the tractive efficiency, defined as (drawbar pull/tractive effort) x (1-slip), for the three track systems with different roadwheel arrangements. Slip is defined as the ratio of the difference between the theoretical and actual forward speeds of the track to the theoretical forward speed, which is equal to the pitch radius multiplied by the angular speed of the sprocket. It can be seen that for the basic track system with 5 roadwheels, increasing the initial track tension to weight ratio from 0.096 to 0.287 causes the value of the tractive efficiency at 20% slip to increase from 0.030 to 0.337. For the same initial track tension to weight ratio of 0.096, increasing the number of roadwheels from 5 to 8 causes the tractive efficiency at 20% slip to increase from 0.030 to 0.222.

The effect of the initial track tension on track sinkage at the rear roadwheel for the three track systems is shown in Fig.3.12. For the basic track system with 5 roadwheels, increasing the initial track tension to weight ratio from 0.096 to 0.287 causes the track sinkage to decrease from 55.2 cm to 51.4 cm. For the same initial track tension to weight ratio of 0.096, increasing the number of roadwheels from 5 to 8 causes the track sinkage to decrease from 55.2 cm to 53.4 cm. Figure 3.13 shows the effect of the initial track tension on the trim angle of the vehicle. It can be seen that the trim angle of the vehicle increases with the increase of the initial track tension. This is mainly due to the fact that the drawbar pull of the vehicle increases with the increase of the initial track tension as described previously. This causes greater load transfer from the front to the rear and hence a higher trim angle.

The effect of ground clearance on tractive performance of the basic vehicle configuration with 5 roadwheels was also examined using NTVPM-85. Figure 3.14 shows the variation of the drawbar pull to weight ratio with slip for the vehicle at various ground clearances. It should be noted that the ground clearance of the baseline vehicle (M113) is 41 cm (16 in.). From Fig.3.14, it can be seen that increasing the ground clearance will enhance the tractive performance over the snow-covered terrain used in this study. For instance, the drawbar pull to weight ratio of the vehicle at 20% slip increases from 0.006 to 0.051 as the ground clearance increases from 41 cm (16 in.) to 61 cm (24 in.).

Figure 3.15 shows the effects of ground clearance on the belly load to weight ratio, belly drag coefficient, total motion resistance coefficient and

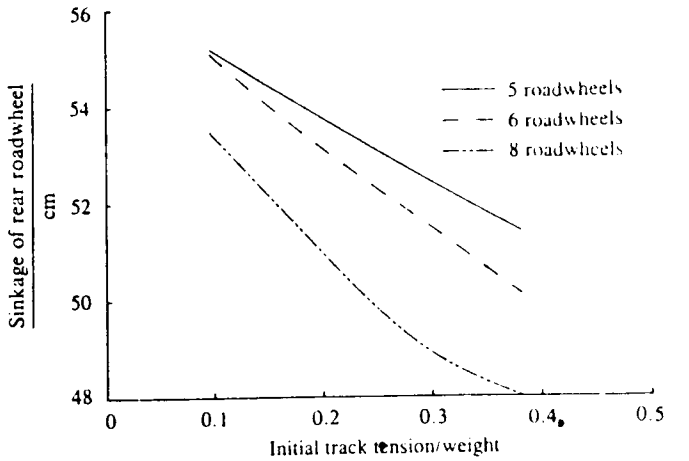

Fig. 3.12 Variation of track sinkage with initial track tension to weight ratio for three track systems (ground clearance 41 cm, slip 20 per cent)

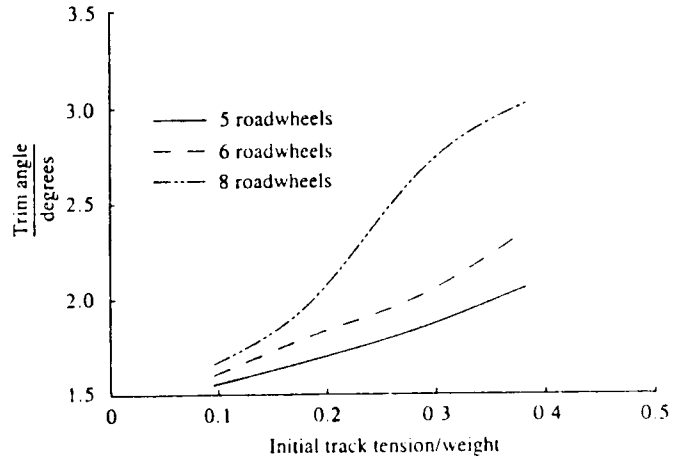

Fig. 3.13 Variation of trim angle with initial track tension to weight ratio for three track systems (ground clearance 41 cm, slip 20 per cent)

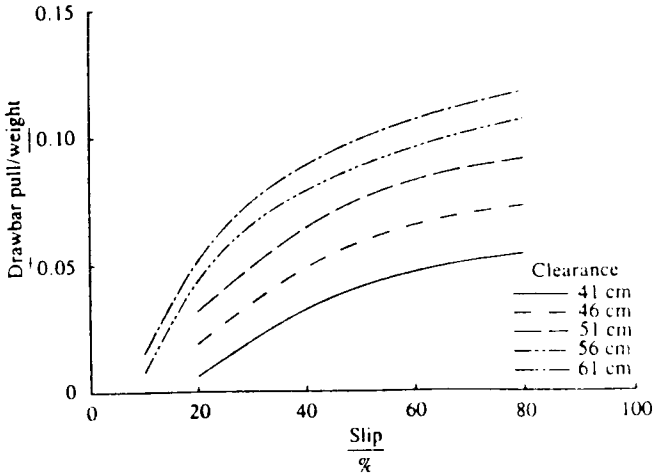

Fig. 3.14 Drawbar performance of a track system with five roadwheels at various ground clearances (initial track tension/weight 0.096)

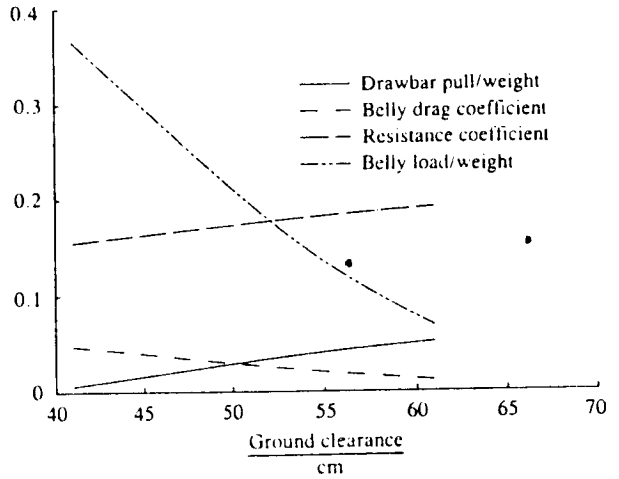

Variation of drawbar pull/weight, belly drag coefficient, total external motion resistance coefficient, and belly load/weight with ground clearance (initial track tension/weight 0.096)

Fig. 3.15

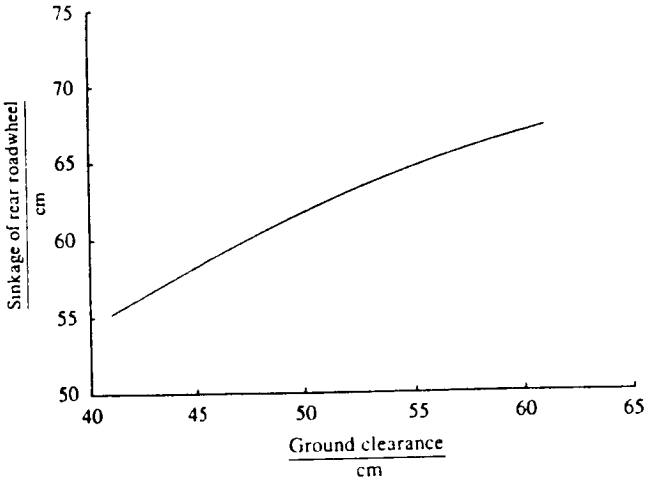

Variation of sinkage with ground clearance for a track system with five roadwheels (initial track tension/weight 0.096)

Fig. 3.16

drawbar pull to weight ratio for the basic track system with 5 roadwheels at 20% slip. It can be seen that the load supported by the belly and hence the belly drag coefficient decreases with the increase of ground clearance. The drawbar pull to weight ratio, however, increases with the increase of ground clearance. This is primarily due to the fact that as the ground clearance increases, the load supported by the track increases. Over a terrain exhibiting significant frictional behaviour, this will result in higher tractive effort at a given slip. Although the total motion resistance also increases with ground clearance, the increase in tractive effort outweighs the increase in total motion resistance. The drawbar pull, therefore, increases with the increase of ground clearance.

The effect of ground clearance on track sinkage at the rear roadwheel for the basic track system with 5 roadwheels is shown in Fig.3.16. It is shown that as the ground clearance increases, the track sinkage increases accordingly. This is because the percentage of the vehicle weight supported by the belly decreases with the increase of ground clearance. As a result, the load supported by the track, and hence track sinkage, increases.

The performance parameters of the three track systems with various initial track tensions at 20% slip on Hope Valley snow are summarized in Tables 3.4, 3.5 and 3.6.

Table 3.4

PERFORMANCE PARAMETERS AT 20% SLIP FOR THE BASELINE TRACKED VEHICLE WITH FIVE ROADWHEELS ON HOPE VALLEY SNOW

Vehicle type	Ground clearance (cm)	Initial track tension to weight ratio	Number of supporting rollers	Belly load to weight ratio	Belly drag coefficient	Track motion resistance coefficient	External motion resistance coefficient	Drawbar pull to weight ratio	Tractive efficiency	Maximum track tension to weight ratio	Sinkage at rear roadwheel (cm)	Trim angle (°)
Standard	41	0.096	0	0.365	0.047	0.108	0.155	0.006	0.030	0.145	55.2	1.55
5-2	41	0.191	0	0.292	0.038	0.101	0.139	0.049	0.209	0.235	53.9	1.69
5-3	41	0.287	0	0.226	0.030	0.095	0.125	0.091	0.337	0.334	52.6	1.85
5-4	41	0.382	0	0.171	0.023	0.089	0.112	0.130	0.429	0.435	51.4	2.06

Table 3.5

PERFORMANCE PARAMETERS AT 20% SLIP FOR A TRACKED VEHICLE WITH SIX ROADWHEELS ON HOPE VALLEY SNOW

Vehicle type	Ground clearance (cm)	Initial track tension to weight ratio	Number of supporting rollers	Belly load to weight ratio	Belly drag coefficient	Track motion resistance coefficient	External motion resistance coefficient	Drawbar pull to weight ratio	Tractive efficiency	Maximum track tension to weight ratio	Sinkage at rear roadwheel (cm)	Trim angle (°)
6-1	41	0.096	3	0.322	0.043	0.107	0.150	0.016	0.077	0.147	54.9	1.6
6-2	41	0.191	3	0.243	0.032	0.099	0.131	0.069	0.276	0.239	53.3	1.79
6-3	41	0.287	3	0.169	0.023	0.091	0.114	0.119	0.409	0.339	51.7	2.03
6-4	41	0.382	3	0.111	0.016	0.083	0.099	0.172	0.507	0.442	50.0	2.47

Table 3.6

PERFORMANCE PARAMETERS AT 20% SLIP FOR A TRACKED VEHICLE WITH EIGHT ROADWHEELS ON HOPE VALLEY SNOW

Vehicle type	Ground clearance (cm)	Initial track tension to weight ratio	Number of supporting rollers	Belly load to weight ratio	Belly drag coefficient	Track motion resistance coefficient	External motion resistance coefficient	Drawbar pull to weight ratio	Tractive efficiency	Maximum track tension to weight ratio	Sinkage at rear roadwheel (cm)	Trim angle (°)
8-1	41	0.096	3	0.252	0.033	0.099	0.132	0.051	0.222	0.150	53.4	1.69
8-2	41	0.191	3	0.151	0.021	0.089	0.110	0.122	0.421	0.245	51.18	2.06
8-3	41	0.287	3	0.087	0.013	0.079	0.092	0.189	0.538	0.349	48.99	2.65
8-4	41	0.382	3	0.067	0.010	0.075	0.085	0.231	0.585	0.449	47.98	2.97

3.2 Effects of Design Parameters on Performance Over Petawawa Muskeg A

Figures 3.17, 3.18 and 3.19 show the variations of the drawbar pull to weight ratio with slip at various initial track tension to weight ratios for the three track systems over Petawawa Muskeg A. It can be seen that over this muskeg, the initial track tension again has a significant effect on tractive performance. For the baseline vehicle with 5 roadwheels, increasing the value of the initial track tension to weight ratio, $\hat{T}_0/W$, from 0.096 to 0.382 results in an increase in the drawbar pull to weight ratio from 0.454 to 0.649, representing an improvement of 43%. It can also be seen from Figs.3.17 and 3.19 that for the same initial track tension to weight ratio of 0.191, the track system with 8 overlapping roadwheels has a drawbar pull to weight ratio of 0.603 at 20% slip, as compared with a value of 0.509 for the track system with 5 roadwheels. This represents an improvement of approximately 18.5%.

Figures 3.20 and 3.21 show the normal pressure distributions under the track system with 6 roadwheels at initial track tension to weight ratios of 0.096 and 0.287, respectively. It again demonstrates that an increase in initial tension results in a decrease in peak pressure and hence improved tractive performance.

The performance parameters of the three track systems with various initial track tensions at 20% slip on Petawawa Muskeg A are summarized in Tables 3.7, 3.8 and 3.9. It can be seen from the tables that for the track systems with 5 and 6 roadwheels at low initial track tensions, the belly comes into contact with the terrain surface. However, the load supported by the belly is small and the belly drag is insignificant. For the track system with 8 overlapping wheels, the belly does not come into contact with terrain surface, even at low initial track tensions.

As shown in Fig.3.22, increasing the initial track tension for a given track system reduces the total motion resistance coefficient of the vehicle. This is particularly significant for the basic track system with 5 roadwheels. For instance, increasing the initial track tension to weight ratio from 0.096 to

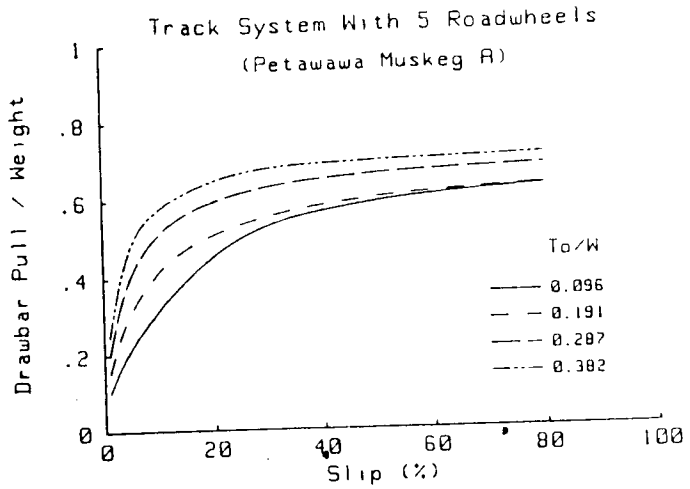

Fig. 3.17 Drawbar performance of a track system with five roadwheels at various ratios of initial track tension to weight on Petawawa Muskeg A.

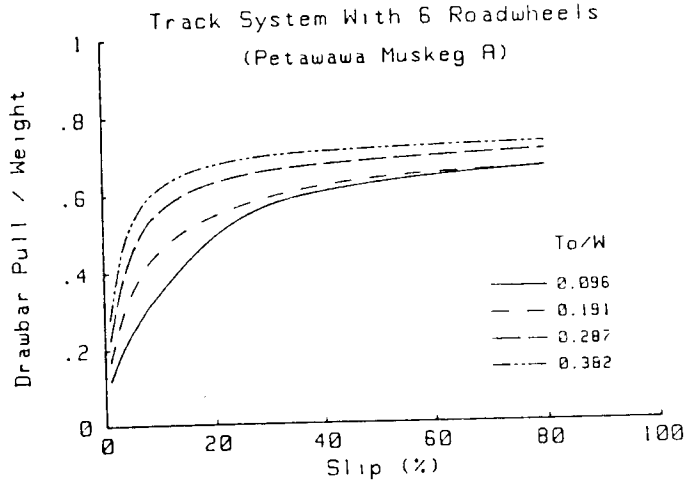

Fig. 3.18 Drawbar performance of a track system with six roadwheels at various ratios of initial track tension to weight on Petawawa Muskeg A.

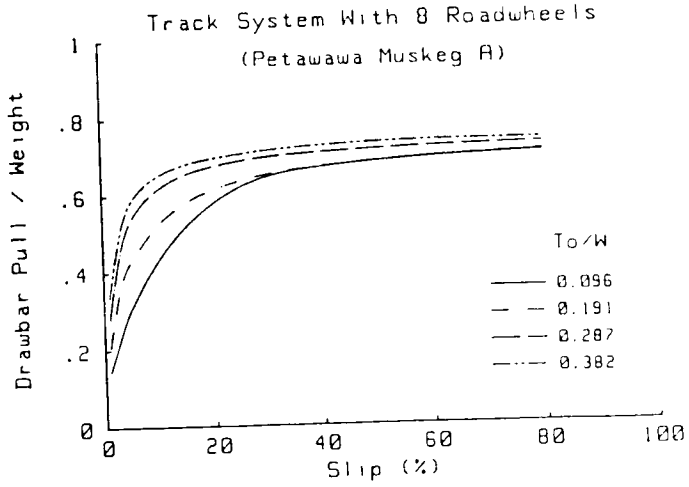

Fig. 3.19 Drawbar performance of a track system with eight overlapping roadwheels at various ratios of initial track tension to weight on Petawawa Muskeg A

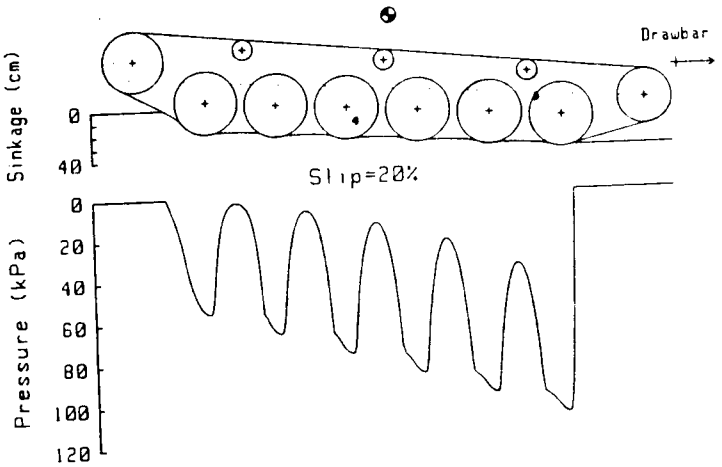

Fig. 3.20 Predicted normal pressure distribution under a track system with six roadwheels at initial track tension to weight ratio of 0.096 on Petawawa Muskeg A

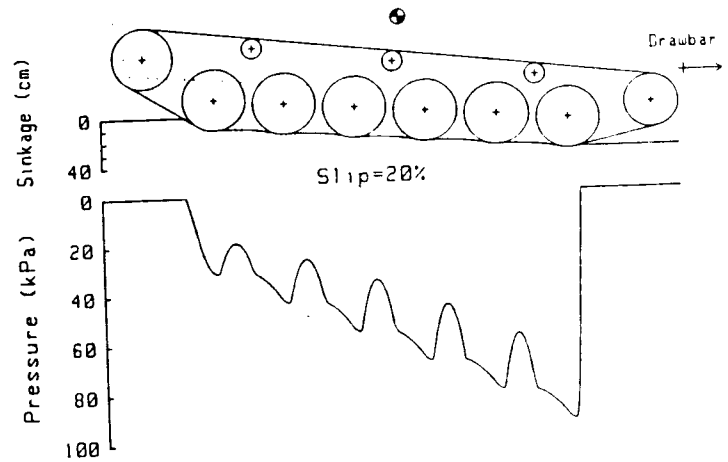

Fig. 3.21 Predicted normal pressure distribution under a track system with six roadwheels at initial track tension to weight ratio of 0.287 on Petawawa Muskeg A

Table 3.7

PERFORMANCE PARAMETERS AT 20% SLIP FOR THE BASELINE TRACKED VEHICLE WITH FIVE ROADWHEELS ON PETAWAWA MUSKEG A

Vehicle type	Ground clearance (cm)	Initial track tension to weight ratio	Number of supporting rollers	Belly load to weight ratio	Belly drag coefficient	Track motion resistance coefficient	External motion resistance coefficient	Drawbar pull to weight ratio	Tractive efficiency	Maximum track tension to weight ratio	Sinkage at rear roadwheel (cm)	Trim angle (°)
Standard	41	0.096	0	0.0248	0.008	0.126	0.134	0.454	0.618	0.301	38.3	3.56
5-2	41	0.191	0	0.009	0.003	0.114	0.117	0.509	0.651	0.353	36.6	4.07
5-3	41	0.287	0	0	0	0.096	0.096	0.596	0.689	0.454	33.9	4.54
5-4	41	0.382	0	0	0	0.088	0.088	0.649	0.704	0.553	32.6	4.80

Table 3.8

PERFORMANCE PARAMETERS AT 20% SLIP FOR A TRACKED VEHICLE WITH SIX ROADWHEELS ON PETAWAWA MUSKEG A

Vehicle type	Ground clearance (cm)	Initial track tension to weight ratio	Number of supporting rollers	Belly load to weight ratio	Belly drag coefficient	Track motion resistance coefficient	External motion resistance coefficient	Drawbar pull to weight ratio	Tractive efficiency	Maximum track tension to weight ratio	Sinkage at rear roadwheel (cm)	Trim angle (°)
6-1	41	0.096	3	0.002	0.0006	0.117	0.118	0.489	0.644	0.310	37	3.65
6-2	41	0.191	3	0	0	0.102	0.102	0.544	0.674	0.359	34.7	3.96
6-3	41	0.287	3	0	0	0.086	0.086	0.630	0.704	0.459	32.2	4.40
6-4	41	0.382	3	0	0	0.081	0.081	0.676	0.714	0.558	31.5	4.66

Table 3.9

PERFORMANCE PARAMETERS AT 20% SLIP FOR THE TRACKED VEHICLE WITH EIGHT ROADWHEELS ON PETAWAWA MUSKEG A

Vehicle type	Ground clearance (cm)	Initial track tension to weight ratio	Number of supporting rollers	Belly load to weight ratio	Belly drag coefficient	Track motion resistance coefficient	External motion resistance coefficient	Drawbar pull to weight ratio	Tractive efficiency	Maximum track tension to weight ratio	Sinkage at rear roadwheel (cm)	Trim angle (°)
8-1	41	0.096	3	0	0	0.089	0.089	0.578	0.693	0.337	32.6	3.82
8-2	41	0.191	3	0	0	0.085	0.085	0.603	0.701	0.363	31.9	4.06
8-3	41	0.287	3	0	0	0.079	0.079	0.673	0.716	0.459	31.2	4.69
8-4	41	0.382	3	0	0	0.078	0.078	0.695	0.719	0.552	31.1	4.83

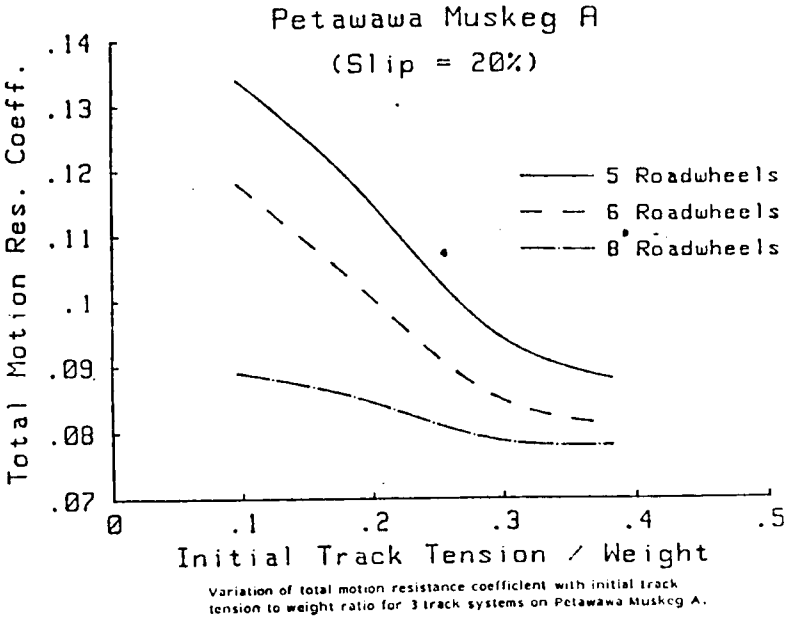

Variation of total motion resistance coefficient with initial track tension to weight ratio for 3 track systems on Petawawa Muskeg A.

Fig. 3.22

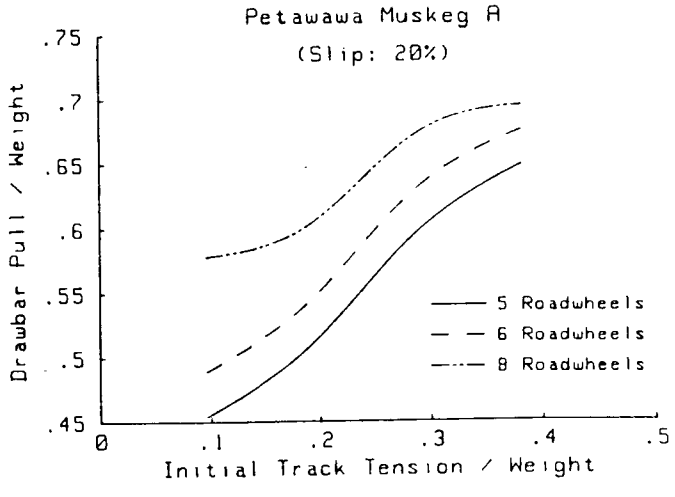

A comparison of the effects of initial track tension on drawbar pull at 20% slip for three track systems on Petawawa Muskeg A.

Fig. 3.23

0.382 causes the total motion resistance coefficient to decrease from 0.134 to 0.088. The track system configuration also has a noticeable effect on the total motion resistance of the vehicle. For instance, at the same initial track tension to weight ratio of 0.096, increasing the number of roadwheels from 5 to 8 causes the total motion resistance coefficient to decrease from 0.134 to 0.089. It is interesting to note, however, that the effects of initial track tension on the total motion resistance for the track system with 8 roadwheels are not as significant as those for the basic track system with 5 roadwheels.

Figure 3.23 shows a comparison of the effects of initial track tension on drawbar pull at 20% slip for the three track systems. It is interesting to point out that on this muskeg the drawbar performance of the track system with 5 roadwheels at an initial track tension to weight ratio of 0.382 is approximately equivalent to that of the track system with 8 overlapping roadwheels at an initial track tension to weight ratio of about 0.25. Figure 3.24 shows a comparison of the effects of initial track tension on tractive efficiency for the three track systems. It is interesting to note that on this muskeg the initial track tension has a more significant effect on the tractive efficiency of the track system with 5 roadwheels than that of the system with 8 overlapping roadwheels.

Figure 3.25 shows the effects of initial track tension on the sinkage of the rear roadwheel for the three track systems. For the basic track system with 5 roadwheels, increasing the initial track tension to weight ratio from 0.096 to 0.382 causes the sinkage of rear roadwheel to decrease from 38.3 to 32.6 cm, representing a reduction of 14.9%. However, for the track system with 8 roadwheels, the initial track tension has less effect on the track sinkage, as can be seen from Fig.3.25.

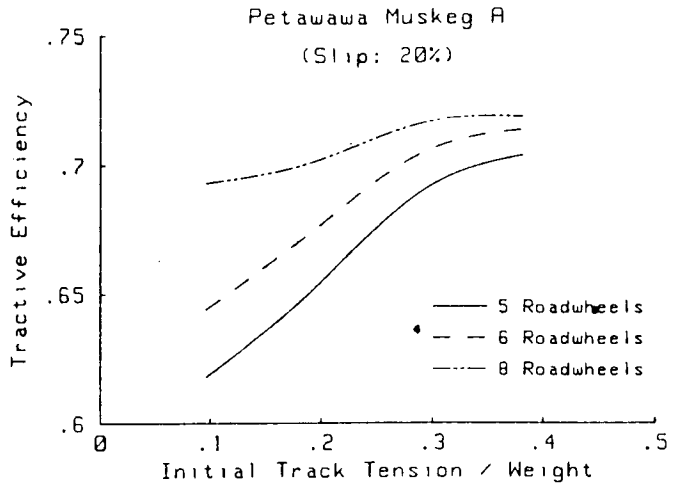

A comparison of the effects of initial track tension on tractive efficiency at 20% slip for three track systems on Petawawa Muskeg A.

Fig. 3.24

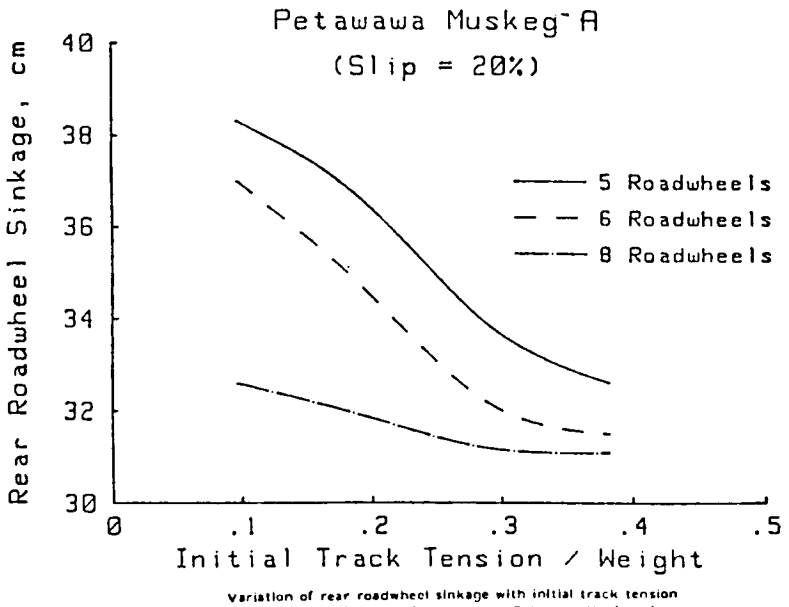

Variation of rear roadwheel sinkage with initial track tension to weight ratio for 3 track systems on Petawawa Muskeg A.

Fig. 3.25

3.3 Effects of Design Parameters on Performance Over LETE Sand

The variations of the drawbar pull to weight ratio with slip at various initial track tension to weight ratios for the three track systems over LETE sand are shown in Figs.3.26, 3.27 and 3.28. It can be seen that on this sandy terrain, the initial track tension has an insignificant effect on tractive performance. For the baseline vehicle with 5 roadwheels, increasing the value of the initial track tension to weight ratio, T_0/W, from 0.096 to 0.382 results in an increase of the drawbar pull to weight ratio of only 8.5%. This is primarily due to the fact that the LETE sand was a relatively firm terrain. The increase in initial track tension does not cause a significant increase in the load supported by the track segments between roadwheels, and thus does not significantly affect the performance. It can also be seen from Figs.3.26 and 3.28 that for the same initial track tension to weight ratio of 0.191, the track system with 8 overlapping roadwheels has similar tractive performance to that of the system with 5 roadwheels. The difference between them in drawbar pull at 20% slip is merely 2.4%.

Figures 3.29 and 3.30 show the normal pressure distributions under the track system with 5 roadwheels at initial track tension to weight ratios of 0.096 and 0.287, respectively. It is shown that the effects of initial track tension on the pressure distribution under the track on LETE sand are much less significant than they are on Hope Valley snow or Petawawa Muskeg A.

Figure 3.31 shows the effects of initial track tension on the track motion resistance coefficient at 20% slip for the three track systems. It indicates that on LETE sand the effects of initial track tension on track motion resistance are relatively insignificant, particularly for the track system with 8 roadwheels.

Figure 3.32 shows a comparison of the effects of initial track tension on drawbar pull at 20% slip for the three track systems. It indicates that on LETE sand the effects of initial track tension on tractive performance are relatively insignificant, compared with those on Hope Valley snow. The effects of initial

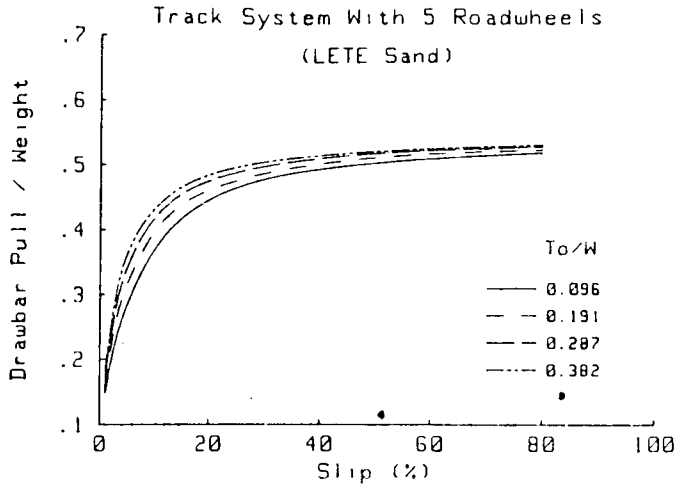

Fig. 3.26 Drawbar performance of a track system with five roadwheels at various ratios of initial track tension to weight on LETE sand.

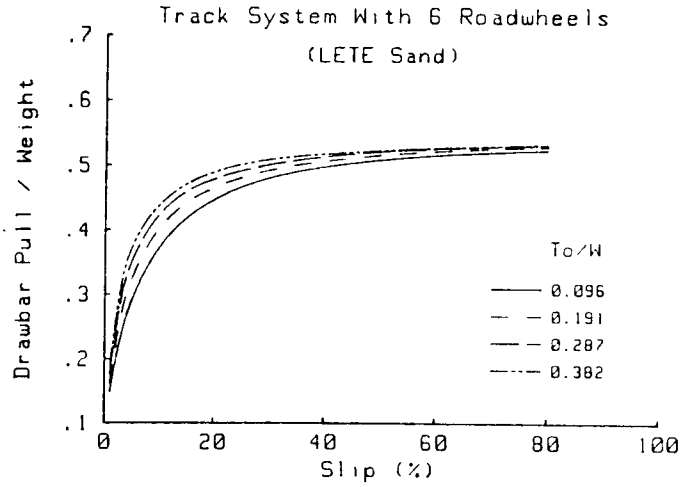

Fig. 3.27 Drawbar performance of a track system with six roadwheels at various ratios of initial track tension to weight on LETE sand.

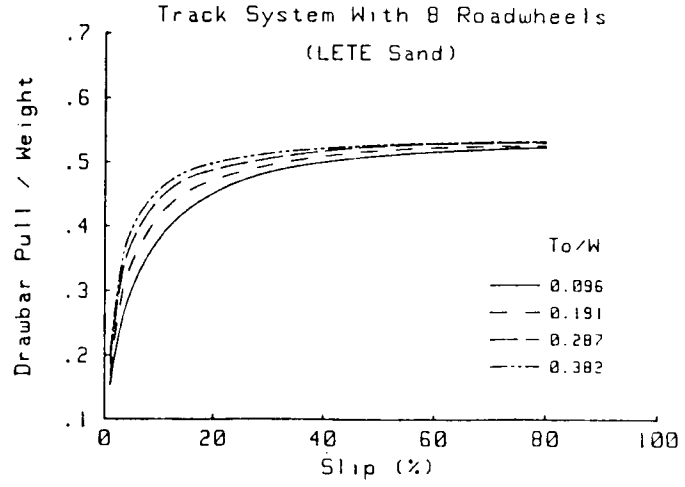

Fig. 3.28 Drawbar performance of a track system with eight overlapping roadwheels at various ratios of initial track tension to weight on LETE sand.

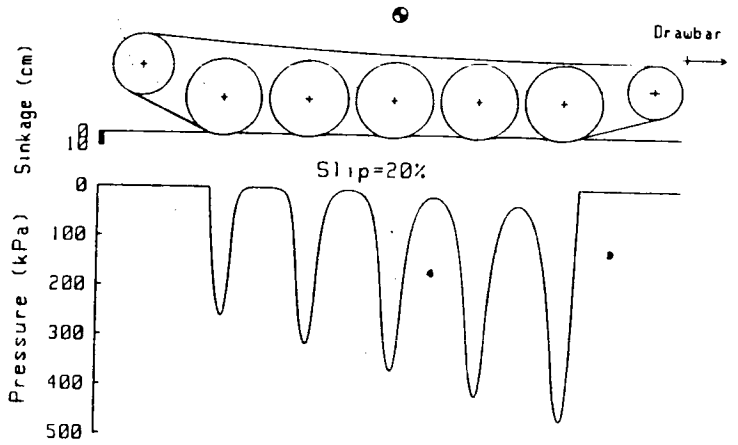

Fig. 3.29 Predicted normal pressure distribution under a track system with five roadwheels at initial track tension to weight ratio of 0.096 on LETE sand.

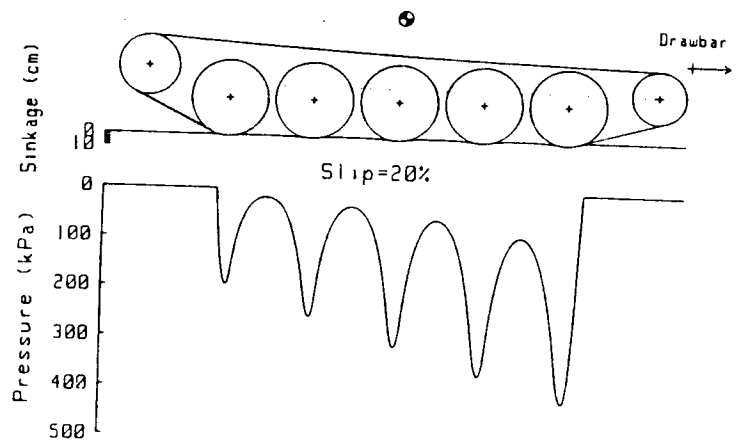

Fig. 3.30 Predicted normal pressure distribution under a track system with five roadwheels at initial track tension to weight ratio of 0.287 on LETE sand.

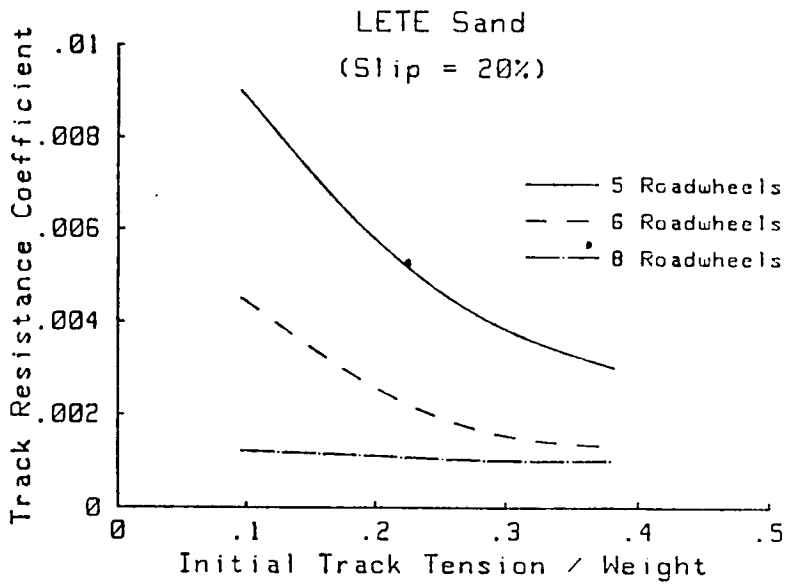

Variation of track resistance coefficient with initial track tension to weight ratio for 3 track systems on LETE sand.

Fig. 3.31

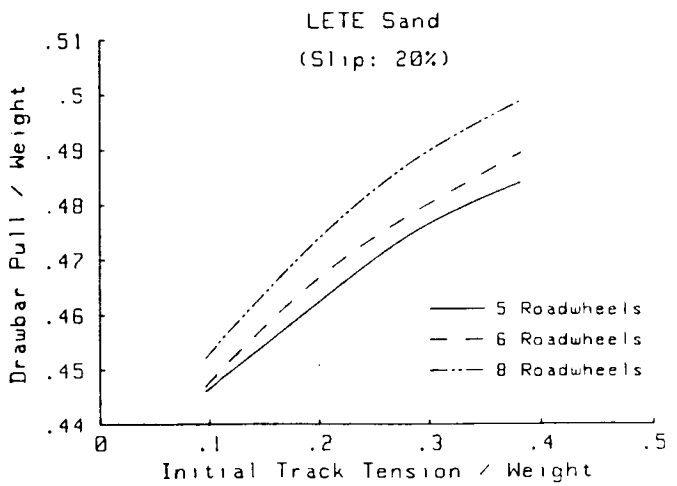

A comparison of the effects of initial track tension on drawbar pull at 20% slip for three track systems on LETE sand.

Fig. 3.32

track tension on tractive efficiency of the three track systems are shown in Fig.3.33. It is shown that while the initial track tension has a minor effect on the tractive efficiency of the track system with 5 roadwheels, it has practically no effect on the tractive efficiency of the system with 8 overlapping roadwheels.

As shown in Fig.3.34, the initial track tension has only minor effects on the sinkage of the rear roadwheel.

The performance parameters of the three track systems with various initial track tensions at 20% slip on LETE sand are summarized in Tables 3.10, 3.11 and 3.12.

Figures 3.35, 3.36 and 3.37 summarize the effects of initial track tension on drawbar pull over the three types of terrain for track systems with 5 roadwheels, 6 roadwheels, and 8 overlapping roadwheels, respectively. It is shown that on LETE sand the initial track tension and track system configuration have little effect on the drawbar performance. On Hope Valley snow and Petawawa Muskeg A, the initial track tension has, in general, a noticeable effect on the drawbar pull of the three track systems. It is interesting to note, however, that on Petawawa Muskeg A the initial track tension has slightly less effect on the drawbar pull of the track system with 8 overlapping roadwheels than that of the track systems with 5 and 6 roadwheels.

Figures 3.38, 3.39 and 3.40 summarize the effects of initial track tension on tractive efficiency over the three types of terrain for the track systems with 5 roadwheels, 6 roadwheels, and 8 overlapping roadwheels, respectively. It can be seen that on LETE sand, both the initial track tension and track system configuration have little effect on tractive efficiency. The tractive efficiency is more sensitive to the initial track tension than to track system configuration on Petawawa Muskeg A. On Hope Valley snow, both the initial track tension and track system configuration have a significant effect on tractive efficiency.

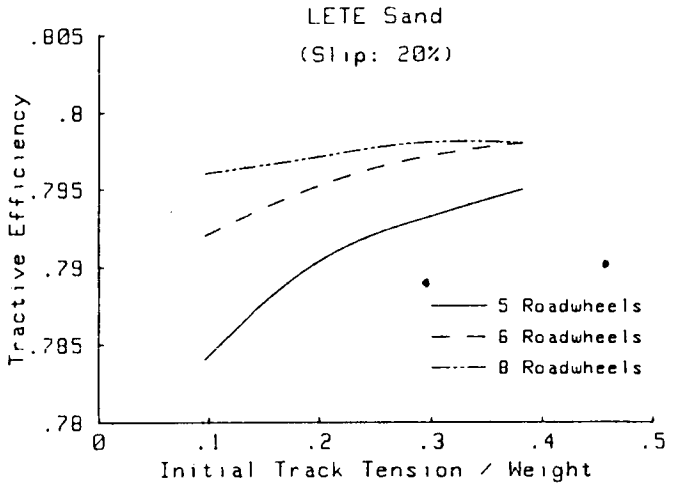

A comparison of the effects of initial track tension on tractive efficiency at 20% slip for three track systems on LETE sand.

Fig. 3.33

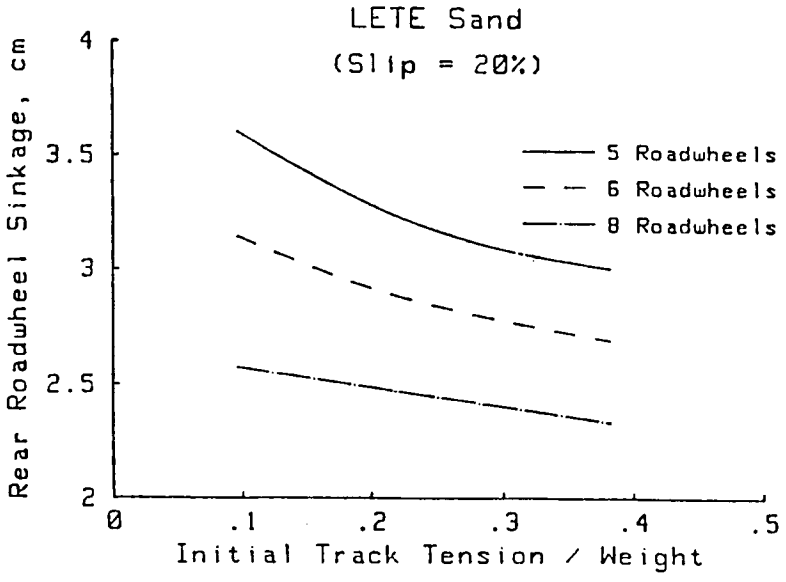

Variation of rear roadwheel sinkage with initial track tension to weight ratio for 3 track systems on LETE sand.

Fig. 3.34

Table 3.10

PERFORMANCE PARAMETERS AT 20% SLIP FOR THE BASELINE TRACKED VEHICLE WITH FIVE ROADWHEELS ON LETE SAND

Vehicle type	Ground clearance (cm)	Initial track tension to weight ratio	Number of supporting rollers	Belly load to weight ratio	Belly drag coefficient	Track motion resistance coefficient	External motion resistance coefficient	Drawbar pull to weight ratio	Tractive efficiency	Maximum track tension to weight ratio	Sinkage at rear roadwheel (cm)	Trim angle (°)
Standard	41	0.096	0	0	0	0.009	0.009	0.446	0.784	0.230	3.6	.40
5-2	41	0.191	0	0	0	0.006	0.006	0.461	0.790	0.307	3.3	.40
5-3	41	0.287	0	0	0	0.004	0.004	0.475	0.793	0.401	3.1	.42
5-4	41	0.382	0	0	0	0.003	0.003	0.484	0.795	0.496	3.0	.43

Table 3.11

PERFORMANCE PARAMETERS AT 20% SLIP FOR A TRACKED VEHICLE WITH SIX ROADWHEELS ON LETE SAND

Vehicle type	Ground clearance (cm)	Initial track tension to weight ratio	Number of supporting rollers	Belly load to weight ratio	Belly drag coefficient	Track motion resistance coefficient	External motion resistance coefficient	Drawbar pull to weight ratio	Tractive efficiency	Maximum track tension to weight ratio	Sinkage at rear roadwheel (cm)	Trim angle (°)
6-1	41	0.096	3	0	0	0.0045	0.0045	0.446	0.792	0.228	3.14	0.306
6-2	41	0.191	3	0	0	0.0027	0.0027	0.465	0.795	0.309	2.93	0.340
6-3	41	0.287	3	0	0	0.0016	0.0016	0.478	0.797	0.402	2.79	0.368
6-4	41	0.382	3	0	0	0.0013	0.0013	0.489	0.798	0.497	2.69	0.384

Table 3.12

PERFORMANCE PARAMETERS AT 20% SLIP FOR A TRACKED VEHICLE WITH EIGHT ROADWHEELS ON LETE SAND

Vehicle type	Ground clearance (cm)	Initial track tension to weight ratio	Number of supporting rollers	Belly load to weight ratio	Belly drag coefficient	Track motion resistance coefficient	External motion resistance coefficient	Drawbar pull to weight ratio	Tractive efficiency	Maximum track tension to weight ratio	Sinkage at rear roadwheel (cm)	Trim angle (°)
8-1	41	0.096	3	0	0	0.0012	0.0012	0.452	0.796	0.228	2.57	0.258
8-2	41	0.191	3	0	0	0.0011	0.0011	0.472	0.798	0.308	2.49	0.317
8-3	41	0.287	3	0	0	0.0010	0.0010	0.488	0.798	0.401	2.41	0.323
8-4	41	0.382	3	0	0	0.0010	0.0010	0.498	0.798	0.499	2.33	0.363

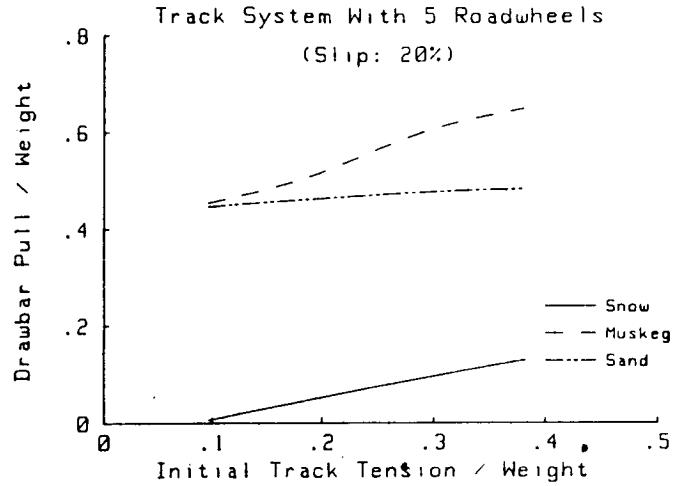

Fig. 3.35 Effects of initial track tension on drawbar pull of a track system with five roadwheels at 20% slip over three types of terrain.

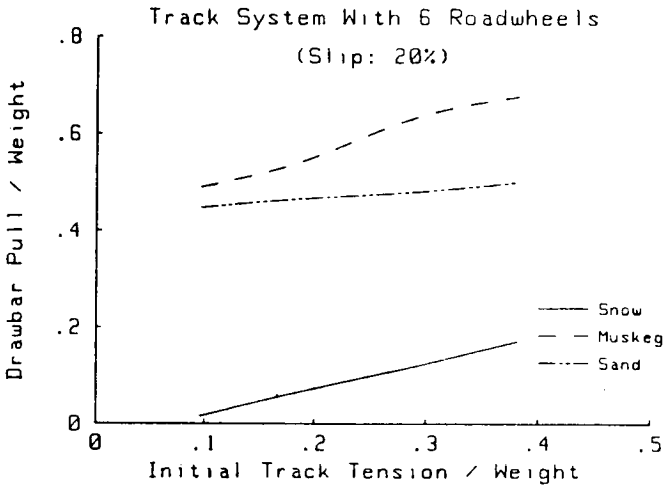

Fig. 3.36 Effects of initial track tension on drawbar pull of a track system with six roadwheels at 20% slip over three types of terrain.

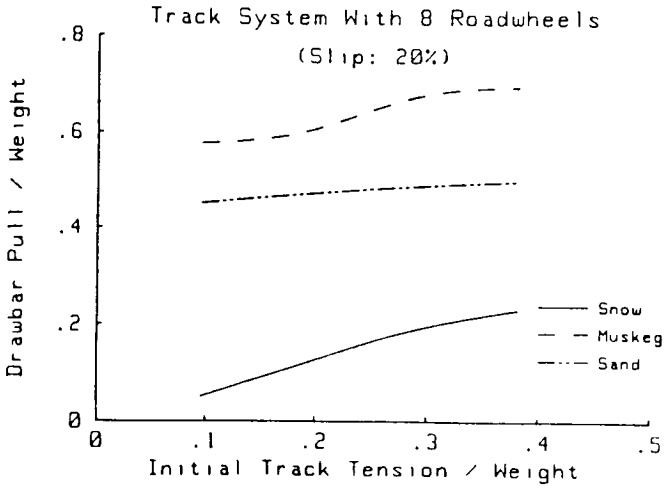

Fig. 3.37 Effects of initial track tension on drawbar pull of a track system with eight overlapping roadwheels at 20% slip over three types of terrain.

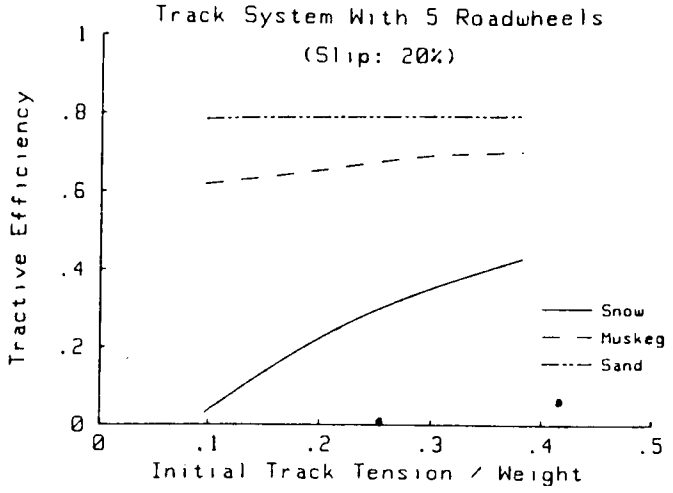

Fig. 3.38 Effects of initial track tension on tractive efficiency of a track system with five roadwheels at 20% slip over three types of terrain.

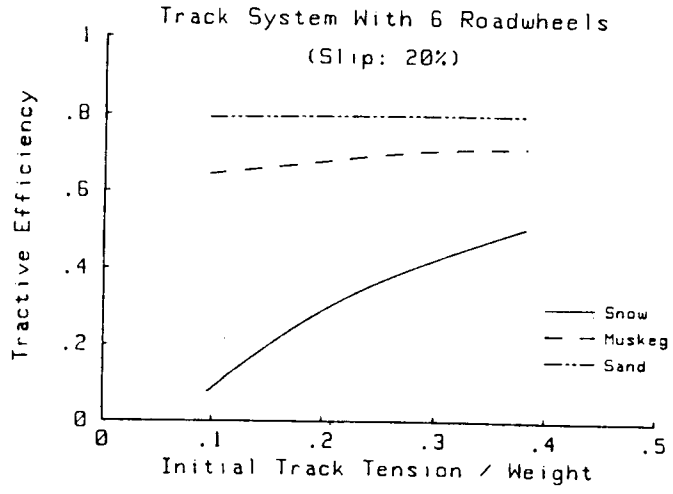

Fig. 3.39 Effects of initial tension on tractive efficiency of a track system with six roadwheels at 20% slip over three types of terrain.

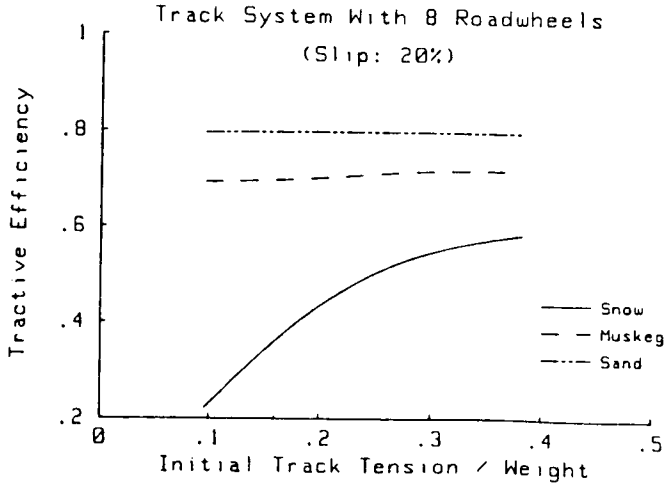

Fig. 3.40 Effects of initial track tension on tractive efficiency of a track system with eight overlapping roadwheels at 20% slip over three types of terrain.

3.4 Discussion

Among the vehicle design parameters examined in this study, the initial track tension is found to have a significant effect on vehicle performance on marginal terrains, such as the Hope Valley snow and Petawawa Muskeg A used in this study. The effect of initial track tension on tractive performance becomes less pronounced as the terrain becomes firmer. For instance, on LETE sand, the increase in initial track tension has an insignificant effect on the performance of the three track systems examined in this study.

Since an increase in initial track tension normally will cause an increase in the internal mechanical losses and wear in the track-suspension system, the increase in tension as a means of improving performance is justifiable only when operating on marginal terrains.

For tracked vehicles that are expected to operate over marginal terrains for any significant period of time, a case can be made for the installation of a central track tension regulating system that can be conveniently controlled by the driver. Over normal terrains, the driver can set the initial track tension at a lower level to minimize the internal mechanical losses and wear of the track-suspension system. When traversing marginal terrains is anticipated, the driver can readily increase the track tension to an appropriate level to improve vehicle mobility. The central track tension regulating system is analogous to the central tire inflation system installed in some off-road wheeled vehicles.

It should be mentioned that the increase of initial track tension will affect the operation of the suspension system. This has to be taken into account when considering the design of the central track tension regulating system.

The track system configuration is also shown to have a noticeable effect on tractive performance over marginal terrain. As the terrain becomes firmer, the effect of track system configuration on performance becomes less significant.

It is interesting to note that the improvement in performance achieved by using 8 overlapping roadwheels at lower initial track tensions can usually be matched by using 5 or 6 roadwheels at higher initial track tensions. Consequently, to improve the mobility of existing tracked vehicles over marginal terrains, increasing the initial track tension would appear to be the most cost-effective means.

Ground clearance of a vehicle is shown to have considerable effects on tractive performance over marginal terrains. In general, the ground clearance should be as high as practicable to minimize belly contact. Belly contact induces additional drag (belly drag) and reduces the load supported by the tracks. Over terrains exhibiting significant frictional behaviour, the reduction in the load supported by the tracks causes a decrease in the tractive effort. All of these will have adverse effects on the tractive performance of the vehicle.

The results described above have demonstrated the usefulness of the computer simulation model NTVPM-85 in parametric analysis of tracked vehicle performance, as it can quantitatively define the effects of design parameters and terrain conditions on vehicle performance. In comparison with the widely used conventional method based on the nominal ground pressure, which is incapable of distinguishing between different track system designs, the computer simulation model NTVPM-85 gives more accurate and realistic predictions of tracked vehicle performance (3.6). Thus, it can be an extremely useful tool for the development and design engineer, as well as the procurement manager, in the selection of the most promising design for a given mission and environment.

The computer simulation model NTVPM-85 has been used to assist tracked vehicle manufacturers in the development and design of new products, as well as governmental agencies in the selection of vehicle candidates. For instance, the model has been employed to assist AB Hagglund of Sweden in the evaluation of competing designs for a new family of armoured fighting vehicles. It has been used to predict the possible changes in mobility of Canada's main battle tank, the Leopard C1, resulting from design modifications for the Canadian Department of National Defence. It has also been employed to compare the off-road mobility of various military logistics vehicles for an agency of the U.S. Department of the Navy.

It should be mentioned that further development of the computer modelling of tracked vehicle performance is being carried out under the auspices of Vehicle Systems Development Corporation (3.8). In the new model NTVPM-86, currently under development, the roadwheel centres are no longer assumed to be rigidly connected, and the characteristics of the independent suspension of the roadwheels are fully taken into account. The model can accommodate both torsion-bar and linear spring suspension systems.

As the tension-elongation relationship of the track link is usually non-linear, in the new model NTVPM-86, the non-linear tension-elongation characteristics of the track link are also taken into account. The measured data on the track tension-elongation relationship may be entered into the simulation model in the form of a table. The inclusion of the non-linear tension-elongation relationship of the track makes the simulation model NTVPM-86 even more realistic. Furthermore, the algorithms that implement the mathematical model have been further improved in the new model, as compared with NTVPM-85.

References

3.1 J.Y. Wong and J. Preston-Thomas, Parametric analysis of tracked vehicle performance using an advanced computer simulation model, Proceedings of the Institution of Mechanical Engineers, Vol.200, Part D, No.2, 1986.

3.2 J.Y. Wong, Computer aided analysis of the effects of design parameters on the performance of tracked vehicles, Journal of Terramechanics, Vol.23, No.2, 1986.

3.3 W.L. Harrison, Vehicle performance over snow, math-model validation study, Technical Report No.268, U.S. Army Corps of Engineers, Cold Regions Research and Engineering Laboratory, December 1975.

3.4 J.Y. Wong, J.R. Radforth and J. Preston-Thomas, Some further studies on the mechanical properties of muskeg in relation to vehicle mobility, Journal of Terramechanics, Vol.21, No.1, 1984.

3.5 J.Y. Wong, M. Garber and J. Preston-Thomas, Theoretical prediction and experimental substantiation of the ground pressure distribution and tractive performance of tracked vehicles, Proceedings of the Institution of Mechanical Engineers, Vol.198, Part D, No.15, 1984.

3.6 J.Y. Wong and J. Preston-Thomas, A comparison between a conventional method and an improved method for predicting tracked vehicle performance, Proceedings of the 8th International Conference of ISTVS, Vol.1, Cambridge, England, 1984.

3.7 J.Y. Wong, An improved method for predicting tracked vehicle performance, Journal of Terramechanics, Vol.21, No.1, 1984.

3.8 J.Y. Wong and J. Preston-Thomas, Investigation into the Effects of Suspension Characteristics and Design Parameters on the Performance of Tracked Vehicles Using An Advanced Computer Simulation Model, Proceedings of Institution of Mechanical Engineers, Vol.202, Part D, No.2, 1988.